Muon decay and physics beyond the standard model

Yoshitaka Kuno* and Yasuhiro Okada[†]

Institute of Particle and Nuclear Studies (IPNS), High Energy Accelerator Research Organization (KEK), Tsukuba, Ibaraki 305-0801, Japan

(Published 12 January 2001)

This article reviews the current theoretical and experimental status of the field of muon decay and its potential to search for new physics beyond the standard model. The importance of rare muon processes with lepton flavor violation is highly stressed, together with precision measurements of normal muon decay. Recent up-to-date motivations of lepton flavor violation based on supersymmetric models, in particular supersymmetric grand unified theories, are described along with other theoretical models. Future prospects of experiments and muon sources of high intensity for further progress in this field are also discussed.

CONTENTS

———
*Current address: Department of Physics, Osaka University, Toyonaka, Osaka 560-0043, Japan. Electronic address: kuno@phys.sci.osaka-u.ac.jp
[†]Electronic address: yasuhiro.okada@kek.jp

I. INTRODUCTION

The muon was discovered in 1937 by Neddermeyer and Anderson (Neddermeyer and Anderson, 1937) in cosmic rays, with a mass found to be about 200 times the

mass of the electron. The discovery was made just after Yukawa postulated the existence of the π meson, a force carrier of the nuclear force, in 1935 (Yukawa, 1935). However, it was demonstrated in 1947 that the muon did not interact via the strong interaction, and thus it could not be the π meson of Yukawa (Conversi *et al.*, 1947). The famous comment by Rabi—"Who ordered that?"— indicates how puzzling the existence of a new lepton was at that time. It was believed that the muon decayed into an electron and a neutral particle. It was assumed that if the muon were simply a heavy electron it would also decay into an electron and a γ ray. The first search for $\mu^+ \to e^+ \gamma$ was made by Hincks and Pontecorvo in 1947 using cosmic-ray muons (Hincks and Pontecorvo, 1947). Its negative result set an upper limit on the branching ratio (B) of less than 10%. This was the beginning of the search for lepton flavor violation, i.e., violation of lepton number conservation for each generation. In 1948, the continuous spectrum of electrons was established, suggesting a three-body decay giving rise to a final state of an electron accompanied by two neutral particles (Steinberger, 1948). Soon afterwards, the search for the process of neutrinoless muon nuclear capture ($\mu^- N \to e^- N$, where N is a nucleus capturing the muon) was also carried out, but with a negative result (Lagarrigue and Peyrou, 1952). Such searches were significantly improved when muons became artificially produced at accelerators. In 1955, the upper limits of $B(\mu \to e\gamma) < 2 \times 10^{-5}$ (Lokonathan and Steinberger, 1955) and $B(\mu^- \text{Cu} \to e^- \text{Cu}) < 5 \times 10^{-4}$ (Steinberger and Wolfe, 1955) were set at the Columbia University Nevis cyclotron.

After the discovery of parity violation, it was suggested that the weak interaction took place through the exchange of charged intermediate vector bosons (Feynman and Gell-Mann, 1958). In 1958, Feinberg pointed out that the intermediate vector boson, if it exists, would lead to $\mu^+ \to e^+ \gamma$ at a branching ratio of 10^{-4} (Feinberg, 1958). The absence of any experimental observation of the $\mu^+ \to e^+ \gamma$ process with $B(\mu \to e\gamma) > 2 \times 10^{-5}$ led directly to the two-neutrino hypothesis (Nishijima, 1957; Schwinger, 1957) in which the neutrino coupled to the muon differs from that coupled to the electron, and the $\mu^+ \to e^+ \gamma$ process is forbidden. The two-neutrino hypothesis was verified experimentally at Brookhaven National Laboratory (BNL) by observing muon production but not electron production from the scattering of neutrinos produced from pion decays (Danby *et al.*, 1962). This introduced the concept of a separate conservation law for individual lepton flavors, electron number (L_e) and muon number (L_μ).

Our understanding of modern elementary particle physics is based on the standard model (SM), which is a gauge theory of the strong and electroweak interactions. The formulation of the SM is based on many theoretical developments of gauge theory in the 1960s and 1970s. Since then, the SM has withstood numerous experimental tests, being entirely consistent with all precision measurements to date. In the minimal version of the SM, where only one Higgs doublet is included and massless
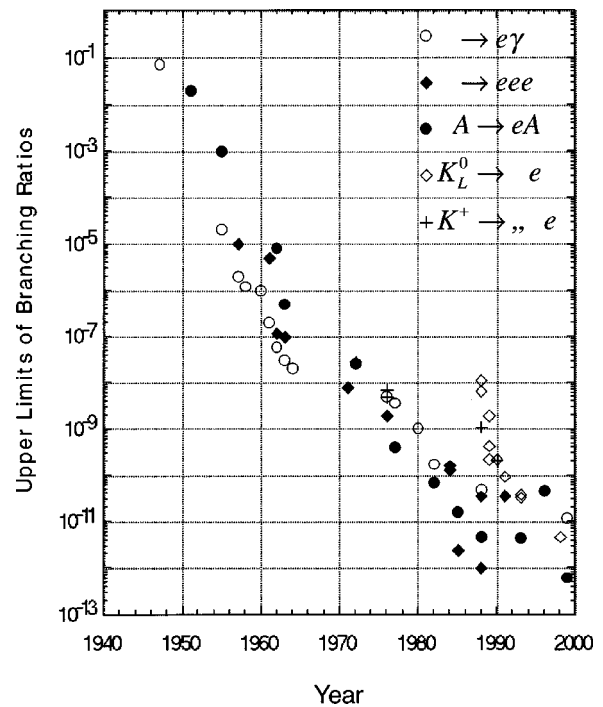
FIG. 1. Historical progress of lepton flavor violation (LFV) searches for various processes of muons and kaons.

neutrinos are assumed, lepton flavor conservation is an automatic consequence of gauge invariance and the renormalizability of the SM Lagrangian. It is the basis of a natural explanation for the smallness of lepton flavor violation (LFV) in charged lepton processes.

However, in extensions of the minimal SM, LFV could occur from various sources. In fact, in many new physics scenarios one would expect LFV at some level. Important LFV processes involving muons are $\mu^+ \to e^+ \gamma$, $\mu^- - e^-$ conversion in a muonic atom ($\mu^- N \to e^- N$), $\mu^+ \to e^+ e^+ e^-$, and muonium to antimuonium conversion (Mu–$\overline{\text{Mu}}$ conversion). The historical progress in various LFV searches in muon and kaon decays is shown in Fig. 1, from which one can see that the experimental upper limits have been continuously improved at a rate of about two orders of magnitude per decade during the 50 years since the first LFV experiment by Hincks and Pontecorvo. The current LFV searches with muons are now sensitive to branching ratios of the order of 10^{-12}–10^{-13}. In general, searches for rare processes could probe new interactions mediated by very heavy particles. For example, in the four-fermion interaction, the LFV branching ratios could be scaled by $(m_W/m_X)^4$, where m_X is the mass of an exotic heavy particle responsible for the LFV interaction and m_W is the mass of the W gauge boson. In such a scenario, the present sensitivities for LFV searches in muon decays could probe m_X up to several hundred TeV, which is not directly accessible at present or planned accelerators.

Recently, considerable interest in LFV processes has arisen based on supersymmetric (SUSY) extensions to the SM, in particular supersymmetric grand unified theories (SUSY GUT). Since the three gauge-coupling constants of the strong, weak, and electromagnetic inter-

actions, which were measured at LEP and SLC, have been shown to be consistent with the assumption that they unify to a single $SU(5)$ gauge-coupling constant at a scale of the order of 10^{16} GeV in SUSY SM, SUSY GUT models have become very attractive candidates for physics beyond the SM. In SUSY models, in general there is a new source of flavor mixing in the mass matrices of SUSY partners for leptons and quarks. This would induce LFV processes for charged leptons whose branching ratios depend on the flavor mixing in the mass matrix of the sleptons, which are the supersymmetric partners of leptons. In the SUSY GUT scenario, the flavor mixing in the slepton sector is naturally induced at the GUT scale because leptons and quarks are in the same GUT multiplet (Hall *et al.*, 1986). It has been shown (Barbieri and Hall, 1994; Barbieri *et al.*, 1995a) that the large top-quark mass has an impact on the calculations of the branching ratios of $\mu^+ \rightarrow e^+ \gamma$ and $\mu^- - e^-$ conversion in SUSY GUT's. The predictions are just one or two orders of magnitude lower than the present experimental limits.

There is considerable evidence for the existence of neutrino masses and mixing based on the experimental results of the solar neutrino deficit (Abdurashitov *et al.*, 1996; Fukuda *et al.*, 1996; Cleveland *et al.*, 1998; Fukuda *et al.*, 1998a; Hampel *et al.*, 1999) and the atmospheric neutrino anomaly (Fukuda *et al.*, 1998b). Since neutrino oscillations indicate that lepton flavor is not conserved, LFV processes in muon decays are also expected to occur. In non-SUSY models, however, the neutrino mixing introduces only small contributions to $\mu^+ \rightarrow e^+ \gamma$. For example, the branching ratio of $\mu^+ \rightarrow e^+ \gamma$ is of the order of 10^{-50} for a neutrino mass-squared difference of $\Delta m_\nu^2 \sim 10^{-3}$ eV^2, due to a suppression factor of $(\Delta m_\nu^2/m_W^2)^2$ (Bilenky *et al.*, 1977; Petcov, 1977). The situation changes drastically in SUSY models. In SUSY models with a neutrino-mass generation mechanism of the see-saw type, the Yukawa coupling constants among the Higgs doublet, lepton doublets, and right-handed neutrinos could induce large flavor-mixing effects in the slepton sector (Borzumati and Masiero, 1986; Hisano, Nomura, and Yanagida, 1998; Hisano and Nomura, 1999). The resulting LFV rates can be as large as (or even exceed) the present experimental upper bounds, depending on the various parameters in question, especially the Majorana mass of the right-handed neutrino. In such a case, the Yukawa coupling constants associated with the right-handed neutrino are responsible for both the neutrino oscillation and the LFV processes of charged leptons.

Thus there are many theoretical scenarios in which the predicted branching ratios for the muon LFV processes can be close to their present experimental upper bounds, and therefore could be accessible to and tested with future experiments.

There has been much progress on the experimental front. First of all, several new results have been obtained using the high-intensity muon beams now available, and ongoing and proposed experiments are aiming for further improvements. Furthermore, in the long term, new attempts to create high-intensity muon sources have been initiated, based on the ideas arising from the $\mu^+ \mu^-$ collider project. The desired muon beam intensity at such a muon source would be about $10^{12} - 10^{13} \mu^\pm/s$, which is several orders of magnitude higher than that presently available. With this increased muon flux, significant improvements in experimental searches can be anticipated.

In this article, we review the current theoretical and experimental status of the field of muon decay and its potential for probing physics beyond the standard model. We particularly stress the importance of rare LFV decays of muons, especially within the framework of SUSY models. In addition, we cover precision measurements of normal muon decay. There have been many excellent review articles on muon decay and lepton flavor violation (Frankel, 1975; Scheck, 1978; Engfer and Walter, 1986; Vergados, 1986; Depommier, 1987; Van der Schaaf, 1993; Depommier and Leroy, 1995), but in order to reflect current renewed interest this article has been written to bring recent topics on muon decay and physics beyond the SM up to date. The phenomenology and experimental status of some of the important muon processes are described in detail.

This article is organized as follows: In Sec. II, we give a short summary of the SM and the muon's properties within the SM. In Sec. III, LFV is discussed in the context of various theoretical models, including SUSY models. Section IV deals with the current status of precision measurements in normal muon decay, such as the muon lifetime, the Michel decay spectrum and its asymmetry, and e^+ polarization. In Sec. V we describe the phenomenology and status of the most recent experiments that search for various lepton-flavor-violating muon decay modes, such as $\mu^+ \rightarrow e^+ \gamma$, $\mu^+ \rightarrow e^+ e^+ e^-$, $\mu^- - e^-$ and $\mu^- - e^+$ conversions in a muonic atom, and Mu–$\overline{\text{Mu}}$ conversion. In Sec. VI, prospects for future experiments and high-intensity muon sources are briefly discussed. Some useful formulas are displayed in the appendixes.

II. BASIC PROPERTIES OF THE MUON IN THE STANDARD MODEL

A. The muon in the standard model

1. The standard model

The current view of elementary particle physics is based on a gauge theory of quarks and leptons. The standard model (SM) postulates three fundamental forces, these being the strong, electromagnetic and weak interactions. They are described by a $SU(3)_C \times SU(2)_L \times U(1)_Y$ gauge theory. Quarks and leptons are classified into three generations. The *up* quark (u), *charm* quark (c), and *top* quark (t) possess 2/3e electric charge, while the *down* quark (d), *strange* quark (s), and *bottom* quark (b) possess $-1/3e$ charge. Correspondingly, there are three leptons with $-e$ electric charge, the electron (e), muon (μ), and tau (τ), and

TABLE I. Quarks and leptons in the standard model.

Electric charge	1st generation	2nd generation	3rd generation
$\frac{2}{3}e$	u	c	t
$-\frac{1}{3}e$	d	s	b
0	ν_e	ν_μ	ν_τ
$-e$	e	μ	τ

their associated neutral partners (neutrinos), ν_e, ν_μ, and ν_τ. These six quarks and six leptons are given in Table I.

In the SM, one introduces the fermionic fields, gauge fields, and a $SU(2)_L$ doublet Higgs field as elementary fields. They are listed along with their quantum numbers in Table II, where the $SU(3)_C$, $SU(2)_L$, and $U(1)_Y$ gauge fields are denoted as G_μ, A_μ, and B_μ, respectively. The subscripts of L and R represent left-handed and right-handed chirality projections [$P_L \equiv (1-\gamma_5)/2$ and $P_R \equiv (1+\gamma_5)/2$], respectively. Here, H represents the Higgs doublet field. The suffix $i(=1-3)$ for the quark and lepton fields is the generation index. The $SU(2)_L$ doublet fields, such as q_{iL}, l_{iL}, and H, have field components given by

$$q_{iL} = \begin{pmatrix} u_{iL} \\ d_{iL} \end{pmatrix}, \quad l_{iL} = \begin{pmatrix} \nu_{iL} \\ e_{iL} \end{pmatrix}, \quad H = \begin{pmatrix} \phi^+ \\ \phi^0 \end{pmatrix}. \tag{1}$$

The SM Lagrangian, $\mathcal{L}_{SM}$, consists of three distinct parts which represent the gauge interaction, the Higgs potential, and the Yukawa interaction. It may be written as

$$\mathcal{L}_{SM} = \mathcal{L}_{gauge} + \mathcal{L}_{Higgs} + \mathcal{L}_{Yukawa}. \tag{2}$$

The Lagrangian for the gauge interaction, $\mathcal{L}_{gauge}$, is given by

$$\mathcal{L}_{gauge} = \sum_{SU(3)_C, SU(2)_L, U(1)_Y} F^{(a)}_{\mu\nu} F^{(a)\mu\nu}$$

$$+ \sum_{quarks, leptons} i\overline{\psi}_{i L(R)} \gamma^\mu \mathcal{D}_\mu \psi_{i_{L(R)}}$$

$$+ |\mathcal{D}_\mu H|^2, \tag{3}$$

where $F_{\mu\nu}$ is the gauge-field strength tensor, and $\mathcal{D}_\mu$ is a covariant derivative defined as

$$\mathcal{D}_\mu = \partial_\mu + ig_s \frac{\lambda^a}{2} G^a_\mu + ig \frac{\tau^a}{2} A^a_\mu + ig' Q_Y B_\mu \tag{4}$$

for the representations with $SU(3)_C$-triplet, $SU(2)_L$-doublet, and Q_Y-$U(1)_Y$ charge quantum numbers. The gauge-coupling constants for $SU(3)_C$, $SU(2)_L$, and $U(1)_Y$ are denoted by g_s, g, and g' respectively. The term λ^a ($a=1-8$) is the Gell-Mann matrix for a $SU(3)$ group, and τ^a ($a=1-3$) is the Pauli matrix for a $SU(2)$ group. The terms for a singlet representation for either the $SU(3)_C$ or $SU(2)_L$ gauge groups are absent in the definition of $\mathcal{D}_\mu$.

The Lagrangian for the Higgs potential, $\mathcal{L}_{Higgs}$, is given by

$$\mathcal{L}_{Higgs} = -(-\mu^2 |H|^2 + \lambda |H|^4). \tag{5}$$

For $\mu^2 > 0$, the Higgs field develops the following vacuum expectation value:

$$\langle H \rangle = \begin{pmatrix} 0 \\ v/\sqrt{2} \end{pmatrix}, \tag{6}$$

where $v = \mu/\sqrt{\lambda}$ ($\cong 246$ GeV). The physical Higgs mass is given by $m_H = \sqrt{2\lambda} v$. After electroweak symmetry breaking, the $SU(2)_L$ and $U(1)_Y$ gauge fields form a massless photon and massive $W^\pm$ and Z^0 bosons. At tree level, their masses are given by $m_W = \frac{1}{2} gv$ and $m_Z = \frac{1}{2}\sqrt{g^2 + g'^2} v$. The $SU(3)$ gauge boson, the gluon, remains massless.

The Yukawa interaction part of the Lagrangian is given by

$$\mathcal{L}_{Yukawa} = (y_e)_{ij} H^\dagger \overline{e}_{iR} l_{jL} + (y_d)_{ij} H^\dagger \overline{d}_{iR} q_{jL}$$

$$+ (y_u)_{ij} \tilde{H}^\dagger \overline{u}_{iR} q_{jL} + \text{H.c.}, \tag{7}$$

where $(y_e)_{ij}$, $(y_d)_{ij}$, and $(y_u)_{ij}$ are the Yukawa coupling constants for the charged leptons, the down-type quarks, and the up-type quarks, respectively; $\tilde{H}$ is given by

$$\tilde{H} = i\tau_2 H^* = \begin{pmatrix} \phi^{0*} \\ -\phi^- \end{pmatrix}. \tag{8}$$

After we substitute the vacuum expectation value for the Higgs field, the Yukawa interaction in Eq. (7) generates the mass terms for quarks and leptons as follows:

$$\mathcal{L}_{mass} = -[\overline{e}_{iR}(m_e)_{ij} e_{jL} + \overline{d}_{iR}(m_d)_{ij} d_{jL}$$

$$+ \overline{u}_{iR}(m_u)_{ij} u_{jL}] + \text{H.c.}, \tag{9}$$

TABLE II. Quantum numbers of elementary fields in the minimal standard model. The $SU(3)_C$, $SU(2)_L$ representation, and $U(1)_Y$ charge are given.

	G_μ	A_μ	B_μ	q_{iL}	u_{iR}	d_{iR}	l_{iL}	e_{iR}	H
$SU(3)_C$	8	1	1	3	3	3	1	1	1
$SU(2)_L$	1	3	1	2	1	1	2	1	2
$U(1)_Y$	0	0	0	$\frac{1}{6}$	$\frac{2}{3}$	$-\frac{1}{3}$	$-\frac{1}{2}$	-1	$\frac{1}{2}$

TABLE III. Assignment of lepton number for the electron (L_e), the muon (L_μ), and the tau (L_τ).

	e^-	ν_e	μ^-	ν_μ	τ^-	ν_τ	e^+	$\overline{\nu_e}$	μ^+	$\overline{\nu_\mu}$	τ^+	$\overline{\nu_\tau}$
L_e	+1	+1	0	0	0	0	−1	−1	0	0	0	0
L_μ	0	0	+1	+1	0	0	0	0	−1	−1	0	0
L_τ	0	0	0	0	+1	+1	0	0	0	0	−1	−1

where $(m_e)_{ij} = -(y_e)_{ij}(v/\sqrt{2})$, $(m_d)_{ij} = -(y_d)_{ij}(v/\sqrt{2})$, and $(m_u)_{ij} = -(y_u)_{ij}(v/\sqrt{2})$. Each mass matrix is diagonalized by unitary transformations for the left-handed fermions and the right-handed fermions with the same charge. Since the unitary matrices for the left-handed up-type quark and the left-handed down-type quark are generally different, flavor mixing is induced in the charged weak-current interaction for quarks. It is given by

$$\mathcal{L}_{W\bar{q}q} = -\frac{g}{\sqrt{2}}[\overline{u}_{iL}\gamma^\mu(V_{CKM})_{ij}d_{jL}W_\mu^+$$
$$+\overline{d}_{iL}\gamma^\mu(V_{CKM})_{ji}^* u_{jL}W_\mu^-], \tag{10}$$

where $(V_{CKM})_{ij}$ represents the flavor mixing matrix for the quark sector, i.e., the Cabibbo-Kobayashi-Maskawa matrix (Kobayashi and Maskawa, 1973). In the above equation, the quark fields are written in the mass-eigenstate basis, and this will be our convention from now on.

On the other hand, the charged-lepton mass matrix in Eq. (9), which is proportional to the lepton Yukawa coupling-constant matrix, is fully diagonalized by unitary transformations on the lepton doublet fields (l_{iL}) and the lepton singlet fields (e_{jR}). In the mass-eigenstate basis, the charged weak-current interaction for leptons remains diagonal as follows:

$$\mathcal{L}_{W\bar{\nu}e} = -\frac{g}{\sqrt{2}}(\overline{\nu}_i L\gamma^\mu e_{iL}W_\mu^+ + \overline{e}_{iL}\gamma^\mu\nu_{iL}W_\mu^-). \tag{11}$$

In the above basis, separate lepton numbers can be defined for each generation, and are thus conserved. They are the electron number (L_e), the muon number (L_μ), and the tau number (L_τ), as defined in Table III.

2. Interactions of the muon in the standard model

At tree level in the SM Lagrangian, the muon interacts with the gauge bosons (the photon and $W^\pm$ and Z^0 bosons) and with the Higgs boson. These interactions may be written as follows:

$$\mathcal{L} = e\overline{\mu}\gamma^\mu\mu A_\mu - \frac{g}{\sqrt{2}}(\overline{\nu_{\mu_L}}\gamma^\mu\mu_L W_\mu^+ + \overline{\mu_L}\gamma^\mu\nu_{\mu L}W_\mu^-)$$
$$-\sqrt{g^2+g'^2}\left\{\overline{\mu_L}\gamma^\mu\left(-\frac{1}{2}+\sin^2\theta_W\right)\mu_L\right.$$
$$+\overline{\mu_R}\gamma^\mu\sin^2\theta_W\mu_R\left.\right\}Z_\mu^0 - \frac{m_\mu}{v}\overline{\mu}\mu H, \tag{12}$$

where the Weinberg angle θ_W is defined by $\sin\theta_W \equiv g'/\sqrt{g^2+g'^2}$, and $e = g\sin\theta_W$ at tree level. Moreover, H denotes the physical Higgs boson field. Here the first term represents the electromagnetic interaction and the second term describes the charged weak-current interaction mediated by the $W^\pm$ boson, while the third term describes neutral weak-current interaction mediated by the Z^0 boson. The other charged leptons, the electron and tau, have identical gauge interactions as the muon while their coupling to the Higgs boson is proportional to the respective lepton mass.

Muon decay in the SM is described by a charged weak-current interaction mediated by the $W^\pm$ gauge boson. The four-fermion interaction is given by

$$\mathcal{L}_{Fermi} = -\frac{G_F}{\sqrt{2}}[\overline{\nu_\mu}\gamma^\mu(1-\gamma_5)\mu\overline{e}\gamma_\mu(1-\gamma_5)\nu_e$$
$$+\overline{\nu_e}\gamma^\mu(1-\gamma_5)e\overline{\mu}\gamma_\mu(1-\gamma_5)\nu_\mu], \tag{13}$$

where G_F is the Fermi coupling constant. At tree level in the SM, this is given by

$$G_F = \frac{g^2}{4\sqrt{2}m_W^2}, \tag{14}$$

where m_W is the $W^\pm$ boson mass. This interaction describes the standard muon decays $\mu^+ \to e^+\nu_e\overline{\nu}_\mu$ and $\mu^- \to e^-\overline{\nu}_e\nu_\mu$.

Lepton universality is a fundamental property of the gauge interaction. The universality in charged weak currents has been tested from the combination of leptonic and semileptonic decays of τ, and leptonic decays of μ, π, and K mesons, whereas that in neutral weak currents has been tested at the Z^0 boson pole (Pich, 1997).

3. Neutrino mass and mixing

Although the minimal SM does not permit massive neutrinos, there is increasing evidence of their mass from the solar neutrino deficit (Abdurashitov et al., 1996; Fukuda et al., 1996; Cleveland et al., 1998; Fukuda et al., 1998a; Hampel et al., 1999) and the atmospheric neutrino anomaly (Fukuda et al., 1998b). If the solar neutrino deficit is due to neutrino oscillations, the mass-squared difference must be in the range of $\Delta m_\nu^2 \approx 10^{-6}-10^{-5}$ eV^2 for the Mikheyev-Smirnov-Wolfenstein solution (Wolfenstein, 1978; Mikheyev and Smirnov, 1985) or $\Delta m_\nu^2 \approx 10^{-11}$ eV^2 for the vacuum oscillation solution (or "just-so" oscillation; Glashow and Krauss, 1987; Glashow et al., 1999). Moreover, the atmospheric neutrino anomaly suggests that the mass-squared difference between the muon neutrino and the

tau (or a sterile) neutrino is of the order of $\Delta m_\nu^2 \approx 10^{-3}–10^{-2}$ eV^2 (Fukuda *et al.*, 1988b). In addition, the LSND (liquid scintillator neutrino detector) experiment has reported the oscillation $\bar{\nu}_\mu(\nu_\mu) \to \bar{\nu}_e(\nu_e)$, suggesting $|m_{\nu_\mu}^2 - m_{\nu_e}^2| \approx 10^{-1}–10^0$ eV^2 (Athanassopoulos *et al.*, 1998), although this has not been confirmed by the KARMEN experiment (Eitel *et al.*, 1999). If neutrino mixing is the correct interpretation of the anomalies, then the SM must be extended. On the other hand, there are direct upper bounds on the neutrino mass for each species: 15 eV/c^2 for the electron neutrino, 170 keV/c^2 for the muon neutrino, and 18.2 MeV/c^2 for the tau neutrino (Caso *et al.*, 1998). Recently, improved measurements of the electron neutrino mass have been reported with superior sensitivities of the order of a few eV/c^2 (Lobashev, 1998; Otten and Weinheimer, 1998).

It is possible to accommodate the Dirac mass terms for the neutrinos if $SU(2)$ singlet fields of the right-handed neutrinos ν_{iR} ($i=1–3$) are added to the minimal SM field content. Then, the following interaction can be added to Eq. (7):

$$\mathcal{L}_{\nu_R} = (y_\nu)_{ij} \tilde{H}^\dagger \overline{\nu}_{iR} l_{jL} + \text{H.c.,} \tag{15}$$

where $(y_\nu)_{ij}$ is the Yukawa coupling for neutrinos. If $(y_\nu)_{ij}$ is very small, the small masses of neutrinos can be explained. For example, the Yukawa coupling constant should be $O(10^{-11})$ for a neutrino mass of 1 eV/c^2. Note that total lepton number is conserved in this scenario, whereas the conservation of lepton flavors could be violated in general.

A more natural explanation for the small neutrino masses is provided by the "see-saw mechanism" (Gell-Mann *et al.*, 1979; Yanagida, 1979). In this scenario, the Majorana mass term is also included for the right-handed neutrino,

$$\mathcal{L}_{\nu_R} = (y_\nu)_{ij} \tilde{H}^\dagger \overline{\nu}_{iR} l_{jL} - \frac{1}{2} \overline{\nu}_{iR} (M_R)_{ij} \nu_{jR}^c + \text{H.c.,} \tag{16}$$

where the charge-conjugation field is defined as $\bar{\psi}^c = -\psi^T C^{-1}$ and the charge-conjugation matrix (C) satisfies $C^{-1}\gamma^\mu C = -\gamma^{\mu T}$. $(M_R)_{ij}$ is the right-handed Majorana neutrino matrix. Substituting the vacuum expectation value for the Higgs field, the neutrino mass terms become

$$\mathcal{L}_{\nu \, mass} = -\frac{1}{2} [\overline{(\nu_{iL})^c}, \ \overline{\nu}_{iR}] \begin{pmatrix} 0 & m_D^T \\ m_D & M_R \end{pmatrix} \begin{pmatrix} \nu_{jL} \\ (\nu_{jR})^c \end{pmatrix}$$
$$+ \text{H.c.,} \tag{17}$$

where the Dirac mass term is $(m_D)_{ij} = -(y_\nu)_{ij}(v/\sqrt{2})$. When the Majorana mass scale is much larger than the Dirac masses, the lighter neutrino masses are given by

$$\mathcal{L}_{\nu \, mass} \approx -\frac{1}{2} \overline{(\nu_{iL})^c} (m_\nu)_{ij} \nu_{jL} + \text{H.c.} \tag{18}$$

and

$$m_\nu = -m_D^T (M_R)^{-1} m_D. \tag{19}$$

For example, if M_R is 10^{15} GeV and the Dirac mass is of the order 100 GeV, then the neutrino mass naturally becomes $O(10^{-2})$ eV.

After diagonalization of the charged lepton and neutrino mass matrices, lepton flavor mixing is induced in the charged weak-current interaction, as follows:

$$\mathcal{L}_{W\nu e} = -\frac{g}{\sqrt{2}} [\overline{\nu}_{iL} \gamma^\mu (V_{MNS})_{ji}^* e_{jL} W_\mu^+$$
$$+ \overline{e}_{iL} \gamma^\mu (V_{MNS})_{ij} \nu_{jL} W_\mu^-], \tag{20}$$

where $(V_{MNS})_{ij}$ is the flavor mixing matrix for the lepton sector, i.e., the Maki-Nakagawa-Sakata matrix (Maki *et al.*, 1962). Note that as in the case of quarks, the lepton fields in Eq. (20) are written in the mass eigenstate basis. The $(V_{MNS})_{ij}$ matrix element represents neutrino mixing, which gives rise to neutrino oscillations. For a review of the field of neutrino masses and mixing, we refer the reader elsewhere (Bilenky and Petcov, 1987; Fukugita and Yanagida, 1994; Mohapatra and Pal, 1998; Fisher, Kayser, and McFarland, 1999).

B. Static properties of the muon

1. Mass and lifetime

The mass and lifetime of the muon are the fundamental input parameters of the SM. The muon mass is (Caso *et al.*, 1998)

$$m_\mu = 106.658\,389(34) \text{ MeV.} \tag{21}$$

It is derived from the ratio of the muon mass to the electron mass, m_μ/m_e, which is measured in a muonium ($\mu^+ e^-$) atom taking into account QED corrections (Cohen and Taylor, 1987).

The experimental value of the muon lifetime is

$$\tau_\mu = 2.197\,03(4) \times 10^{-6} \text{ s.} \tag{22}$$

In the framework of the SM with QED corrections, the muon lifetime (τ_μ) is related to the Fermi coupling constant (G_F) as follows (Kinoshita and Sirlin, 1959b; Marciano and Sirlin, 1988):

$$\tau_\mu^{-1} = \frac{G_F^2 m_\mu^5}{192\pi^3} F\left(\frac{m_e^2}{m_\mu^2}\right) \left(1 + \frac{3}{5} \frac{m_\mu^2}{m_W^2}\right)$$
$$\times \left[1 + \frac{\alpha(m_\mu)}{2\pi} \left(\frac{25}{4} - \pi^2\right)\right], \tag{23}$$

where $F(x) = 1 - 8x + 8x^3 - x^4 - 12x^2 \ln x$, and m_μ and m_e are the masses of the muon and the electron, respectively. The value of α at the scale m_μ, denoted by $\alpha(m_\mu)$, turns out to be

$$\alpha(m_\mu)^{-1} = \alpha^{-1} - \frac{2}{3\pi} \ln\left(\frac{m_\mu}{m_e}\right) + \frac{1}{6\pi} \approx 136. \tag{24}$$

From Eq. (23), the Fermi coupling constant is determined and has the value $G_F = 1.166\,39(1) \times 10^{-5}$ GeV^{-2} (Caso *et al.*, 1998). The higher-order two-loop corrections to the muon lifetime have recently been calculated (van Ritbergen and Stuart, 1999).

TABLE IV. Decay modes of muons.

Decay mode	Branching ratio	References
$\mu^-\rightarrow e^-\bar{\nu}_e\nu_\mu$	$\sim100\%$	
$\mu^-\rightarrow e^-\bar{\nu}_e\nu_\mu\gamma$	$1.4\pm0.4\%$ (for $E_\gamma>10\,\mathrm{MeV}$)	Crittenden *et al.* (1961)
$\mu^-\rightarrow e^-\bar{\nu}_e\nu_\mu e^+e^-$	$(3.4\pm0.4)\times10^{-5}$	Bertl *et al.* (1985)
$\mu^-\rightarrow e^-\nu_e\bar{\nu}_\mu$	$<1.2\%$	Freedman *et al.* (1993)
$\mu^-\rightarrow e^-\gamma$	$<1.2\times10^{-11}$	Brooks *et al.* (1999)
$\mu^-\rightarrow e^-e^-e^+$	$<1.0\times10^{-12}$	Bellgardt *et al.* (1988)
$\mu^-\rightarrow e^-\gamma\gamma$	$<7.2\times10^{-11}$	Bolton *et al.* (1988)

2. Magnetic moment

Since the muon is a Dirac particle, the g factor of its magnetic moment is 2, if radiative corrections are neglected. A deviation from 2, namely $g-2\neq0$, is very important for investigating quantum corrections. The present experimental value of $a_\mu=(g_\mu-2)/2$ is given by (Caso *et al.*, 1998)

$$a_\mu^{exp}=11\,659\,230(84)\times10^{-10} \quad (\pm7\,\mathrm{ppm}). \tag{25}$$

A new experiment, E821, is currently in progress at BNL and aims to reduce the above experimental error by a factor of 20. The result from the first run gives $a_\mu^{exp}=1\,165\,925(15)\times10^{-9}$ ($\pm13\,\mathrm{ppm}$; Carey *et al.*, 1999a).

Theoretically, this quantity is known very precisely (Hughes and Kinoshita, 1999). The correction is divided into higher-order QED corrections, hadronic contributions, and electroweak contributions. A recent update of theoretical calculations gives (Czarnecki and Marciano, 1999)

$$a_\mu^{QED}=11\,658\,470.56(0.29)\times10^{-10}, \tag{26}$$

$$a_\mu^{hadron}=673.9(6.7)\times10^{-10}, \tag{27}$$

$$a_\mu^{EW}=15.1(0.4)\times10^{-10}. \tag{28}$$

By adding the above contributions, the SM prediction is

$$a_\mu^{SM}=a_\mu^{QED}+a_\mu^{hadron}+a_\mu^{EW}$$
$$=11\,659\,159.6(6.7)\times10^{-10}. \tag{29}$$

The theoretical prediction is in good agreement with the experimental value.

To calculate the QED correction, the fine-structure constant is needed as an input parameter. Equation (26) was estimated by using the fine-structure constant obtained from the quantum Hall effect, which gives $\alpha^{-1}(qH)=137.036\,003\,70(270)$. It is consistent with the value determined from the electron anomalous magnetic moments (a_e) by assuming a theoretical evaluation based on the SM. One obtains $\alpha^{-1}(a_e)=137.035\,999\,59(38)$, and the experimental values of the electron anomalous magnetic moments are $a_{e^-}^{exp}=1\,159\,652\,188.4(4.3)\times10^{-12}$ and $a_{e^+}^{exp}=1\,159\,652\,187.9(4.3)\times10^{-12}$.

Although the electron $g-2$ factor is experimentally measured with more accuracy than the muon $g-2$ factor, the latter is much more sensitive to short-distance physics. For example, the electroweak correction of a_μ^{EW} quoted in Eq. (28) is much larger than a_e^{EW}, which is $O(10^{-14})$. Moreover, in SUSY models, the muon $g-2$ factor receives a significant contribution if the slepton, charginos, and neutralinos possess masses of the order of a few hundred GeV (Lopez *et al.*, 1994; Chattopadhyay and Nath, 1996; Moroi, 1996; Carena *et al.*, 1997; Gabrielli and Sarid, 1997). Therefore the ongoing experiment E821 is expected to put very strong constraints on SUSY models.

C. Decay modes of the muon

The measured decay modes of muons are $\mu^-\rightarrow e^-\bar{\nu}_e\nu_\mu$ (Michel decay), $\mu^-\rightarrow e^-\bar{\nu}_e\nu_\mu\gamma$ (radiative muon decay), and $\mu^-\rightarrow e^-\bar{\nu}_e\nu_\mu e^+e^-$. The branching ratios for these modes and the upper bounds on other exotic decay modes at 90% confidence level are summarized in Table IV. Although these branching fractions have been measured in experiments with positive muon decays, they are listed for negative muons by assuming CP invariance. Since $\mu^-\rightarrow e^-\bar{\nu}_e\nu_\mu\gamma$ cannot be clearly separated from $\mu^-\rightarrow e^-\bar{\nu}_e\nu_\mu$ with a soft photon, the branching ratio for the radiative decay is shown for $E_\gamma>10\,\mathrm{MeV}$. There is no evidence of lepton-flavor-violating processes such as $\mu^-\rightarrow e^-\gamma$, $\mu^-\rightarrow e^-e^-e^+$, or $\mu^-\rightarrow e^-\gamma\gamma$. Moreover, an upper bound is set for those with $|\Delta L_i|=2$, such as $\mu^-\rightarrow e^-\nu_e\bar{\nu}_\mu$ decay, which is allowed if the lepton flavor number is conserved multiplicatively instead of additively.

1. Normal muon decay

In the SM, muon decay is described by the $V-A$ interaction. In extensions of the SM, any new interactions of the muon would affect observables such as the energy spectrum of a decay positron (electron), its angular distribution if muons are polarized, and its spin polarization in $\mu^+\rightarrow e^+\nu_e\bar{\nu}_\mu$ (or $\mu^-\rightarrow e^-\bar{\nu}_e\nu_\mu$). If general four-fermion interactions with no derivatives are assumed, the muon differential decay rate is given by (Fetscher and Gerber, 1998)

$$\frac{d^2\Gamma(\mu^\pm\rightarrow e^\pm\nu\bar{\nu})}{dx\,d\cos\theta_e}=\frac{m_\mu}{4\pi^3}W_{e\mu}^4G_F^2\sqrt{x^2-x_0^2}$$
$$\times(F_{IS}(x)\pm P_\mu\cos\theta_e F_{AS}(x))$$
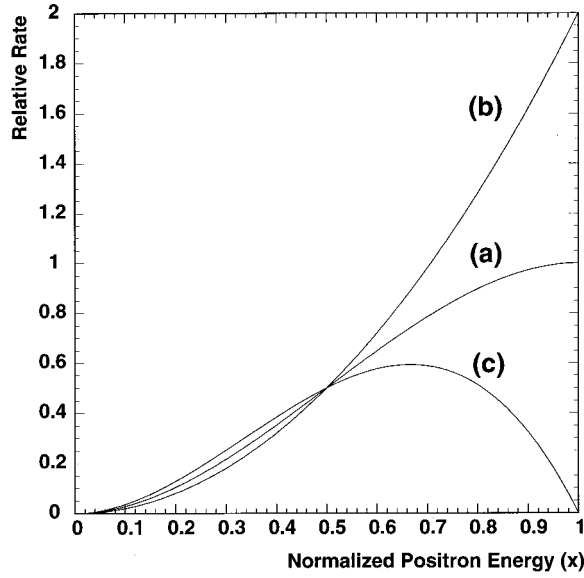$$\times[1+\vec{P}_e(x,\theta_e)\cdot\hat{\zeta}], \tag{30}$$

FIG. 2. Michel e^+ energy spectrum of polarized $\mu^+ \rightarrow e^+ \nu_e \bar{\nu}_\mu$ decay with 100% muon polarization ($P_\mu = 1$): (a) $\cos \theta_e = 0$; (b) $\cos \theta_e = 1$; and (c) $\cos \theta_e = -1$.

where $W_{e\mu} = (m_\mu^2 + m_e^2)/(2m_\mu)$, $x = E_e/W_{e\mu}$, and $x_0 = m_e/W_{e\mu} (= 9.7 \times 10^{-3}) \leqslant x \leqslant 1$. Here E_e is the energy of the $e^\pm$, while m_e and m_μ are the masses of the $e^\pm$ and the $\mu^\pm$, respectively. The plus (minus) sign in Eq. (30) corresponds to $\mu^+ (\mu^-)$ decay, θ_e is the angle between the muon polarization ($\vec{P}_\mu$) and the $e^\pm$ momentum, and $\hat{\zeta}$ is the directional vector of the measurement of the $e^\pm$ spin polarization. Moreover, $\vec{P}_e(x, \theta_e)$ is the polarization vector of the $e^\pm$. The functions $F_{IS}(x)$ and $F_{AS}(x)$ are, respectively, the isotropic and anisotropic parts of the $e^\pm$ energy spectrum. They are given by

$$F_{IS}(x) = x(1-x) + \frac{2}{9}\rho(4x^2 - 3x - x_0^2) + \eta x_0(1-x),$$
(31)

$$F_{AS}(x) = \frac{1}{3}\xi\sqrt{x^2 - x_0^2}\left(1 - x + \frac{2}{3}\delta[4x - 3\right.$$

$$\left. + (\sqrt{1 - x_0^2} - 1)]\right),$$
(32)

where ρ, η, ξ, and δ are called Michel parameters (Michel, 1950; Bouchiat and Michel, 1957).

In the SM, these parameters take the values $\rho = \frac{3}{4}$, $\eta = 0$, $\xi = 1$, and $\delta = \frac{3}{4}$. If the positron (electron) polarization is not measured and x_0 is neglected, the differential branching ratio in the SM in Eq. (30) leads to the simpler form of

$$\frac{d^2\Gamma(\mu^\pm \rightarrow e^\pm \nu \bar{\nu})}{dx \, d\cos\theta_e} = \frac{m_\mu^5 G_F^2}{192\pi^3} x^2 [(3 - 2x)$$

$$\pm P_\mu \cos\theta_e(2x - 1)].$$
(33)

Figure 2 shows the e^+ energy spectrum for $\mu^+ \rightarrow e^+ \nu_e \bar{\nu}_\mu$ decay in the SM, for the cases of $\cos\theta_e = 0$, $\cos\theta_e = +1$, and $\cos\theta_e = -1$ with 100% polarized positive

muons. As can be seen, the spectrum is high at $x \approx 1$, and the sign of the $e^\pm$ asymmetry changes at $x = 1/2$.

If the SM is not assumed, the muon lifetime in Eq. (23) should be replaced by (Scheck, 1978; Fetscher and Gerber, 1995; Pich and Silva, 1995)

$$\tau_\mu^{-1} = \frac{G_F^2 m_\mu^5}{192\pi^3}\left[F\left(\frac{m_e^2}{m_\mu^2}\right) + 4\eta\frac{m_e}{m_\mu}G\left(\frac{m_e^2}{m_\mu^2}\right)\right.$$

$$- \frac{32}{3}\left(\rho - \frac{3}{4}\right)\frac{m_e^2}{m_\mu^2}\left(1 - \frac{m_e^4}{m_\mu^4}\right)\right]$$

$$\times \left(1 + \frac{3}{5}\frac{m_\mu^2}{m_W^2}\right)\left[1 + \frac{\alpha(m_\mu)}{2\pi}\left(\frac{25}{4} - \pi^2\right)\right],$$
(34)

where $G(x) = 1 + 9x - 9x^2 - x^3 + 6x(1+x)\ln x$. Radiative corrections based on the SM [in Eq. (23)] are used, since it can be assumed that the SM contribution dominates in the normal muon decay process. From Eq. (34), we see that the correction from the η parameter is proportional to $O(m_e/m_\mu)$, whereas that from the ρ parameter is very small, being of the order of $O(m_e^2/m_\mu^2)$. Since the η parameter is presently measured with an accuracy of around 1%, the uncertainty from the η correction introduces an uncertainty of the order of 10^{-4} to the estimation of the muon lifetime in the non-SM case.

If the spin polarization of $e^+ (e^-)$ in the $\mu^+ \rightarrow e^+ \nu_e \bar{\nu}_\mu$ ($\mu^- \rightarrow e^- \nu_\mu \bar{\nu}_e$) decay is detected, $\vec{P}_e(x, \theta_e)$ in Eq. (30) can be measured. It is given by

$$\vec{P}_e(x, \theta_e) = P_{T1} \cdot \frac{(\vec{z} \times \vec{P}_\mu) \times \vec{z}}{|(\vec{z} \times \vec{P}_\mu) \times \vec{z}|}$$

$$+ P_{T2} \cdot \frac{\vec{z} \times \vec{P}_\mu}{|\vec{z} \times \vec{P}_\mu|} + P_L \cdot \frac{\vec{z}}{|\vec{z}|},$$
(35)

where $\vec{z}$ is the direction of the $e^\pm$ momentum, and $\vec{P}_\mu$ is the muon spin polarization. The terms P_L, P_{T1}, and P_{T2} are, respectively, the $e^\pm$ polarization component parallel to the $e^\pm$ momentum direction, that transverse to the $e^\pm$ momentum within the decay plane, and that transverse to the $e^\pm$ momentum and normal to the decay plane. They are given by

$$P_{T1}(x, \theta_e) = \frac{P_\mu \sin\theta_e F_{T1}(x)}{F_{IS}(x) \pm P_\mu \cos\theta_e F_{AS}(x)},$$
(36)

$$P_{T2}(x, \theta_e) = \frac{P_\mu \sin\theta_e F_{T2}(x)}{F_{IS}(x) \pm P_\mu \cos\theta_e F_{AS}(x)},$$
(37)

$$P_L(x, \theta_e) = \frac{\pm F_{IP}(x) + P_\mu \cos\theta_e F_{AP}(x)}{F_{IS}(x) \pm P_\mu \cos\theta_e F_{AS}(x)},$$
(38)

where the $\pm$ sign corresponds to $\mu^\pm$ decays, and

$$F_{T1}(x) = \frac{1}{12}\left\{-2\left[\xi'' + 12\left(\rho - \frac{3}{4}\right)\right](1-x)x_0\right.$$

$$\left. - 3\eta(x^2 - x_0^2) + \eta''(-3x^2 + 4x - x_0^2)\right\},$$
(39)

TABLE V. Experimental values of some of the Michel decay parameters.

Michel parameter	SM value	Experimental value	Sensitive observables
ρ	3/4	0.7518 ± 0.0026	F_{IS}
η	0	-0.007 ± 0.013	F_{IS} and P_{T1}
δ	3/4	0.7486 ± 0.0038	F_{AS} and P_L
ξ	1	1.0027 ± 0.0084	F_{AS}[a] and P_L
ξ'	1	1.00 ± 0.04	P_L
ξ''	1	0.65 ± 0.36	P_L

[a]Only the product of ξP_μ is measured.

$$F_{T2}(x) = \frac{1}{3}\sqrt{x^2 - x_0^2}\left\{3\frac{\alpha'}{A}(1-x) + 2\frac{\beta'}{A}\sqrt{1-x_0^2}\right\}, \tag{40}$$

$$F_{IP}(x) = \frac{1}{54}\sqrt{x^2 - x_0^2}\left\{9\xi'(-2x + 2 + \sqrt{1-x_0^2}) + 4\xi\left(\delta - \frac{3}{4}\right)(4x - 4 + \sqrt{1-x_0^2})\right\}, \tag{41}$$

$$F_{AP}(x) = \frac{1}{6}\left\{\xi''(2x^2 - x - x_0^2) + 4\left(\rho - \frac{3}{4}\right)(4x^2 - 3x - x_0^2) + 2\eta''(1-x)x_0\right\}, \tag{42}$$

where ξ', ξ'', η'', (α'/A), and (β'/A) are newly defined Michel parameters (Kinoshita and Sirlin, 1957; Fetscher and Gerber, 1998). A nonzero value of the triple T-odd correction, P_{T2}, would imply violation of time-reversal invariance. In the SM, $\xi' = \xi'' = 1$ and $\eta'' = (\alpha'/A) = (\beta'/A) = 0$.

The muon-decay Lagrangian for the general four-fermion couplings with ten complex parameters is expressed as (Fetscher *et al.*, 1986)

$$\mathcal{L}_{\mu \to e\nu\bar{\nu}} = -\frac{4G_F}{\sqrt{2}}\left[g_{RR}^S(\bar{e}_R\nu_{eL})(\overline{\nu_{\mu L}}\mu_R) + g_{RL}^S(\bar{e}_R\nu_{eL})(\overline{\nu_{\mu R}}\mu_L) + g_{LR}^S(\bar{e}_L\nu_{eR})(\overline{\nu_{\mu L}}\mu_R) + g_{LL}^S(\bar{e}_L\nu_{eR})(\overline{\nu_{\mu R}}\mu_L)\right.$$

$$+ g_{RR}^V(\bar{e}_R\gamma^\mu\nu_{eR})(\overline{\nu_{\mu R}}\gamma_\mu\mu_R) + g_{RL}^V(\bar{e}_R\gamma^\mu\nu_{eR})(\overline{\nu_{\mu L}}\gamma_\mu\mu_L) + g_{LR}^V(\bar{e}_L\gamma^\mu\nu_{eL})(\overline{\nu_{\mu R}}\gamma_\mu\mu_R) + g_{LL}^V(\bar{e}_L\gamma^\mu\nu_{eL})$$

$$\times(\overline{\nu_{\mu L}}\gamma_\mu\mu_L) + \frac{g_{RL}^T}{2}(\bar{e}_R\sigma^{\mu\nu}\nu_{eL})(\overline{\nu_{\mu R}}\sigma_{\mu\nu}\mu_L) + \frac{g_{LR}^T}{2}(\bar{e}_L\sigma^{\mu\nu}\nu_{eR})(\overline{\nu_{\mu L}}\sigma_{\mu\nu}\mu_R) + \text{H.c.}\right], \tag{43}$$

where there is a normalization condition of

$$\frac{1}{4}(|g_{RR}^S|^2 + |g_{LL}^S|^2 + |g_{RL}^S|^2 + |g_{LR}^S|^2) + (|g_{RR}^V|^2 + |g_{LL}^V|^2$$
$$+ |g_{RL}^V|^2 + |g_{LR}^V|^2) + 3(|g_{RL}^T|^2 + |g_{LR}^T|^2) = 1. \tag{44}$$

Note that in the $V-A$ interaction of the SM, $g_{LL}^V = 1$ and the remainder is zero.

The Michel decay parameters of ρ, η, ξ, and δ are given by

$$\rho = \frac{3}{4} - \frac{3}{4}[|g_{LR}^V|^2 + |g_{RL}^V|^2 + 2|g_{LR}^T|^2 + 2|g_{RL}^T|^2$$
$$+ \text{Re}(g_{RL}^S g_{RL}^{T*} + g_{LR}^S g_{LR}^{T*})], \tag{45}$$

$$\eta = \frac{1}{2}\text{Re}[g_{RR}^V g_{LL}^{S*} + g_{LL}^V g_{RR}^{S*} + g_{RL}^V(g_{LR}^{S*} + 6g_{LR}^{T*})$$
$$+ g_{LR}^V(g_{RL}^{S*} + 6g_{RL}^{T*})], \tag{46}$$

$$\xi = 1 - \left[\frac{1}{2}|g_{RR}^S|^2 + \frac{1}{2}|g_{LR}^S|^2 + 2|g_{RR}^V|^2 + 4|g_{RL}^V|^2\right.$$
$$- 2|g_{LR}^V|^2 - 2|g_{RL}^T|^2 + 8|g_{RL}^T|^2$$
$$\left. + 4\,\text{Re}(g_{RL}^S g_{RL}^{T*} - g_{LR}^S g_{LR}^{T*})\right], \tag{47}$$

$$\xi\delta = \frac{3}{4} - \frac{3}{4}\left[|g_{LR}^V|^2 + |g_{RL}^V|^2 + 4|g_{LR}^T|^2 + 2|g_{RL}^T|^2\right.$$
$$+ 2|g_{RR}^V|^2 + \frac{1}{2}|g_{RR}^S|^2 + \frac{1}{2}|g_{LR}^S|^2$$
$$\left. + \text{Re}(g_{RL}^S g_{RL}^{T*} - g_{LR}^S g_{LR}^{T*})\right]. \tag{48}$$

Table V summarizes the present knowledge of the Michel decay parameters (Caso *et al.*, 1998). More precise measurements would place constraints on various new physics contributions, which would induce small deviations from the $V-A$ couplings. The current constraints on the general four-fermion couplings are summarized in Fetscher and Gerber (1998).

2. Radiative muon decay

The spectrum of the radiative muon decay, $\mu^{\pm} \rightarrow e^{\pm} \nu \bar{\nu} \gamma$, has been calculated by several authors (Kinoshita and Sirlin, 1959a; Eckstein and Pratt, 1959; Fronsdal and Überall, 1959). Within the framework of the $V-A$ interaction, the differential branching ratio of the radiative muon decay, where the final positron (electron) and photon are emitted at energy intervals of dx and dy with solid angles of $d\Omega_e$ and $d\Omega_{\gamma}$, respectively, in the muon rest frame, is expressed by

$$dB(\mu^{\pm} \rightarrow e^{\pm} \nu \bar{\nu} \gamma) = \frac{\alpha}{64\pi^3} \beta \, dx \, \frac{dy}{y} d\Omega_e \, d\Omega_{\gamma} [F(x,y,d)$$

$$\mp \beta \vec{P}_{\mu} \cdot \hat{p}_e G(x,y,d)$$

$$\mp \vec{P}_{\mu} \cdot \hat{p}_{\gamma} H(x,y,d)]. \tag{49}$$

Here $\vec{P}_{\mu}$ is the muon polarization vector; $\vec{p}_e$ and $\vec{p}_{\gamma}$ are the momenta of the positron (electron) and the photon in the muon rest frame, respectively; $\hat{p}_e$ and $\hat{p}_{\gamma}$ are their unit vectors defined by $\hat{p}_e \equiv \vec{p}_e / |\vec{p}_e|$ and $\hat{p}_{\gamma} \equiv \vec{p}_{\gamma} / |\vec{p}_{\gamma}|$, respectively; β is defined as $\beta \equiv |\vec{p}_e| / E_e$; d is given by $d \equiv 1 - \beta \hat{p}_e \cdot \hat{p}_{\gamma}$; and x and y are normalized positron (electron) and photon energies, $x = 2E_e / m_{\mu}$ and $y = 2E_{\gamma} / m_{\mu}$ in the muon rest frame. From the four-body kinematics, the allowed ranges of x and y are given by

$$2\sqrt{r} < x < 1 + r \quad \text{for} \quad 0 < y \leqslant 1 - \sqrt{r},$$

$$(1-y) + r/(1-y) \leqslant x \leqslant 1 + r \quad \text{for} \quad 1 - \sqrt{r} < y \leqslant 1 - r, \tag{50}$$

where $r = (m_e / m_{\mu})^2$. $F(x,y,d)$, $G(x,y,d)$, and $H(x,y,d)$ in the SM are given in Appendix A.

The decay probability distribution is high for an energetic $e^{\pm}$ with a soft photon, namely $x \approx 1$ and $y \approx 0$. In the soft-photon limit ($y \rightarrow 0$), the distribution has an infrared singularity which is canceled by the radiative correction of the Michel decay.

The photon spectrum is obtained by integrating over the positron (electron) energy and angle variables. By neglecting the terms suppressed by m_e / m_{μ}, the differential branching ratio is given by (Kuno et al., 1997)

$$\frac{dB(\mu^{\pm} \rightarrow e^{\pm} \nu \bar{\nu} \gamma)}{dy \, d\cos\theta_{\gamma}} = \frac{1}{y} [J_+(y)(1 \pm P_{\mu} \cos\theta_{\gamma})$$

$$+ J_-(y)(1 \mp P_{\mu} \cos\theta_{\gamma})], \tag{51}$$

where $J_+(y)$ and $J_-(y)$ are defined by

$$J_+(y) = \frac{\alpha}{6\pi}(1-y)\left[\left(3\ln\frac{1-y}{r} - \frac{17}{2}\right)\right.$$

$$+ \left(-3\ln\frac{1-y}{r} + 7\right)(1-y)$$

$$\left. + \left(2\ln\frac{1-y}{r} - \frac{13}{3}\right)(1-y)^2\right], \tag{52}$$
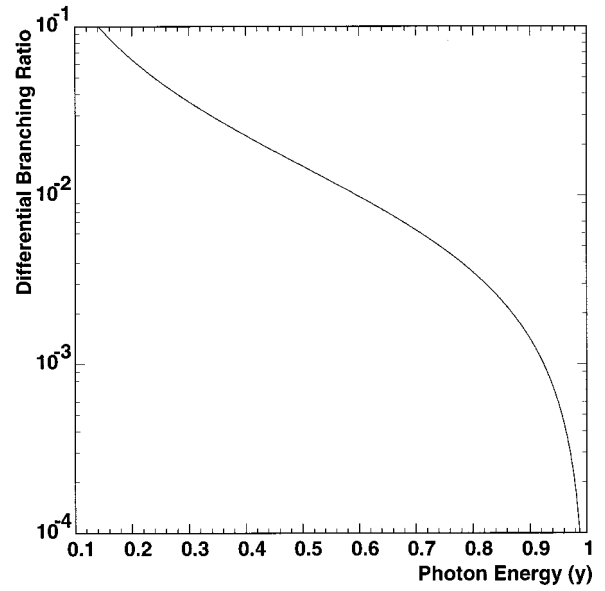

FIG. 3. Differential branching ratio of the $\mu^{\pm} \rightarrow e^{\pm} \nu \bar{\nu} \gamma$ decay as a function of the photon energy ($y \equiv 2E_{\gamma}/m_{\mu}$). This branching ratio is obtained by integrating over the e^+ energy and the angle between an e^+ and a photon.

$$J_-(y) = \frac{\alpha}{6\pi}(1-y)^2\left[\left(3\ln\frac{1-y}{r} - \frac{93}{12}\right)\right.$$

$$+ \left(-4\ln\frac{1-y}{r} + \frac{29}{3}\right)(1-y)$$

$$\left. + \left(2\ln\frac{1-y}{r} - \frac{55}{12}\right)(1-y)^2\right], \tag{53}$$

and θ_{γ} is the angle between the muon spin polarization and the photon momentum. The photon spectrum for unpolarized muons is shown in Fig. 3. Note that at the maximum photon energy ($y \sim 1$), the photon distribution is approximately given by $(1 + P_{\mu}\cos\theta_{\gamma})$ for the $\mu^+ \rightarrow e^+ \nu_e \bar{\nu}_{\mu} \gamma$ decay, because $J_+(y)$ has a first-order term in $(1-y)$, but $J_-(y)$ only contains the second- and higher-order terms. This fact is important for the suppression of accidental background in a $\mu^+ \rightarrow e^+ \gamma$ search using polarized muons, as mentioned in Sec. V.A.5.

In generalized interactions, the differential branching ratio of $\mu^{\pm} \rightarrow e^{\pm} \nu \bar{\nu} \gamma$ decay has been calculated (Lenard, 1953; Behrends et al., 1956; Fronsdal and Überall, 1959). Here, the spectra of $e^{\pm}$ and a photon depend not only on the Michel parameters of ρ and δ in the standard muon decay, but also on an additional parameter, $\bar{\eta}$, which should be zero in the $V-A$ interaction of the SM. Moreover, the asymmetry of $e^{\pm}$ in $\mu^{\pm} \rightarrow e^{\pm} \nu \bar{\nu} \gamma$ from polarized muons is parametrized by another parameter, $\xi \cdot \kappa$ (Fetscher and Gerber, 1995). Measurements of these parameters would give additional constraints on the four-fermion coupling constants (Eichenberger et al., 1984). Time-reversal violation in radiative muon decay has also been discussed (Pratt, 1958), but it was concluded that the T-odd effects have to include either the $e^{\pm}$ polarization or those terms suppressed by the electron mass.

III. LEPTON FLAVOR VIOLATION AND PHYSICS BEYOND THE STANDARD MODEL

In the minimal SM, neutrinos are massless and lepton flavor is conserved separately for each generation. This is not necessarily true if new particles or new interactions are introduced. In this section we shall discuss various theoretical models with LFV in the charged lepton processes. In particular, we emphasize those in which LFV effects could be large enough to be detected in present or future experiments in $\mu^+ \to e^+ \gamma$ decay, $\mu^+ \to e^+ e^+ e^-$ decay, $\mu^- - e^-$ conversion, and other LFV processes. Among the theoretical models that predict observable LFV effects, SUSY models have recently received much attention. In SUSY models, the origin of LFV could be interactions at a very high energy scale, such as the GUT scale or the mass scale of a heavy right-handed Majorana neutrino that appears in the see-saw mechanism. Searches for rare muon decays, thereby, could provide indirect evidence for physics at a very high energy scale. In the following sections, we first present and explain the effective Lagrangians for various muon LFV processes of $|\Delta L_i|=1$ (Sec. III.A). This is followed by a discussion of LFV in specific models which we classify as either "supersymmetric" (Sec. III.B) or "other theoretical models" (Sec. III.C). Then the phenomenology of LFV with polarized muons is presented (Sec. III.D). Finally, the muon LFV processes with $|\Delta L_i|=2$ are discussed (Sec. III.E).

A. Effective Lagrangians for lepton-flavor-violating processes

In this section we present the effective Lagrangians for muon LFV processes of $|\Delta L_i|=1$, such as $\mu^+ \to e^+ \gamma$ decay, $\mu^+ \to e^+ e^+ e^-$ decay, and $\mu^- - e^-$ conversion in a muonic atom. The possible LFV contributions can be grouped into two types: photonic interaction and four-fermion interaction.

First, the effective Lagrangian for $\mu^+ \to e^+ \gamma$ process is given by

$$\mathcal{L}_{\mu \to e\gamma} = -\frac{4G_F}{\sqrt{2}}[m_\mu A_R \overline{\mu_R}\sigma^{\mu\nu}e_L F_{\mu\nu}$$

$$+ m_\mu A_L \overline{\mu_L}\sigma^{\mu\nu}e_R F_{\mu\nu} + \text{H.c.}], \qquad (54)$$

where A_R and A_L are coupling constants that correspond to the processes $\mu^+ \to e_R^+ \gamma$ and $\mu^+ \to e_L^+ \gamma$, respectively.

For $\mu^+ \to e^+ e^+ e^-$ decay and $\mu^- - e^-$ conversion, off-shell photon emission also contributes. The general photonic $\mu - e$ transition amplitude is then written as

$$M_{photonic} = -eA_\mu^*(q)\bar{u}_e(p_e)\left[(f_{E0}(q^2)\right.$$

$$+ \gamma_5 f_{M0}(q^2))\gamma_\nu\left(g^{\mu\nu} - \frac{q^\mu q^\nu}{q^2}\right) + (f_{M1}(q^2)$$

$$\left. + \gamma_5 f_{E1}(q^2))\frac{i\sigma_{\mu\nu}q^\nu}{m_\mu}\right]u_\mu(p_\mu), \qquad (55)$$

where p_μ and p_e are the μ^- and e^- four momenta, and $q \equiv p_\mu - p_e$ is the four-momentum transfer. The electromagnetic form factors (f_{E0}, f_{E1}, f_{M0}, and f_{M1}) are functions of q^2. For $\mu^+ \to e^+ \gamma$ decay, only $f_{E1}(0)$ and $f_{M1}(0)$ can contribute, whereas all four form factors could contribute to $\mu^+ \to e^+ e^+ e^-$ decay and $\mu^- - e^-$ conversion. The coupling constants A_R and A_L are related to the dipole form factors by

$$A_R = -\frac{\sqrt{2}e}{8G_F^2 m_\mu^2}(f_{E1}^*(0) + f_{M1}^*(0)), \qquad (56)$$

$$A_L = \frac{\sqrt{2}e}{8G_F^2 m_\mu^2}(f_{E1}^*(0) - f_{M1}^*(0)). \qquad (57)$$

The direct four-fermion interactions could introduce $\mu^+ \to e^+ e^+ e^-$ decay and $\mu^- - e^-$ conversion, in addition to the photonic $\mu - e$ transition in Eq. (55). For the $\mu^+ \to e^+ e^+ e^-$ decay, the general four-fermion couplings are given by

$$\mathcal{L}_{\mu \to 3e}^{non-photo} = -\frac{4G_F}{\sqrt{2}}[g_1(\overline{\mu_R}e_L)(\overline{e_R}e_L) + g_2(\overline{\mu_L}e_R)$$

$$\times(\overline{e_L}e_R) + g_3(\overline{\mu_R}\gamma^\mu e_R)(\overline{e_R}\gamma_\mu e_R)$$

$$+ g_4(\overline{\mu_L}\gamma^\mu e_L)(\overline{e_L}\gamma_\mu e_L) + g_5(\overline{\mu_R}\gamma^\mu e_R)$$

$$\times(\overline{e_L}\gamma_\mu e_L) + g_6(\overline{\mu_L}\gamma^\mu e_L)(\overline{e_R}\gamma_\mu e_R)$$

$$+ \text{H.c.}], \qquad (58)$$

where the Fierz rearrangement for the four fermion operators is used. For the $\mu^- - e^-$ conversion process, the relevant interactions are written as

$$\mathcal{L}_{\mu-e\ conv}^{non-photo} = -\frac{G_F}{\sqrt{2}}\sum_{q=u,d,s\cdots}\left[(g_{LS(q)}\overline{e_L}\mu_R\right.$$

$$+ g_{RS(q)}\overline{e_R}\mu_L)\bar{q}q + (g_{LP(q)}\overline{e_L}\mu_R$$

$$+ g_{RP(q)}\overline{e_R}\mu_L)\bar{q}\gamma_5 q + (g_{LV(q)}\overline{e_L}\gamma^\mu\mu_L$$

$$+ g_{RV(q)}\overline{e_R}\gamma^\mu\mu_R)\bar{q}\gamma_\mu q$$

$$+ (g_{LA(q)}\overline{e_L}\gamma^\mu\mu_L$$

$$+ g_{RA(q)}\overline{e_R}\gamma^\mu\mu_R)\bar{q}\gamma_\mu\gamma_5 q$$

$$+ \frac{1}{2}(g_{LT(q)}\overline{e_L}\sigma^{\mu\nu}\mu_R$$

$$\left. + g_{RT(q)}\overline{e_R}\sigma^{\mu\nu}\mu_L)\bar{q}\sigma_{\mu\nu}q + \text{H.c.}\right], \qquad (59)$$

where $g_{LX(q)}$ and $g_{RX(q)}$ are the coupling constants for the left-handed and right-handed lepton currents, respectively, and $X = S,P,V,A,T$ represent scalar, pseudoscalar, vector, axial vector, and tensor interactions, respectively. Here, the flavor-changing quark currents are not included. The four-fermion coupling constants introduced in Eqs. (58) and (59) arise from specific contributions in the model in question. For example, box diagrams in supersymmetric models, tree diagrams involving Z', supersymmetric models with R-parity breaking, etc.
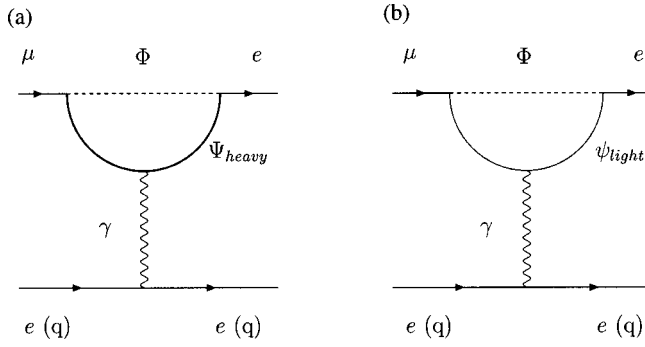
(a)

(b)

FIG. 4. Photonic penguin diagrams for $\mu - e$ transitions, such as $\mu^+ \to e^+ e^+ e^-$ or $\mu^- - e^-$ conversion: (a) the case of a heavy particle (Ψ_{heavy}) in the loop; (b) the case of a light fermion (ψ_{light}) in the loop. Φ is a scalar field.

The form factors f_{E0} and f_{M0} contribute to off-shell photons and not to real photon emission. Therefore they vanish in the $q^2 \to 0$ limit. They can be rewritten as

$$f_{E0}(q^2) = \frac{q^2}{m_\mu^2} \tilde{f}_{E0}(q^2), \qquad (60)$$

$$f_{M0}(q^2) = \frac{q^2}{m_\mu^2} \tilde{f}_{M0}(q^2), \qquad (61)$$

where $\tilde{f}_{E0}(q^2)$ and $\tilde{f}_{M0}(q^2)$ are finite at $q^2 \to 0$. If these transitions are induced by loop diagrams including heavy particles, $\tilde{f}_{E0}(q^2)$ and $\tilde{f}_{M0}(q^2)$ are then regarded as slowly varying functions of q^2. One example of such a diagram is shown in Fig. 4(a). In such a case, these form factors can be considered as additional contributions that should be added to the corresponding four-fermion coupling constants in Eqs. (58) and (59). These additional contributions are

$$\Delta g_3 = \Delta g_5 = \frac{\sqrt{2}}{4 G_F} \frac{e^2}{m_\mu^2} (\tilde{f}_{E0}^*(0) + \tilde{f}_{M0}^*(0)), \qquad (62)$$

$$\Delta g_4 = \Delta g_6 = \frac{\sqrt{2}}{4 G_F} \frac{e^2}{m_\mu^2} (\tilde{f}_{E0}^*(0) - \tilde{f}_{M0}^*(0)), \qquad (63)$$

for g_3, g_4, g_5, and g_6, correspondingly, and

$$\Delta g_{LV(u)} = -2\Delta g_{LV(d)}$$
$$= -\frac{2}{3} \frac{\sqrt{2}}{G_F} \frac{e^2}{m_\mu^2} (\tilde{f}_{E0}(0) + \tilde{f}_{M0}(0)), \qquad (64)$$

$$\Delta g_{RV(u)} = -2\Delta g_{RV(d)}$$
$$= -\frac{2}{3} \frac{\sqrt{2}}{G_F} \frac{e^2}{m_\mu^2} (\tilde{f}_{E0}(0) - \tilde{f}_{M0}(0)), \qquad (65)$$

for $g_{LV(u)}$, $g_{LV(d)}$, $g_{RV(u)}$, and $g_{RV(d)}$, respectively.

If these form factors are generated by penguin diagrams with a photon coupled to an internal line of a light fermion, as seen in Fig. 4(b), $\tilde{f}_{E0}(q^2)$ and $\tilde{f}_{M0}(q^2)$ have a logarithmic dependence on q^2 that is cut off by the light-fermion mass. Such diagrams may occur in models with a doubly charged Higgs boson or SUSY models with R-parity violation, which are discussed in Sec.

III.C. The logarithmic factor could enhance the rates of $\mu^+ \to e^+ e^+ e^-$ decay and $\mu^- - e^-$ conversion, but not that of $\mu^+ \to e^+ \gamma$ decay.

If $f_{E1}(q^2)$ and $f_{M1}(q^2)$ dominate, the following simple relations among the branching ratios of $\mu^+ \to e^+ \gamma$, $\mu^+ \to e^+ e^+ e^-$, and $\mu^- - e^-$ conversion can be derived:

$$\frac{\Gamma(\mu T_i \to e T_i)}{\Gamma(\mu T_i \to \text{capture})} \simeq \frac{1}{240} B(\mu^+ \to e^+ \gamma), \qquad (66)$$

$$B(\mu^+ \to e^+ e^+ e^-) \simeq \frac{1}{160} B(\mu^+ \to e^+ \gamma). \qquad (67)$$

These relations hold in some models of SUSY GUT, which are discussed in the next subsection. Regarding $\mu^- - e^-$ conversion, more detailed discussions of Eq. (66), including the nuclear dependence, are given in Sec. V.C.1.

B. Supersymmetric models

1. Introduction to supersymmetric models

Phenomenological applications of SUSY theories have been considered since the late 1970s in connection with the naturalness problem (or the hierarchy problem) in the SM. The SM can be regarded as being a low-energy approximation of a more complete theory, the latter being the correct theory at high energy scales. The naturalness problem in the SM arises essentially due to the many-orders-of-magnitude difference between the electroweak scale ($\approx 10^2$ GeV) and the Planck scale ($\approx 10^{19}$ GeV). If one requires the SM to remain valid up to very high energies (e.g., the Planck scale) while maintaining a Higgs mass of the order of the electroweak scale, one must invoke a precise fine tuning between the bare mass of the Higgs scalar and its radiative corrections, the latter being quadratically divergent with the high energy scale. If SUSY particles are introduced, such quadratic divergences are canceled and the mass of the Higgs scalar may be naturally of the order of the electroweak scale. For general reviews on SUSY models, we refer the reader elsewhere (Nilles, 1984; Haber and Kane, 1985).

The minimal SUSY extension of the SM is called the minimal supersymmetric standard model (MSSM). In the MSSM, the SUSY partners (which differ by 1/2 unit of spin from the corresponding SM particle) are introduced for each particle in the SM. For quarks and leptons, one introduces the complex scalar fields squark ($\tilde{q}$) and slepton ($\tilde{l}$). The superpartner of the gauge boson is a gauge fermion (gaugino), and that of the Higgs field is called a Higgsino ($\tilde{H}$). The superpartners of the gluon, $SU(2)$ and $U(1)$ gauge bosons are, respectively, the gluino ($\tilde{G}$), the wino ($\tilde{W}$), and the bino ($\tilde{B}$). After electroweak symmetry breaking, the wino, bino, and Higgsino mix with each other and form two charged Dirac fermions called charginos ($\tilde{\chi}_i^\pm$; $i=1,2$), and four Majorana fermions called neutralinos ($\tilde{\chi}_i^0$; $i=1-4$). Regarding the Higgs sector, SUSY models contain at least two Higgs doublet fields in order to keep the SUSY in-

TABLE VI. Particle content in the MSSM.

| Ordinary particles | | SUSY particles | |
Particle	Spin	Particle	Spin
quark (q)	$\frac{1}{2}$	squark ($\tilde{q}$)	0
lepton (l)	$\frac{1}{2}$	slepton ($\tilde{l}$)	0
gluon (G)	1	gluino ($\tilde{G}$)	$\frac{1}{2}$
$W^\pm, Z^0, \gamma$	1	chargino ($\tilde{\chi}_i^\pm$) ($i=1-2$)	$\frac{1}{2}$
Higgs boson ($h, H, A, H^\pm$)	0	neutralino ($\tilde{\chi}_i^0$) ($i=1-4$)	$\frac{1}{2}$

variance for three types of the Yukawa coupling constants. Namely, one Higgs field provides the mass terms for up-type quarks while another provides mass terms for the down-type quarks and charged leptons. The particle content of the MSSM are listed in Table VI.

The MSSM Lagrangian consists of two parts. These are the SUSY-invariant Lagrangian and the soft SUSY-breaking terms, as follows:

$$\mathcal{L} = \mathcal{L}_{SUSY\ inv} + \mathcal{L}_{SUSY\ breaking}. \qquad (68)$$

The MSSM Lagrangian is described in more detail in Appendix B. One of the important features of the SUSY-invariant Lagrangian is that various bosonic and fermionic interactions are related to each other by the requirement of SUSY invariance. For example, the gauge-coupling constants appear not only in the covariant derivative, but also in the gaugino-scalar-fermion interactions and the scalar self-couplings.

The ordinary Yukawa coupling constants are included in a scalar function called the superpotential $[W(\phi_i)]$. The Lagrangian specified by the superpotential ($\mathcal{L}_{superpotential}$) contains a set of fermionic interactions and scalar potentials, as follows:

$$\mathcal{L}_{superpotential} = -\sum_i \left| \frac{W(\phi)}{\partial \phi_i} \right|^2$$
$$- \frac{1}{2} \frac{\partial^2 W(\phi)}{\partial \phi_i \partial \phi_j} (\psi_{iL})^c \psi_{jL} + \text{H.c.}, \qquad (69)$$

where the scalar field (ϕ_i) and the left-handed Weyl field (ψ_{iL}) form a chiral multiplet of SUSY. The superpotential of the MSSM is given by

$$W_{MSSM} = (y_e)_{ij} H_1 E_i^c L_j + (y_d)_{ij} H_1 D_i^c Q_j$$
$$+ (y_u)_{ij} H_2 U_i^c Q_j - \mu H_1 H_2, \qquad (70)$$

where E_i^c and L_i represent the supermultiplets of $SU(2)_L$ lepton singlets and doublets, respectively. Moreover, Q_i, U_i^c, and D_i^c are the supermultiplets for quark doublets, up-type quark singlets, and down-type

quark singlets, respectively. H_1 and H_2 are distinct Higgs doublet fields. From the superpotential in Eq. (70), the following Yukawa interactions are induced:

$$\mathcal{L}_{Yukawa} = -[(y_e)_{ij} H_1 \overline{e}_{iR} l_{jL} + (y_d)_{ij} H_1 \overline{d}_{iR} q_{jL}$$
$$+ (y_u)_{ij} H_2 \overline{u}_{iR} q_{jL}] + \text{H.c.} \qquad (71)$$

In addition to Eq. (71), the superpotential in Eq. (70) generates the Higgsino mass term, various Yukawa-type interactions, and the two-, three-, and four-point scalar interactions, according to Eq. (69).

2. Flavor problems in supersymmetric models

In the MSSM the masses of superparticles, i.e., squarks, sleptons, and gauginos, are generated by the soft SUSY-breaking mass terms, which are defined as SUSY-breaking terms that do not induce quadratic divergences. In general, the soft SUSY-breaking mass terms become a new source of flavor mixing in the MSSM, which is not necessarily related to the flavor mixing in the Yukawa coupling constants in Eq. (70). For the slepton sector, the soft SUSY-breaking mass terms are given by

$$\mathcal{L}_{soft} = -(m_E^2)_{ij} \tilde{e}_{iR}^* \tilde{e}_{jR} - (m_L^2)_{ij} \tilde{l}_{iL}^* \tilde{l}_{jL}$$
$$- \{m_0(A_e)_{ij} H_1 \tilde{e}_{iR}^* \tilde{l}_{jL} + \text{H.c.}\}, \qquad (72)$$

where $(m_E)_{ij}$ and $(m_L)_{ij}$ are, respectively, the mass matrices for the right-handed sleptons ($\tilde{e}_R$) and left-handed sleptons ($\tilde{l}_L$); m_0 is a SUSY-breaking parameter and A_e is a dimensionless scalar trilinear coupling matrix.

In the basis where the lepton mass matrix is diagonalized, the presence of nonzero off-diagonal matrix elements in the slepton mass matrix would introduce LFV. From Fig. 5, one can place constraints on the off-diagonal elements of the slepton mass matrix, e.g., the $\tilde{\mu} - \tilde{e}$ element ($\Delta m_{\tilde{\mu}\tilde{e}}$), from considering their contribution to the decay $\mu^+ \rightarrow e^+ \gamma$. From the present upper limit on the latter's branching ratio, one finds
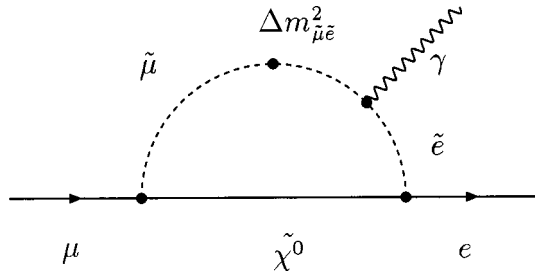
FIG. 5. Feynman diagram for $\mu^+ \to e^+ \gamma$ decay induced by slepton flavor mixing ($\Delta m^2_{\tilde{\mu}\tilde{e}}$).

$$\frac{\Delta m^2_{\tilde{\mu}\tilde{e}}}{m^2_{\tilde{l}}} \lesssim 10^{-3} \left(\frac{m_{\tilde{l}}}{100\,\text{GeV}}\right)^2, \tag{73}$$

where $m_{\tilde{l}}$ is the mass of a slepton. Similar constraints on the squark mass-matrix elements are obtained from the flavor-changing neutral current processes in the quark sector. For example, the observed value of $K^0 - \bar{K}^0$ mixing requires any possible SUSY contribution to be small. Therefore the squarks of the first and second generations must be degenerate at the level of a few percent, assuming that the squark mass is a few hundred GeV and that the squark mixing angle is of similar magnitude to the Cabibbo angle. These constraints from LFV and flavor-changing neutral current processes suggest that there should be a special suppression mechanism for the flavor mixing of sfermions (squarks and sleptons) from the dynamics of SUSY breaking. This is called the SUSY flavor problem.

There are several scenarios that solve the SUSY flavor problem:

• The soft SUSY-breaking mass terms have a universal structure at a very high energy scale, such as the Planck scale (*Gravity-mediated SUSY-breaking scenario*; Nilles, 1984).

• The SUSY-breaking effects are mediated by the SM gauge interaction so that squarks and sleptons with the same quantum numbers receive the same magnitude of soft SUSY-breaking mass (*gauge-mediated SUSY-breaking scenario*; Dine and Nelson, 1993; Dine *et al.* 1995; 1996; Giudice and Rattazzi, 1999).

• There is some approximate flavor symmetry that produces nearly degenerate masses for squarks and sleptons, at least for the first two generations (*flavor symmetry scenario*; Barbieri *et al.*, 1996).

• Squarks and sleptons can be diagonalized in the same basis as the quarks and leptons (*alignment scenario*; Nir and Seiberg, 1993).

• The squark and slepton masses are heavy enough (10–100 TeV) to avoid constraints from flavor-changing neutral current processes and LFV, at least for the sfermions of the first two generations (*effective SUSY scenario*; Cohen *et al.*, 1996).

The minimal supergravity model (SUGRA) is a realization of the first scenario. There are many phenomenological analyses based on the supergravity model. In this model, all squarks and sleptons receive the same magnitudes of the soft SUSY-breaking mass through the

coupling of supergravity at the Planck scale, so that the mass matrices are diagonal with the same diagonal elements. Therefore there is neither flavor-changing neutral current nor LFV at that energy scale. This does not necessarily imply that LFV effects are absent in this scenario. In fact, if there is some interaction which breaks lepton flavor conservation between the Planck ($\approx 10^{19}$ GeV) and the electroweak scales ($\approx 10^2$ GeV), the LFV effect could be induced in the slepton mass matrices through radiative corrections (Hall *et al.*, 1986). In recent years, it has been noticed that such an effect can induce muon LFV processes with large branching ratios in some models of SUSY GUT (Barbieri and Hall, 1994; Barbieri *et al.*, 1995a).

3. Supersymmetric grand unified theory and lepton flavor violation

In SUSY GUT's (Dimopoulos and Georgi, 1981; Sakai, 1981), the SM gauge groups of $SU(3)_C$, $SU(2)_L$, and $U(1)_Y$ are assumed to be unified by a larger group at a high energy scale. In recent years, SUSY GUT's have attracted much attention because the three gauge-coupling constants determined at LEP and SLC are consistent with the $SU(5)$ GUT prediction if contributions from SUSY particles are taken into account in the renormalization-group evolution of the coupling constants. The three coupling constants are then unified at 2×10^{16} GeV (Amaldi *et al.*, 1991; Ellis *et al.*, 1991; Langacker and Luo, 1991), which suggests that SUSY GUT's with the $SU(5)$ group or other gauge groups that include $SU(5)$ are well-motivated extensions of the SM.

Let us first discuss how LFV would be induced in $SU(5)$ SUSY GUT. In this model, quarks and leptons are classified in the three generations of $\bar{\mathbf{5}}$ and $\mathbf{10}$ representations of the $SU(5)$ group, where the $\bar{\mathbf{5}}$ representation ($\bar{F}_i$) contains d^c_{iL}, l_{iL}, and their superpartners, and the $\mathbf{10}$ representation (T_i) contains q_{iL}, u^c_{iL}, e^c_{iL}, and their superpartners. The Yukawa coupling constants at the GUT scale are determined by the superpotential,

$$W_{SU(5)} = \frac{1}{8}(y_u)_{ij} T_i \cdot T_j \cdot H(5) + (y_d)_{ij} \bar{F}_i \cdot T_j \cdot \bar{H}(5), \tag{74}$$

where $H(5)$ and $\bar{H}(5)$ are two Higgs fields associated with the $\mathbf{5}$ and $\bar{\mathbf{5}}$ representations, respectively. By substituting the fermionic fields for $\bar{F}_i$ and T_i, and also the Higgs boson fields for $H(5)$ and $\bar{H}(5)$, the Yukawa couplings responsible for the quark and lepton masses are obtained. Here, the matrix $(y_u)_{ij}$ corresponds to the Yukawa coupling matrix for the up-type quarks, and $(y_d)_{ij}$ to that for the down-type quarks and leptons.

In the minimal supergravity model, all of the scalar partners of the quarks and leptons, namely squarks and sleptons, are assumed to have a common SUSY-breaking mass from the coupling of the gravitational interaction. In addition to the mass terms, the triple scalar couplings also have a universal structure so that they are
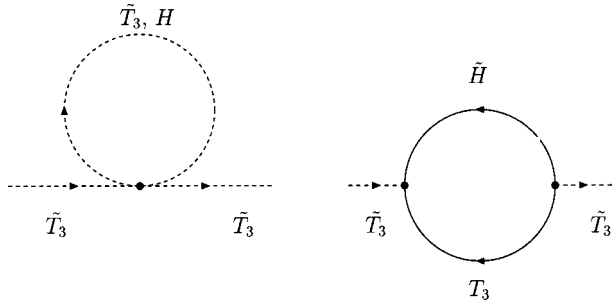
FIG. 7. Feynman diagrams for the $\mu^+ \to e^+ \gamma$ decay in $SU(5)$ SUSY GUT. The closed blobs represent the flavor transitions due to the off-diagonal terms of the slepton mass matrices.

FIG. 6. Feynman diagrams that contribute to the renormalization effect on the slepton masses from the Planck to the GUT energy scales. Here $\tilde{T}_3$ and T_3 are the scalar and fermionic components of the third-generation **10** representation of $SU(5)$, respectively. H and $\tilde{H}$ are scalar and fermionic components of the **5**-representation Higgs fields, respectively.

proportional to the corresponding Yukawa coupling constants. At the Planck scale, the soft SUSY-breaking mass terms are given by

$$\mathcal{L}_{soft} = -m_0^2 \{\tilde{T}_i^\dagger \tilde{T}_i + \tilde{\bar{F}}_i^\dagger \tilde{\bar{F}}_i\}$$
$$-\left[m_0 A_0\left(\frac{1}{8}(y_u)_{ij}\tilde{T}_i \cdot \tilde{T}_j \cdot H(5)\right.\right.$$
$$\left.\left.+(y_d)_{ij}\tilde{\bar{F}}_i \cdot \tilde{T}_j \cdot \bar{H}(5)\right) + \text{H.c.}\right], \tag{75}$$

where m_0 is the universal scalar mass, and A_0 is the universal trilinear coupling. At this stage, there is no LFV in the slepton sector. When the lepton Yukawa coupling constants (in this case y_d) are diagonalized by unitary transformations on the bosons and fermions of $\bar{F}_i$ and T_i for each generation index, the soft SUSY-breaking mass terms for the sleptons also become diagonal in the same basis. This is no longer true if we take into account the radiative corrections to the soft SUSY-breaking mass terms due to the Yukawa coupling constants. In particular, since the Yukawa coupling constant corresponding to the top-quark mass is surprisingly large, its effects on the soft SUSY-breaking mass terms are expected to be sizeable. In the basis where the matrix of up-type Yukawa coupling constants is diagonal, all members of T_i, including the right-handed slepton masses, are obtained by

$$m_T^2 \simeq \begin{pmatrix} m^2 & & \\ & m^2 & \\ & & m^2 + \Delta m^2 \end{pmatrix} \quad \text{and} \tag{76}$$

$$\Delta m^2 \simeq -\frac{3}{8\pi^2}|(y_u)_{33}|^2 m_0^2(3+|A_0|^2)\ln\left(\frac{M_P}{M_G}\right), \tag{77}$$

where M_P and M_G denote the reduced Planck mass ($\sim 2\times 10^{18}$ GeV) and the GUT scale ($\sim 2\times 10^{16}$ GeV). The term Δm^2 arises from the evolution of the renormalization-group equation between the Planck and the GUT scales through the diagrams in Fig. 6.

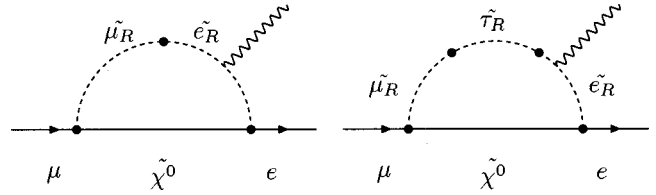Since the physical LFV effect is induced by a mis-

match of the lepton and slepton diagonalization, the off-diagonal terms of the slepton mass matrix can be examined in the basis where the Yukawa coupling constant for leptons is diagonalized. If it is diagonalized by

$$V_R y_e V_L^\dagger = \text{diagonal}, \tag{78}$$

the off-diagonal elements of the right-handed slepton mass matrix in this new basis are given by

$$(m_{\tilde{e}_R}^2)_{ij} \simeq -\frac{3}{8\pi^2}(V_R)_{i3}(V_R)_{j3}^*|y_u^{33}|^2$$
$$\times m_0^2(3+|A_0|^2)\ln\left(\frac{M_P}{M_G}\right). \tag{79}$$

This becomes a source of $\mu^+ \to e^+ \gamma$ decay through the diagrams in Fig. 7. If one uses the $SU(5)$ GUT relation for the down-type quark and lepton Yukawa coupling constants, given by

$$y_e = y_d^T, \tag{80}$$

then V_R is given by the Cabibbo-Kobayashi-Maskawa matrix at the GUT scale as follows:

$$(V_R)_{ij} = (V_{CKM}^{GUT})_{ji}, \tag{81}$$

where V_{CKM}^{GUT} can be obtained from the Cabibbo-Kobayashi-Maskawa matrix at the electroweak scale by taking into account the effects of running coupling constants from the electroweak to the GUT scales.

The prediction of the branching ratio of $\mu^+ \to e^+ \gamma$ decay is presented in Fig. 8 for typical SUSY parameters in $SU(5)$ SUSY GUT. The branching ratio reaches the order of 10^{-14} for a slepton mass of a few hundred GeV/c^2.

Some remarks on $SU(5)$ SUSY GUT are presented in the following:

• In the $SU(5)$ SUSY GUT model, LFV appears only in the right-handed slepton sector for small or moderate values of $\tan\beta$, which is defined by the ratio of two Higgs vacuum expectation values, $\tan\beta \equiv \langle H_2^0 \rangle / \langle H_1^0 \rangle$. This is because the renormalization effects contribute only to $\tilde{e}_R$, and not to $\tilde{l}_L$. As a result, the helicity of an electron (positron) in LFV processes becomes only right handed (left handed). For instance, only $\mu^+ \to e_L^+ \gamma$ decay occurs, not $\mu^+ \to e_R^+ \gamma$. These two processes could be distinguished if the angular distribution of the $\mu^+ \to e^+ \gamma$ signal were measured using polarized muons.

• There is partial cancellation among the Feynman diagrams that contribute to the $\mu^+ \to e^+ \gamma$ amplitudes in

FIG. 9. Predicted $\mu^+ \to e^+ \gamma$ branching ratios in the $SU(5)$ SUSY GUT model with higher dimensional operators in the GUT superpotential. The branching ratios are shown as a function of the right-handed selectron mass for $\tan\beta = 6$ (dashed lines) and 30 (solid lines). The thick lines are for the nonminimal case in which $V_{\bar{e}}$ and V_l are the same as V_{CKM}, and the thin lines are for the minimal case in which $V_{\bar{e}} = V_{CKM}$ and $V_l = \mathbf{1}$, where $V_{\bar{e}}$ is the mixing matrix for the right-handed sleptons, and V_l is that for the left-handed sleptons. The bino mass of $M_1 = 60 \text{ GeV}/c^2$, the trilinear scalar coupling constant of $A_0 = 0$, the positive Higgsino mass ($\mu > 0$), and the top quark mass of $175 \text{ GeV}/c^2$ are used. The experimental bound shown in the dashed line is $B(\mu^+ \to e^+ \gamma) \leq 4.9 \times 10^{-11}$ (Bolton *et al.*, 1988), and it is noted that the recent best limit is $B(\mu^+ \to e^+ \gamma) \leq 1.2 \times 10^{-11}$ (Brooks *et al.*, 1999). For detail on the calculations, see Hisano, Nomura, Okada, *et al.* (1998). From Hisano, Nomura, Okada, *et al.*, 1998.
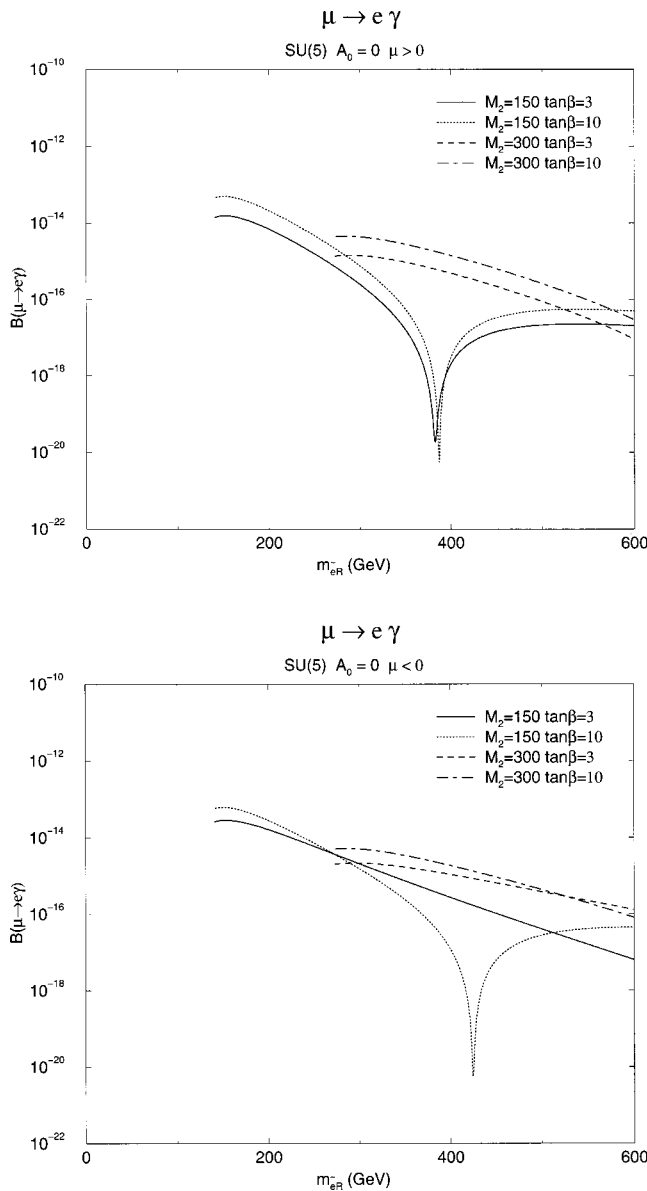

FIG. 8. Predicted branching ratios for the $\mu^+ \to e^+ \gamma$ decay in the $SU(5)$ SUSY GUT based on the minimal supergravity model as a function of the right-handed slepton mass for four different sets of the SUSY input parameters of M_2 [the $SU(2)$ gaugino mass] and $\tan\beta$ (the ratio of the two Higgs vacuum expectation values). For the other parameters, the trilinear scalar coupling constant $A_0 = 0$ and $m_t = 175 \text{ GeV}$. The following Cabibbo-Kobayashi-Maskawa matrix elements are used: $|(V_{CKM})_{cb}| = 0.04$ and $|(V_{CKM})_{td}| = 0.01$. The two graphs correspond to a positive and negative sign of the Higgsino mass parameter μ, respectively.

the $SU(5)$ SUSY GUT (Hisano *et al.*, 1997). This cancellation can be seen in Fig. 8.

• In Eqs. (79) and (81), the off-diagonal elements of the right-handed slepton mass matrix are determined by the Cabibbo-Kobayashi-Maskawa matrix elements. When the favorable values of the Cabibbo-Kobayashi-Maskawa matrix elements are used, $|\lambda_\tau| \equiv |(V_R)_{13}(V_R)_{23}^*|$ of $(3-5) \times 10^{-4}$ is obtained. This results from the assumption that all of the Yukawa cou-
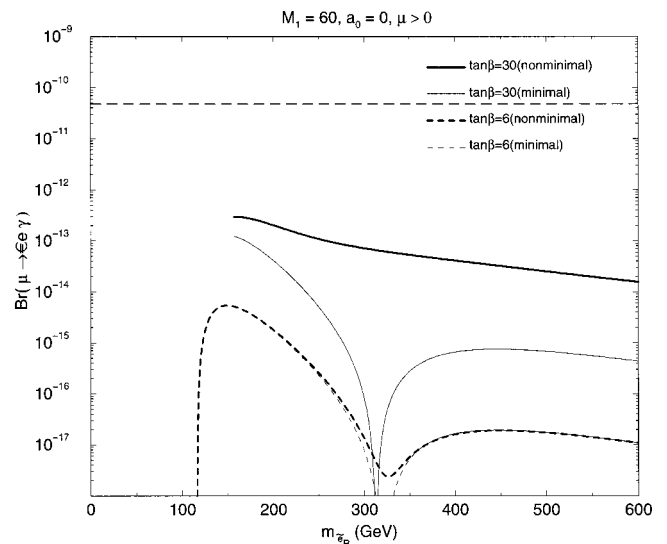
pling constants are generated from the superpotential in Eq. (74). However, it is known that this assumption does not yield a realistic mass relation for the down-type quarks and charged leptons of the first and second generations. If higher-dimensional terms or different $SU(5)$ representations of Higgs fields are included to resolve this problem, the simple relationship between the slepton mixing matrix and the Cabibbo-Kobayashi-Maskawa matrix in Eq. (81) would be lost, and λ_τ would essentially become a free parameter. As a consequence, the predicted branching ratios could be different from those in Fig. 8. For example, if $|\lambda_\tau| \approx 10^{-2}$, the branching ratio is enhanced by three orders of magnitude compared to those in Fig. 8. In addition, for large $\tan\beta$, a further enhancement can be expected (Arkani-Hamed, Cheng, and Hall, 1996). One example of the $\mu^+ \to e^+ \gamma$ branching ratio for large $\tan\beta$ is shown in Fig. 9 (Hisano, Nomura, Okada, *et al.*, 1998). When the higher-dimensional terms are included, the mass matrix for left-handed sleptons also has off-diagonal elements owing to the large bottom Yukawa coupling constant, and therefore the branching ratio of $\mu^+ \to e^+ \gamma$ decay is enhanced by $(m_\tau/m_\mu)^2 \approx 10^2$, just as in the case of $SO(10)$ SUSY GUT discussed below. This enhancement can be seen in
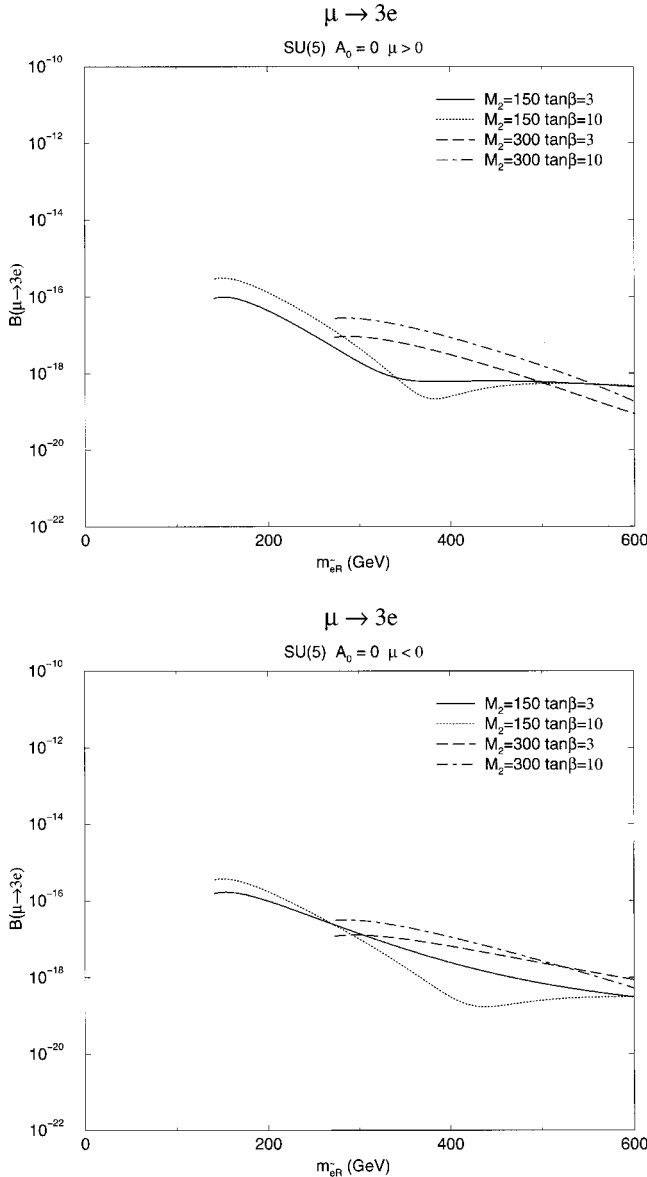
$\mu \to 3e$

SU(5) $A_0 = 0$ $\mu > 0$

$\mu \to 3e$

SU(5) $A_0 = 0$ $\mu < 0$

FIG. 10. Predicted branching ratios for the $\mu^+ \to e^+ e^+ e^-$ decay in the $SU(5)$ SUSY GUT based on the minimal supergravity model. The input parameters are the same as in Fig. 9.

the nonminimal case in Fig. 9. Furthermore, the previously discussed destructive interference between the different diagrams in the minimal $SU(5)$ SUSY GUT may disappear.

• The decay $\mu^+ \to e^+ e^+ e^-$ and the $\mu^- - e^-$ conversion process both receive contributions from the off-shell photon, Z-penguin, and box diagrams, in addition to the photonic penguin diagram contributing to the $\mu^+ \to e^+ \gamma$ decay. In $SU(5)$ SUSY GUT, the relative magnitudes of different contributions vary over the SUSY parameter space. This implies that the relations in Eqs. (66) and (67) may change for different SUSY input values. The predictions of the $\mu^+ \to e^+ e^+ e^-$ decay and the $\mu^- - e^-$ conversion in $SU(5)$ SUSY GUT are shown in Figs. 10 and 11, respectively.

Large LFV effects are also expected in $SO(10)$ SUSY GUT. In the minimal $SO(10)$ SUSY GUT, the superpotential is given by

$$W_{SO(10)} = \frac{1}{2}(y_u)_{ij} \Psi_i \cdot \Phi_u \cdot \Psi_j + \frac{1}{2}(y_d)_{ij} \Psi_i \cdot \Phi_d \cdot \Psi_j,$$

(82)

where Ψ_i is the 16-dimensional representation of $SO(10)$ and Φ_u and Φ_d are two 10-dimensional Higgs fields. In this model, both the left-handed and right-handed sleptons receive LFV effects. In particular, the diagrams shown in Fig. 12 attribute a large contribution to the amplitude of $\mu^+ \to e^+ \gamma$ decay because they are proportional to m_τ. Hence the branching ratio is enhanced by $(m_\tau/m_\mu)^2$ compared to the minimal $SU(5)$ SUSY GUT. Owing to this enhancement, the branching ratios for muon LFV processes can become comparable to the present experimental upper bounds if the slepton mixing matrices are related to the observed Cabibbo-Kobayashi-Maskawa matrix elements. The predictions for the branching ratio of $\mu^+ \to e^+ \gamma$ decay in $SO(10)$ SUSY GUT are shown in Fig. 13. In $SO(10)$ SUSY GUT, since the photon-penguin diagrams dominate in the amplitudes of $\mu^+ \to e^+ e^+ e^-$ decay and $\mu^- - e^-$ conversion, their predicted branching ratios with respect to $\mu^+ \to e^+ \gamma$ decay would follow Eqs. (66) and (67) over a wide SUSY parameter space (Barbieri *et al.*, 1995a).

The rates of muon LFV processes depend on the structure on the Yukawa coupling constants at the GUT scale. The branching ratios for the muon LFV processes are calculated in various realistic $SO(10)$ SUSY GUT models (Arkani-Hamed, Cheng, and Hall, 1996; Ciafaloni *et al.*, 1996; Duong *et al.*, 1996; Gómez and Goldberg, 1996). In $SO(10)$ SUSY GUT models, the diagrams relevant for the $\mu^+ \to e^+ \gamma$ amplitude would induce electric dipole moments for the electron and neutron (Dimopoulos and Hall, 1995). The branching ratios for muon LFV processes were compared with the prediction of electric dipole moments, flavor-changing neutral current processes in the quark sector, and CP violations in B and K meson decays in both $SU(5)$ and $SO(10)$ SUSY GUT models, and the leptonic signals were shown to be very sensitive to the interaction at the GUT scale (Barbieri *et al.*, 1995b). The LFV process has also been investigated in the breaking pattern of $SO(10) \to SU(3) \times SU_L(2) \times SU_R(2) \times U_{B-L}(1) \to SU(3) \times SU_L(2) \times U_Y(1)$ (Deshpande *et al.*, 1996) and in the $SU(4) \times SU_L(2) \times SU_R(2)$ model without GUT unification (King and Oliveira, 1999).

In some theoretical scenarios in which the mass matrices for squarks and sleptons at very high energy scale are not universal, but instead have some correlation or alignment with the corresponding fermion matrices, it is possible to avoid the SUSY flavor problem and at the same time still have muon LFV branching ratios large enough to be detected. One such realization has been investigated concerning the dynamical alignment mechanism (Rattazzi and Sarid, 1996). An interesting possibility is a class of models based on $U(2)$ flavor symmetry where both the Yukawa coupling constants and the soft SUSY-breaking mass terms are controlled by the same approximate symmetry. In this case, the branching ratio
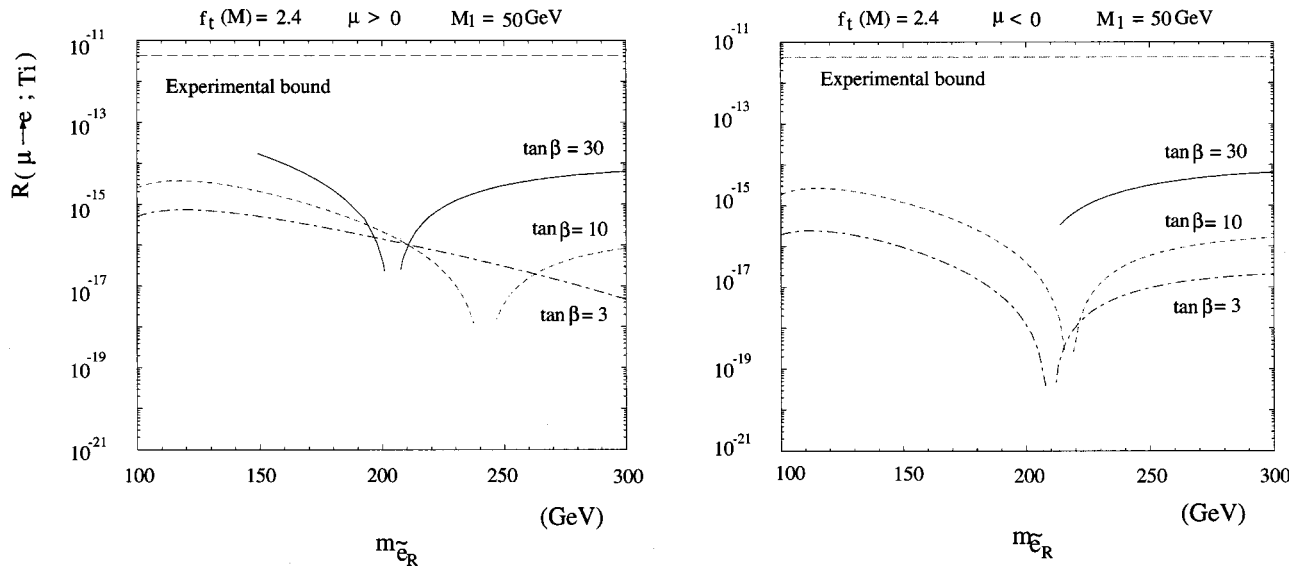
FIG. 11. Predicted branching ratios for the $\mu^- - e^-$ conversion in $SU(5)$ SUSY GUT. The SUSY gaugino mass of M_1 $=50$ GeV, and the top Yukawa coupling at the reduced Planck scale of $f_t=2.4$ are used. The left and right figures correspond to a positive and negative sign of the Higgsino mass parameter μ, respectively. The experimental bound shown is $B(\mu^-\mathrm{Ti}\rightarrow e^-\mathrm{Ti})$ $\leq 4.3\times 10^{-12}$ (Dohmen *et al.*, 1993), and it is noted that the recent best limit is $B(\mu^-\mathrm{Ti}\rightarrow e^-\mathrm{Ti})\leq 6.1\times 10^{-13}$ (Wintz, 1998). From Hisano *et al.*, 1997.

for $\mu^+\rightarrow e^+\gamma$ decay is expected to receive large SUSY contributions (Barbieri *et al.*, 1996).

4. Supersymmetric models with a right-handed neutrino

A large LFV effect can be expected if the supermultiplets of the right-handed Majorana neutrino are included in the SUSY standard model (Borzumati and Masiero, 1986). As explained in Sec. II.A.3, the smallness of the neutrino masses can be accommodated by the see-saw mechanism. To include this see-saw mechanism, part of the lepton sector in the Lagrangian in Eq. (70) is replaced by

$$W_N=(y_e)_{ij}H_1E_i^cL_j+(y_\nu)_{ij}H_2N_iL_j+\frac{1}{2}(M_R)_{ij}N_iN_j,$$
(83)

where N_i is the right-handed neutrino supermultiplets and $(M_R)_{ij}$ is the Majorana mass matrix, and a new Yukawa coupling constant matrix, y_ν, is introduced. Since there are two Yukawa coupling matrices (y_e and y_ν) in the lepton sector, flavor mixing would arise and lepton flavor would no longer be conserved separately
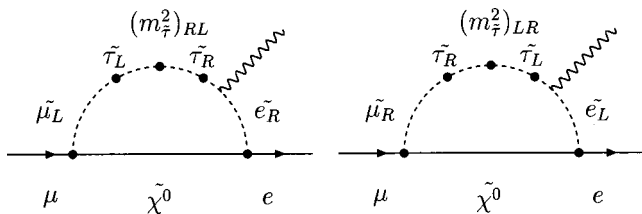
for each generation, just as in the quark sector. In SUSY models with universal soft SUSY breaking at the Planck scale, the flavor mixing in left-handed sleptons would induce sizeable LFV effects in muon and tau decays through the renormalization effects from the Planck to the Majorana mass scales.

The expected magnitudes of the LFV effects depend on the Yukawa coupling constant and the flavor mixing in the lepton sector. In the basis where the Yukawa coupling constant matrix for charged leptons is diagonalized, the mass matrix of light neutrinos is given by

$$(m_\nu)_{ij}=-(y_\nu)_{ki}(M_R^{-1})_{kl}(y_\nu)_{lj}\frac{v^2\sin^2\beta}{2},$$
(84)

where v is the SM Higgs vacuum expectation value, and β is the Higgs vacuum angle for the two Higgs doublets. On the other hand, the off-diagonal terms of the left-handed slepton mass matrix induced by the renormalization effect are

$$(m_{\tilde{l}_L}^2)_{ij}\simeq-\frac{1}{8\pi^2}(y_\nu)_{ki}^*(y_\nu)_{kj}m_0^2(3+|A_0|^2)\ln\left(\frac{M_P}{M_R}\right).$$
(85)

In general, there is no direct relationship between the neutrino mixing in Eq. (84) and the slepton mixing relevant to $\mu\rightarrow e\gamma$, $\tau\rightarrow\mu\gamma$, and $\tau\rightarrow e\gamma$ in Eq. (85). If, however, we assume that the neutrino mixing mostly originates from the neutrino Yukawa coupling constants, $(y_\nu)_{ij}$, the information from atmospheric and solar neutrinos can be related to the slepton mixing. Then, the branching ratios for $\mu^+\rightarrow e^+\gamma$ and $\tau\rightarrow\mu\gamma$ decays can be evaluated by using the neutrino mixing parameters (Hisano *et al.*, 1995; 1996; Hisano, Nomura, and Yanagida, 1998; Hisano and Nomura, 1999). Figure 14
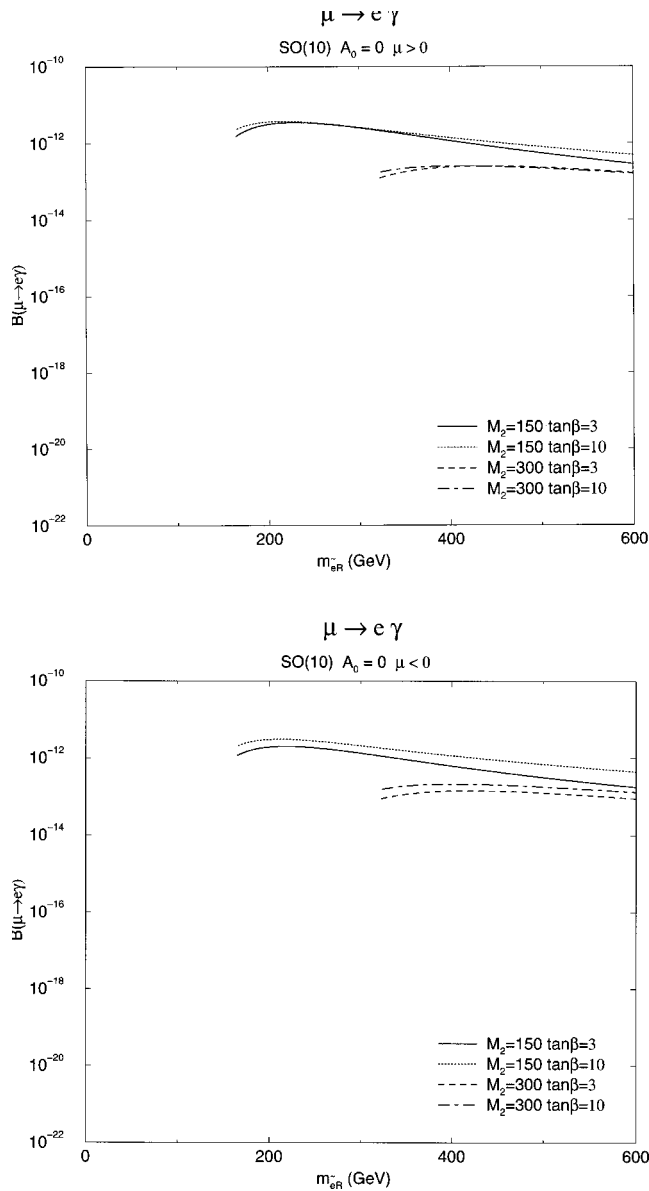

FIG. 12. Feynman diagrams in $SO(10)$ SUSY GUT that give dominant contributions to the $\mu^+\rightarrow e^+\gamma$ process; $(m_{\tilde{\tau}}^2)_{RL}$ and $(m_{\tilde{\tau}}^2)_{LR}$ are proportional to m_τ.

μ → e γ

SO(10) $A_0 = 0$ $\mu > 0$

μ → e γ

SO(10) $A_0 = 0$ $\mu < 0$

FIG. 13. Predicted branching ratios for $\mu^+ \to e^+ \gamma$ decay in the $SO(10)$ SUSY GUT based on the minimal supergravity model. Input parameters are the same as in Fig. 9.

shows the predicted branching ratio for the $\mu^+ \to e^+ \gamma$ decay for different solutions of the solar neutrino mixing. As can be seen in Fig. 14, it can reach the present experimental bound if the Majorana mass is larger than $O(10^{14})$ GeV and if the large-angle Mikheyev-Smirnov-Wolfenstein solution for the solar neutrino problem is chosen. It is noted that from Eq. (84), given a fixed value of the light neutrino mass (m_ν), the Yukawa coupling constant (y_ν) becomes larger for a larger value of the Majorana mass scale (M_R), resulting in the LFV rate becoming larger in Eq. (85). The LFV rate increases approximately as the second power of M_R and, therefore, it could possibly probe the mass scale of the right-handed Majorana neutrino (M_R) in this scenario. Note that this prediction is in contrast to the see-saw mechanism without SUSY, in which the LFV rates for charged leptons are extremely suppressed, as discussed in Sec. III.C.

μ→eγ in the MSSMRN with the MSW large-angle solution
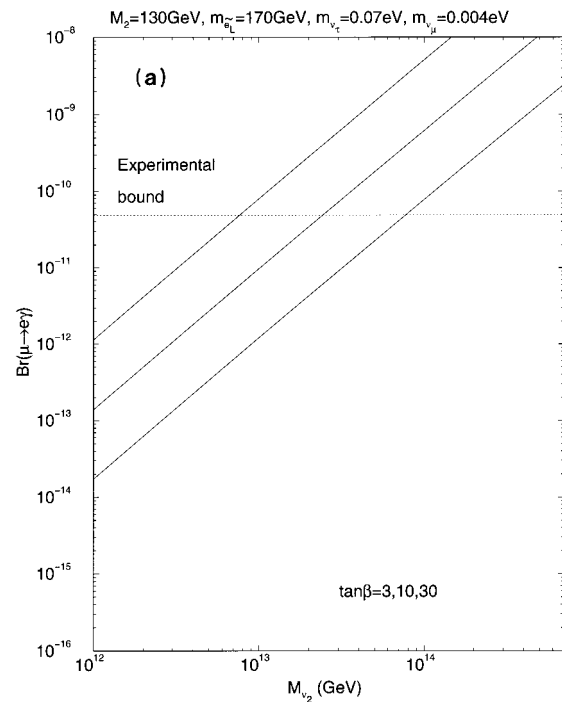
μ→eγ in the MSSMRN with the MSW small-angle solution
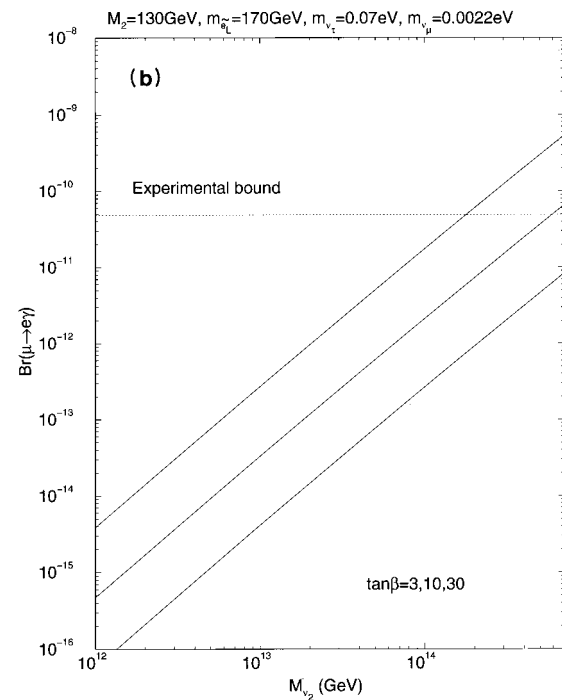
FIG. 14. Predicted branching ratios of $\mu^+ \to e^+ \gamma$ decay as a function of the Majorana mass of the second-generation right-handed neutrino (M_{ν_2}) in the MSSM model with right-handed neutrino. They are given for the Mikheyev-Smirnov-Wolfenstein large-angle and small-angle solutions. The three curves correspond to $\tan\beta$=30, 10, and 3 from top to bottom for both figures. The other parameters are shown in the top of the figures. The experimental bound shown is the previous limit from Bolton et al. (1988). From Hisano and Nomura, 1999.

5. Other supersymmetric models

Observable effects of muon LFV processes may arise through renormalization effects in the slepton mass matrix. Because these effects may come from anywhere between the Planck and the electroweak scale, it is possible to consider some other interaction at a high energy scale as a new source of LFV.

Such an example is given in the context of the gauge-mediated SUSY breaking. If the mixing between the messenger fields of gauge mediation and the ordinary matter fields is allowed, a sizable LFV effect can be generated through the renormalization of the slepton mass matrix (Dine *et al.*, 1997; Dubovsky and Gorbunov, 1998). A similar effect appears in a supersymmetric model with vectorlike leptons, where a large LFV effect could be induced via the slepton mixing (Kitano and Yamomoto, 2000).

6. Lepton flavor violation in slepton production and decay

If the charged sleptons are discovered in experiments at future colliders (like LHC and LC), LFV due to slepton mixing could be directly sought in their production and decay processes (Krasnikov, 1994; 1996; Arkani-Hamed, Cheng, Feng, *et al.*, 1996). For example, a process like $e^+e^- \to \tilde{l}^+\tilde{l}^- \to e^{\pm}\tilde{\chi}_1^0 \mu^{\mp}\tilde{\chi}_1^0$ breaks lepton flavor conservation, where the slepton $\tilde{l}^{\pm}$ is assumed to decay to a lepton and the neutralino $\tilde{\chi}_1^0$. Direct searches for the $e\mu$ final states in e^+e^- and e^-e^- collisions can probe the slepton mixing angle between the selectron ($\tilde{e}$) and the smuon ($\tilde{\mu}$). Figure 15 shows a contour plot of the cross section for right-handed selectron and smuon pair production in the parameter space of the right-handed slepton mixing angle ($\sin 2\theta_R$) and the mass difference of two right-handed scalars ($\Delta m_R^2/m_R^2$) for future e^+e^- linear collider experiments. Depending on the parameters in the slepton mass matrix, the direct production can cover parameter space comparable to or even larger than indirect searches for muon LFV processes (Arkani-Hamed, Cheng, Feng *et al.*, 1996).

The production cross section for the slepton LFV processes depends on the masses and mixing of the sleptons. If two sleptons, like $\tilde{e}$ and $\tilde{\mu}$, are almost degenerate in their masses, a possible oscillation between them would occur in the decay process. Another interesting possibility is a *CP*-violating signal in the slepton oscillation, which may arise due to a new complex phase in the slepton mixing matrices (Arkani-Hamed *et al.*, 1997; Bowser-Chao and Keung, 1997).

In $SU(5)$ SUSY GUT, lepton flavor violation in the slepton pair production and decays, in particular with a tau in the final state, has been investigated, and was found to be more sensitive than the searches for $\tau \to e(\mu)\gamma$ (Hirouchi and Tanaka, 1998). Lepton-flavor-violating signals in the production of left-handed sleptons at $\mu^+\mu^-$ and e^+e^- colliders are also considered in the framework of MSSM with right-handed neutrinos motivated by the atmospheric-neutrinos data. It is shown that the decay modes of either $\tau + \mu + 4$ *jets*
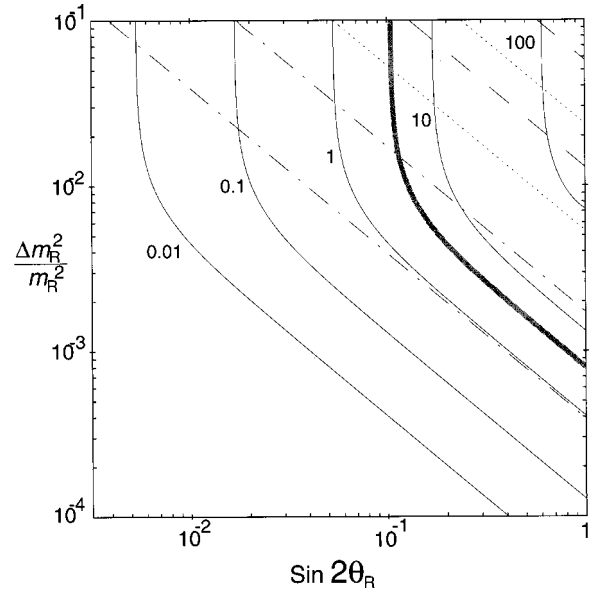

FIG. 15. Contours of the cross section $\sigma(e^+e_R^- \to e^{\pm}\mu^{\mp}\tilde{\chi}_1^0\tilde{\chi}_1^0)$ in a unit of fb for Next Linear Collider (solid line) with center-of-mass energy of 500 GeV, $m_{\tilde{e}_R}, m_{\tilde{\mu}_R} \sim 200$ GeV, and $M_1 = 100$ GeV. The thick gray contour represents the experimental reach in one year with 50 fb^{-1}. Constant contours of $B(\mu \to e\gamma) = 4.9 \times 10^{-11}$ and 2.5×10^{-12} are also plotted for degenerate left-handed sleptons with mass of 350 GeV and $\tilde{t} \equiv -(A + \mu \tan\beta)/m_R = 0$ (dotted), 2 (dashed), and 50 (dot-dashed). From Arkani-Hamed, Cheng, Feng *et al.*, 1996b.

+missing energy or $\tau + \mu + l + 2$ *jets+missing energy* could be useful to see the signals with suppressing any potential background (Hisano *et al.*, 1999). Other possible LFV searches at a $e\mu$ collider (Choi *et al.*, 1998) and a $e\gamma$ collider (Cao *et al.*, 1999) are also considered.

7. Summary of lepton-flavor-violating supersymmetric processes in models

We have seen that the branching ratios for muon LFV processes can be large for many models based on SUSY. Particularly interesting cases are the various models of SUSY GUT and the SUSY model with right-handed neutrinos that accommodates neutrino mass generation by the see-saw mechanism. In these cases, the interaction at very high energy scale becomes an origin of the flavor mixing in the slepton mass matrix. Therefore the muon LFV processes can offer a unique opportunity to explore interactions at the unification scale.

The search for LFV processes would become even more important, were (some) SUSY particles to be discovered in future collider experiments. The existence of SUSY implies new sources of flavor mixing in the scalar sector, in addition to the Cabibbo-Kobayashi-Maskawa and Mikheyev-Smirnov-Wolfenstein matrices in the fermion sector. A fundamental question such as how SUSY is broken in the SUSY model could be addressed with studies of the flavor structure of the scalar mass matrices. Therefore a study of muon LFV processes will con-

tinue to play a crucial role, even after all of the SUSY particles are experimentally discovered.

C. Other theoretical models

In the late 1970s, especially in 1977, the false rumor of $\mu^+ \to e^+ \gamma$ signals at SIN (Schweizerisches Institut für Nuklearforschung) gave rise to a surge in the number of theoretical papers on models with heavy neutrinos inducing LFV (Altarelli *et al.*, 1977; Bjorken *et al.*, 1977; Cheng and Li, 1977a, 1977b; Lee *et al.*, 1977; Lee and Shrock, 1977). In this section, we discuss LFV effects in theoretical models other than SUSY models. Although there may be many ways to induce LFV effects, we discuss only a few specific examples. For other references, see, for instance, Vergados (1986) and Depommier and Leroy (1995).

1. Models with a massive neutrino

The simplest way to violate lepton flavor conservation is to introduce neutrino masses and mixing. However, it has been known that the branching ratio of $\mu^+ \to e^+ \gamma$ decay from ordinary neutrino mixing is very suppressed if the neutrino mass and mixing suggested by the atmospheric- and solar-neutrino experiments are used. For example, the predicted branching ratio from the Dirac neutrino masses and mixing is given by (Bilenky *et al.*, 1977; Petcov, 1977)

$$B(\mu \to e\gamma) = \frac{3\alpha}{32\pi} \left| \sum_i (V_{MNS})^*_{\mu i}(V_{MNS})_{ei} \frac{m^2_{\nu_i}}{m^2_W} \right|^2,$$
(86)

where $(V_{MNS})_{ai}$ is the lepton flavor mixing matrix (Mikheyev-Smirnov-Wolfenstein matrix) defined in Eq. (20). It is represented by

$$\nu_{La} = \sum_i (V_{MNS})_{ai}\nu_{Li},$$
(87)

where ν_{La} is the neutrino field in the weak-flavor basis, and ν_{Li} in the mass eigenstate basis. Even if a 1-eV neutrino mass with maximal mixing is considered, Eq. (86) only gives a branching ratio of the order of 10^{-47}.

For the Majorana neutrino model of the see-saw type (Cheng and Li, 1980), the suppression factor of $(m^2_{\nu_i}/m^2_W)$ in Eq. (86) is replaced by a factor of $O(m_{\nu_i}/M_R)$, where M_R is the mass of a heavy Majorana neutrino. Then the branching ratio is still $O(10^{-40})$ or less for $m_\nu = 1$ eV and $M_R = 10^{10}$ GeV. It is therefore difficult to expect observable LFV effects from the ordinary neutrino masses and mixing indicated by the atmospheric and solar neutrinos.

2. Models with a doubly charged Higgs boson

There is a wide class of theoretical models that allow interesting enhancements for $\mu^+ \to e^+ e^+ e^-$ decay and $\mu^- - e^-$ conversion. If LFV is induced by a penguin diagram with a heavy boson and a light charged fermion, the photonic form factors $f_{E0}(q^2)$ and $f_{M0}(q^2)$ receive

an enhancement factor of $\ln(m_{boson}/m_{fermion})$ from the loop diagrams in which a photon is attached to the internal light-fermion line (Marciano and Sanda, 1977a; 1977b; Wilczek and Zee, 1977; Raidal and Santamaria, 1998). Since this factor is absent for $f_{E1}(q^2)$ and $f_{M1}(q^2)$, the branching ratio of $\mu^+ \to e^+ \gamma$ decay has no enhancement. An example of such a model is one that contains a doubly charged Higgs boson with the following interaction:

$$\mathcal{L} = h_{ij}\overline{e^c_{iR}}e_{jR}\phi^{++} + \text{H.c.},$$
(88)

where the loop diagrams with internal charged leptons and doubly charged scalar ϕ^{++} could induce a logarithmic enhancement (Raidal and Santamaria, 1998).

3. Supersymmetric models with *R*-parity violation

Another important class of models that might induce a logarithmic enhancement are SUSY models with *R*-parity violation. In the MSSM, if we required only gauge invariance when writing all possible superpotentials, the following interactions would also be allowed:

$$W = \lambda_{ijk}L_iL_jE^c_k + \lambda'_{ijk}L_iQ_jD^c_k + \lambda''_{ijk}U^c_iD^c_jD^c_k$$
$$- \mu_iL_iH_2.$$
(89)

These interactions violate baryon or lepton number conservation. To forbid proton decays that are too fast, a parity that distinguishes superparticles from ordinary particles is often imposed. This parity is called the *R* parity, and is defined as $R \equiv (-1)^{3B+L+2S}$, where B, L, and S are, respectively, the baryon number, lepton number, and spin. However, the diagrams leading to proton decay require both lepton and baryon number violation, i.e., a combination of the couplings above. Hence one may still consider models with *R*-parity violation which maintain proton stability if one suppresses the baryon-number-violating terms while keeping the lepton-number-violating terms (or vice versa) in the superpotential above.

Some combinations of the coupling constants are severely constrained by the LFV processes. It is known that the allowed values of $\lambda\lambda$, $\lambda\lambda'$, and $\lambda'\lambda'$ still give large contributions at a tree level to the $\mu^+ \to e^+ e^+ e^-$ and $\mu^- - e^-$ conversion processes (Kim *et al.*, 1982; Huitu *et al.*, 1998; Faessler *et al.*, 1999). Typical tree-level diagrams are shown in Fig. 16.

In SUSY models with *R*-parity violation, there also exist loop contributions to muon LFV processes, such as $\mu^+ \to e^+ \gamma$ decay (Chaichian and Huitu, 1996), $\mu^+ \to e^+ e^+ e^-$ decay, and $\mu^- - e^-$ conversion. The latter two processes would receive a logarithmic enhancement (Huitu *et al.*, 1998). Figure 17 shows typical loop diagrams. From the one-loop diagram, the $\mu^- - e^-$ conversion process can also be induced from the $\lambda\lambda$ coupling constants. For example, from the loop diagrams with internal leptons, the following four form factors are given by
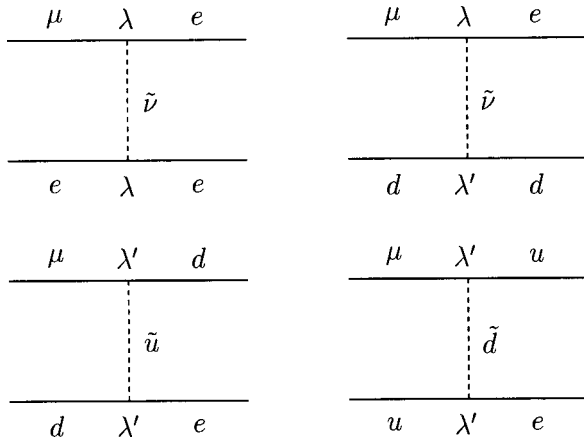
FIG. 16. Tree diagrams for LFV processes in SUSY models with R-parity violation.

$$f_{E0}(q^2) = \pm f_{M0}(q^2)$$

$$= -\frac{2(\lambda\lambda)}{3(4\pi)^2} \frac{-q^2}{m_{\tilde{\nu}}^2} \left(\ln \frac{-q^2}{m_{\tilde{\nu}}^2} + F(r) \right), \qquad (90)$$

$$f_{M1}(0) = \mp f_{E1}(0) = -\frac{(\lambda\lambda)}{3(4\pi)^2} \frac{m_\mu^2}{m_{\tilde{\nu}}^2}, \qquad (91)$$

where $r = m_{\tilde{\nu}}^2/(-q^2)$. For $r \gg 1$, $F(r) = \ln r + \frac{4}{3}$; otherwise, it takes a value of $O(1)$.

As a result, some of the $\lambda\lambda$ combinations are more severely constrained by $\mu^- - e^-$ conversion than by the tree-level process of $\mu^+ \to e^+ e^+ e^-$ decay.

The present constraints for the combinations of $\lambda\lambda$ and $\lambda'\lambda'$ couplings are summarized in Huitu *et al.* (1998) and Faessler *et al.* (1999).

4. Models with Z'

There are many models where nonphotonic LFV transitions occur at tree level. Typical examples are models with a Z' that has flavor off-diagonal couplings, or models with extra fermion families which mix with the SM fermions at tree level so that the Z boson has LFV couplings (Bernabeu *et al.*, 1993). In such cases, the $\mu^+ \to e^+ e^+ e^-$ and $\mu^- - e^-$ conversion processes are expected to be much more important than $\mu^+ \to e^+ \gamma$ decay.

5. Models with Lorentz noninvariance

Recently, a possible violation of Lorentz invariance has been suggested (Coleman and Glashow, 1999). In this context, the Lorentz transformation is not invariant, but only the translational and rotational symmetries are
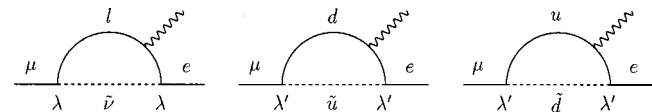

FIG. 17. One-loop diagrams for LFV processes in SUSY models with R-parity violation.

assumed to be exact in a preferred system. Thus the maximum attainable velocity could be different for each species of particle, and this would give rise to many unique phenomena in particle physics and cosmic-ray physics.

Muon LFV processes provide a good test for the violation of Lorentz invariance (Coleman and Glashow, 1999). If a small Lorentz-noninvariant interaction exists in the SM Lagrangian, flavor mixing couplings are in general allowed in the photon-fermion interaction. The current limit on the branching ratio of $\mu^+ \to e^+ \gamma$ puts a strong constraint on the relevant coupling constants. Another interesting effect is a change in the muon lifetime at high energies. Since the contribution to the decay width of $\mu \to e\gamma$ due to the Lorentz-noninvariant interaction increases with γ^3, where γ is the Lorentz factor, this would dominate over the ordinary contribution to muon decay which decreases with $1/\gamma$. Therefore the muon lifetime might start decreasing as γ^{-3} at a sufficiently high energy. The current limit on the energy dependence of the muon lifetime has been obtained from the experiment that measures the muon anomalous magnetic moment.

D. Lepton flavor violation with polarized muons

In this subsection, we discuss the usefulness of polarized muons in searches for $\mu^+ \to e^+ \gamma$ and $\mu^+ \to e^+ e^+ e^-$ decays. As discussed later in Sec. IV, highly polarized μ^+'s (surface muons) are available experimentally. Therefore it would be useful to examine what kind of new information can be obtained by measuring the angular distribution of decay products with respect to the muon polarization.

When the initial muon is polarized in $\mu^+ \to e^+ \gamma$ decay, the angular distribution of the positron is given by

$$\frac{dB(\mu^+ \to e^+ \gamma)}{d\cos\theta_e} = 192\pi^2 [|A_R|^2 (1 - P_\mu \cos\theta_e)$$

$$+ |A_L|^2 (1 + P_\mu \cos\theta_e)], \qquad (92)$$

where θ_e is the angle between the muon polarization and the positron momentum in the muon rest frame. The terms A_R and A_L are given in Eqs. (56) and (57), and P_μ is the magnitude of the muon polarization. A measurement of the e^+ polarization would give the relative amplitudes of A_R and A_L, which correspond to the emission of right-handed e^+ ($\mu^+ \to e_R^+ \gamma$) and left-handed e^+ ($\mu^+ \to e_L^+ \gamma$), respectively. This is shown schematically in Fig. 18.

Since A_L and A_R are model dependent, it would be useful to discriminate between different LFV mechanisms. For instance, the minimal $SU(5)$ SUSY GUT model predicts a vanishing A_R and a nonzero A_L, yielding a $(1 + P_\mu \cos\theta_e)$ distribution. On the other hand, the $SO(10)$ SUSY GUT model predicts the helicity amplitudes for both right-handed and left-handed e^+s. For nonunified supersymmetric models with a right-handed neutrino, A_R is nonzero but A_L vanishes, giving a $(1 - P_\mu \cos\theta_e)$ distribution. Thus a measurement of the an-
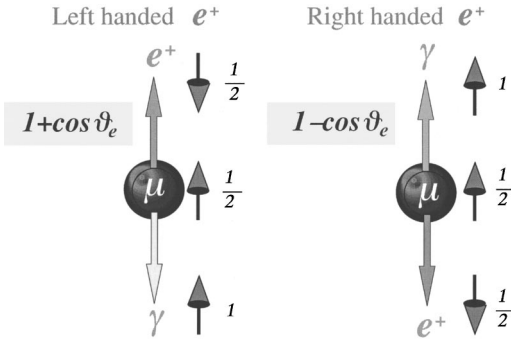
FIG. 18. Angular distribution of e^+ in polarized $\mu^+ \rightarrow e^+ \gamma$ decay.

FIG. 19. Examples of theoretical models to induce Mu-$\overline{\text{Mu}}$ conversion, which are mediated by (a) a doubly charged Higgs boson, (b) heavy Majorana neutrinos, (c) a neutral scalar particle like a tau sneutrino, and (d) a bilepton X^{--}. From Willmann et al., 1999.

gular distribution of e^+ with respect to the direction of muon polarization would provide a valuable means to clearly discriminate between these models.

The $\mu^+ \rightarrow e^+ e^+ e^-$ decay with polarized muons would provide us with an interesting possibility of measuring T violation (Treiman et al., 1977; Zee, 1985). A T-odd triple vector correlation, $\vec{\sigma}_\mu \cdot (\vec{p}_1 \times \vec{p}_2)$, can be defined, where $\vec{\sigma}_\mu$ is the muon spin, and $\vec{p}_1$ and $\vec{p}_2$ are two independent momenta of the e^+ in the final state. If CPT invariance holds, the information on CP violation in the LFV interaction may be obtained from the T-odd correlations of the decay products. The T-odd asymmetry would arise as an interference between the photon-penguin terms and the four-fermion terms. Details are discussed in Sec. V.B.1. In particular, the T-odd asymmetry has been evaluated in the $SU(5)$ SUSY GUT model based on supergravity (Okada et al., 1998). It was shown that an asymmetry of up to 20% is possible if CP-violating phases are introduced in the soft SUSY-breaking mass terms. This would give information independent from that obtained from the electric dipole moment of the electron and neutron.

In the $\mu^+ \rightarrow e^+ e^+ e^-$ decay, parity-odd asymmetries can be also defined if the initial muons are polarized. These asymmetries are sensitive to the chiralities of the terms in the effective Lagrangian, both the photon-penguin terms (A_L and A_R) and the four-fermion coupling terms (g_i). Measurements of the parity-odd asymmetries in $\mu^+ \rightarrow e^+ e^+ e^-$ decay, together with the branching ratios of $\mu^+ \rightarrow e^+ \gamma$ and $\mu^+ \rightarrow e^+ e^+ e^-$ decays, are useful for distinguishing between different SUSY GUT models (Okada et al., 2000).

E. $|\Delta L_i| = 2$ processes

Examples of LFV processes with $|\Delta L_i| = 2$ are the muonium to antimuonium conversion (Mu$-\overline{\text{Mu}}$ conversion) and wrong-flavor muon decay ($\mu^+ \rightarrow e^+ \nu_\mu \bar{\nu}_e$). The phenomenology of Mu$-\overline{\text{Mu}}$ conversion can be described with an effective four-fermion interaction. As an example, an interaction of the type $(V-A)(V-A)$ was considered by Feinberg and Weinberg (1961). It is given by
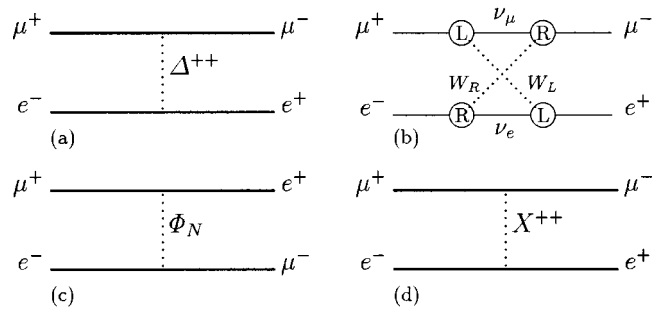
$$H_{\text{Mu}\overline{\text{Mu}}} = \left(\frac{G_{\text{Mu}\overline{\text{Mu}}}}{\sqrt{2}}\right) \bar{\mu} \gamma_\lambda (1-\gamma_5) e \, \bar{\mu} \gamma^\lambda (1-\gamma_5) e + \text{H.c.},$$

(93)

in which $G_{\text{Mu}\overline{\text{Mu}}}$ is a coupling constant characterizing the strength of the Mu$-\overline{\text{Mu}}$ conversion. As described in Sec. V.E.3, the present experimental limits require $G_{\text{Mu}\overline{\text{Mu}}} \lesssim 3.0 \times 10^{-3} G_F$ (Willmann et al., 1999).

In general, there could be various combinations of different types of four-fermion interactions, such as $(V+A)(V+A)$, $(V-A)(V+A)$, $(S-P)(S-P)$, $(S+P)(S+P)$, $(S-P)(S+P)$, SS, and PP, where V, A, S, and P are, respectively, vector, axial-vector, scalar, pseudoscalar effective interactions. The type of interaction is determined by the theoretical model in question. Figure 19 shows example diagrams of speculative theoretical models responsible for the Mu$-\overline{\text{Mu}}$ conversion. The models involve the exchange of (a) doubly charged Higgs bosons, (b) heavy Majorana neutrinos, (c) a neutral scalar particle (including a superparticle), and (d) a bilepton gauge boson. They are briefly described below.

A simple example that induces the $|\Delta L_i| = 2$ process is provided by a model with a doubly charged singlet scalar boson (Chang and Keung, 1989). In this model, only the $(V+A)(V+A)$ interaction is generated and the Mu$-\overline{\text{Mu}}$ conversion rate can be as large as the present experimental limit, within the constraints from the measurements of the anomalous muon magnetic moment and high-energy Bhabha scattering. A more general case with the doubly charged scalar boson is also considered (Swartz, 1989).

In the left-right symmetric model with a triplet Higgs boson field, the Mu$-\overline{\text{Mu}}$ conversion could be induced by a doubly charged Higgs boson Δ^{++} (Halprin, 1982). In this model, if the mass of the muon neutrino is greater than $35\,\text{keV}/c^2$ and less than the present direct experimental bound of $170\,\text{keV}/c^2$, one can derive an upper limit on the neutrino lifetime from the requirement that the neutrino energy density in the universe does not exceed the present total energy density. A lower bound for $G_{\text{Mu}\overline{\text{Mu}}}$ can then be obtained as a function of the mass of the muon neutrino m_{ν_μ} (Herczeg and

Mohapatra, 1992). For the range $35 \leqslant m_{\nu_\mu} \leqslant 170 \, \text{keV}/c^2$, a lower limit of $G_{\text{Mu}\overline{\text{Mu}}} \geqslant (1-40) \times 10^{-4} G_F$ can be derived.

If neutrinos are of a Majorana nature, $\text{Mu}-\overline{\text{Mu}}$ conversion could take place by an intermediate pair of neutrinos. This coupling is related to neutrinoless double-β decays, yielding $G_{\text{Mu}\overline{\text{Mu}}} \leqslant 10^{-5} G_F$ (Halprin, 1982).

There is a class of models with a neutral scalar boson, which has a flavor-changing coupling to introduce the $|\Delta L_i| = 2$ processes (Hou and Wong, 1996). An important example of these kinds of models is the supersymmetric model with R-parity violation, where a tau sneutrino exchange induces the $\text{Mu}-\overline{\text{Mu}}$ conversion (Mohapatra, 1992; Halprin and Masiero, 1993). In this case, the four-fermion coupling is of the $(S-P)(S+P)$ type. The present experimental limit for $\text{Mu}-\overline{\text{Mu}}$ conversion gives a constraint on the relevant coupling constant, $|\lambda_{132}\lambda^*_{231}| \leqslant 3 \times 10^{-4}$, for a superpartner mass of order $100 \, \text{GeV}/c^2$. Moreover, the four-fermion coupling constant for the $\mu^+ \to e^+ \nu_\mu \bar{\nu}_e$ decay is predicted to be similar in magnitude to that for $\text{Mu}-\overline{\text{Mu}}$ conversion.

In some extensions of the SM gauge groups, there appear doubly charged gauge bosons (called bileptons), X^{--}, which couple only to leptons. They occur, for instance, in $SU(15)$ GUT models (Frampton and Lee, 1990), or in a gauge model with $SU(3)_C \times SU(3)_L \times U(1)_Y$ (331 model; Frampton, 1992a). In these models, singly charged and doubly charged bilepton gauge bosons appear from breaking of the $SU(3)_L$ gauge symmetry to $SU(2)_L$ of the SM gauge groups. The mass bound for the bilepton gauge bosons is obtained from a precise determination of the Michel parameters for normal muon decay (Carlson and Frampton, 1992), the muonium hyperfine splitting, and the decay $\mu^+ \to e^+ \nu_\mu \bar{\nu}_e$ (Fujii et al., 1994). They give a lower bound of roughly $200 \, \text{GeV}/c^2$. In these models, $\text{Mu}-\overline{\text{Mu}}$ conversion could occur by the exchange of a doubly charged bilepton (Fujii et al., 1993; Horikawa and Sasaki, 1996). The effective interaction is of the form $(V-A)(V+A)$, in contrast to the traditional $(V-A)(V-A)$ interaction by Feinberg and Weinberg. The bilepton interaction is given by

$$\mathcal{L} = -\frac{g_{3l}}{2\sqrt{2}} X_\mu^{--} \bar{l} \gamma^\mu \gamma_5 C \bar{l}^T + \text{H.c.}, \tag{94}$$

where $l = e, \mu, \tau$, and C is the charge-conjugation matrix. The gauge-coupling constant, g_{3l}, is of the order of $O(1)$, and is determined from model in question. The $\text{Mu}-\overline{\text{Mu}}$ conversion rate $(P_{\text{Mu}\overline{\text{Mu}}})$ is given by

$$P_{\text{Mu}\overline{\text{Mu}}} = 4.5 \times 10^3 \times \left(\frac{g_{3l}}{m_X} \right)^4, \tag{95}$$

where m_X is the mass of the bilepton gauge boson. From the current experimental bound for $\text{Mu}-\overline{\text{Mu}}$ conversion, a constraint of $m_X/g_{3l} \geqslant 2.6 \, \text{TeV}/c^2$ is obtained (Willmann et al., 1999).

It has long been known that the reaction $e^- e^- \to \mu^- \mu^-$ is useful for studying $|\Delta L_i| = 2$ processes

TABLE VII. Three fundamental values in the standard model.

Parameter	Experimental value	Uncertainty
$1/\alpha$	$137.0359895 \pm 0.0000061$	0.045 ppm
G_F	$(1.16639 \pm 0.00001) \times 10^{-5} \, \text{GeV}^{-2}$	9 ppm
m_Z	$91.1867 \pm 0.0021 \, \text{GeV}/c^2$	23 ppm

(Glashow, 1961). Such experiments were carried out to place a constraint on $G_{\text{Mu}\overline{\text{Mu}}}$ (Barber et al., 1969). Recently, similar scattering processes at high energy, such as at a ee linear collider or a $\mu\mu$ collider have been discussed, and are mostly based on bilepton models (Frampton, 1992b; Hou, 1996; Raidal, 1998).

IV. NORMAL MUON DECAY

Normal muon decay remains the only pure leptonic process of the weak interaction accessible to precise measurements with high statistics. The studies are free from the complications of the strong interaction and hadronic structure. For this reason, precise studies of normal muon decay would provide information that is unambiguously interpreted.

The experimental progress has benefited from the high-intensity muon beams available at the three meson factories, the Paul Scherrer Institute (PSI) in Switzerland, TRIUMF in Canada, LAMPF in the U.S.A. (which was unfortunately shut down), and also lately at the Rutherford Appleton Laboratory (RAL) in England. Particularly useful is a surface μ^+ beam, which arises from the decay of pions stopped at the surface of a pion-production target. It has a kinetic energy of 4.1 MeV ($29.8 \, \text{MeV}/c$ in momentum) and 100% muon polarization antiparallel to its momentum direction. This high polarization of the surface muons is useful for various measurements requiring muon polarization.

In the past, studies of normal muon decay have greatly contributed to the development of the SM. They are now playing the role of probing for possible deviations from the SM. For example, see reviews by Fetscher and Gerber (1995) and Herczeg (1995). In the following sections, the current status of the studies of normal muon decay is discussed, in particular those that are being prepared or planned for the future. These include measurements of the muon lifetime, the Michel spectrum, and the longitudinal polarization of e^+'s in polarized $\mu^+ \to e^+ \nu_e \bar{\nu}_\mu$ decay. Other important muon experiments, such as the muon anomalous magnetic moment and the muon electric dipole moment, will not be discussed.

A. Muon lifetime

1. Phenomenology

The Fermi coupling constant G_F is one of the three precisely measured inputs of the SM, along with the fine-structure constant (α) and the Z-boson mass (m_Z). Their updated values are given in Table VII. Note that the m_Z value in the Particle Data Group (Caso et al.,

1998) is $m_Z = 91.187 \pm 0.007$ (77 ppm). However, after a recent improvement in the measurement in m_Z (LEP and SLD Electroweak Working Group, 1999), the uncertainties of G_F and m_Z have become comparable in order, as can be seen in Table VII. Here G_F is determined from the muon lifetime (τ_μ) given by Eq. (23). The complete two-loop QED corrections to the estimation of the muon lifetime have been calculated (van Ritbergen and Stuart, 1999). The theoretical errors in deriving G_F from the muon lifetime are now reduced to negligible proportions, compared with the experimental uncertainty in the measurement of the muon lifetime. It would be necessary to improve the accuracy of G_F, if experimentally possible. To test the SM, a comparison is necessary between measurements of G_F from the muon lifetime with those determined from other measurements, such as tau leptonic decays, or the M_W and other observables at the M_Z pole with similar accuracies (Marciano, 1999).

2. Experimental status

Experimentally, measurements of the muon lifetime were carried out at TRIUMF (Giovanetti *et al.*, 1984) and at Saclay (Bardin *et al.*, 1984). Since then, for more than a decade, no experimental efforts to improve the situation have been made. The present value of τ_μ is $\tau_\mu = 2.197 \, 03(4) \times 10^{-6}$ (± 18 ppm) (Caso *et al.*, 1998). Recently, however, an experimental proposal at Rutherford Appleton Laboratory (RAL) to reduce the uncertainty of G_F by an order of magnitude has been undertaken (Nakamura *et al.*, 1998), and two experimental proposals to PSI (Carey *et al.*, 1999b; Cavallo *et al.*, 1999) have been submitted.

An ongoing experiment at the RIKEN-RAL muon facility, R77, uses a pulsed muon beam. In previous experiments with a continuous muon beam, only one incident muon within the time window of measurement was allowed in order to avoid any possible confusion from the decay of other muons occurring in the same time window. It would otherwise introduce distortion of the time spectrum of muon decay. This requirement, however, would lead to a limitation on muon beam intensity, and the sensitivity would be statistically limited. To overcome this problem, R77 at RIKEN-RAL has adopted a pulsed beam, with a pulse interval of 20 msec that is much longer than the measurement window. Since all muons come at the same time, multiple muon decays within the measurement time window are allowed. There are several sources of systematic errors. One of them is from counting losses due to pileup e^+ events and the dead time of detection, since the instantaneous beam intensity is high. To avoid this effect, segmentation of the detectors is required. In R77, multiwire proportional chambers are used. Another systematic error might come from a precession of muon spin under an earth field. A special magnetic material will be adopted for the muon-stopping target to depolarize the muon spin polarization. By accumulating 10^{11} muon decays, it aims to achieve statistical and systematic errors

of about 3 ppm (a total of 4 ppm) in the τ_μ measurement. Its initial phase, which plans to accumulate 10^{10} muon decays, started in 1999.

There are two new planned experiments at PSI: R-99-06 (Cavallo *et al.*, 1999) and R-99-07 (Carey *et al.*, 1999b). R-99-07 was approved in 1999 and R-99-06 has been approved in 2000. Both experiments are aiming at an improvement of a factor of 20 over the current world average of τ_μ.

The experiment R-99-07 is to use a chopped surface-muon beam at PSI. The muons are stopped in a sulfur target to reduce the residual muon polarization, and a transverse magnetic field of 75 G is applied to further dephase it. The e^+ detector (μLan detector) consists of 180 triangular scintillating tiles distributed within 20 supertriangles in an icosahedral geometry centered on the target. Each scintillating tile is viewed by a photomultiplier, and the signal is recorded by a wave-form digitizer developed in the $g-2$ experiment at BNL. This 4π geometry of the μLan detector, especially a sum of the pointlike symmetric tile pairs with respect to the center, would further reduce any asymmetries due to spin rotation.

The other experiment, R-99-06, uses a fiber-active scintillator target, which comprises plastic scintillating fibers in an overall active volume of $20 \times 20 \times 20 \, cm^3$. A π^+ beam is stopped in the fiber-active-scintillator target, and a $\pi^+ \rightarrow \mu^+ \rightarrow e^+$ decay chain is observed in the target. Owing to the high granularity and fast response of the fiber-active-scintillator-target detector, many individual muon decays can be recorded in parallel with a high event rate.

B. Michel decay spectrum

1. Phenomenology

The $e^\pm$ spectrum of normal muon decay is given in Eq. (30) with the four Michel parameters of ρ, ξ, δ, and η. It includes all possible Lorentz-invariant interactions. A precise determination of the Michel parameters would allow stringent testing of the $(V-A)$ structure of electroweak interactions in the SM, and would be sensitive to any deviations caused by physics beyond the SM.

2. Experimental status

In the past, each of the Michel parameters in normal muon decay was determined in dedicated experiments: for instance, the ρ parameter (Derenzo, 1969), the η parameter (Burkard *et al.*, 1985b), the δ parameter (Balke *et al.*, 1988), $P_\mu \xi$ (Beltrami *et al.*, 1987), and $P_\mu \xi(\delta/\rho)$ (Jodidio *et al.*, 1986).

A new experiment, E614 at TRIUMF, is being prepared to measure the entire differential spectrum of positrons from the decay of polarized muons (Abegg *et al.*, 1996). By accumulating 10^9 muon decays, the goal of the E614 experiment is to measure the Michel parameters to precisions of $\Delta\rho < 1 \times 10^{-4}$, $\Delta\delta < 3 \times 10^{-4}$, and $\Delta(P_\mu \xi) < 2 \times 10^{-4}$. The aimed precisions are 3–10 times better
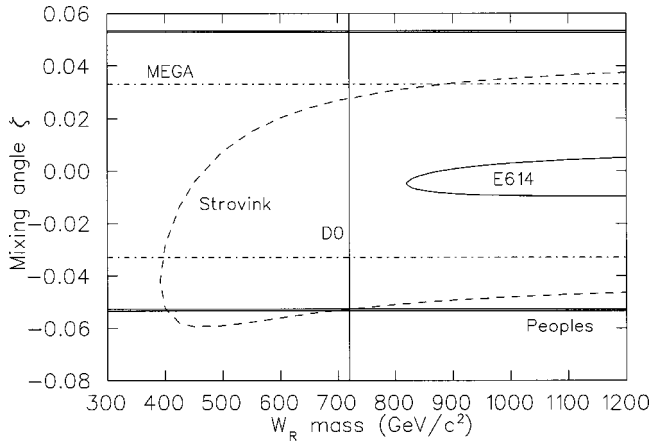
FIG. 20. Constraints on the mass of W_R vs its mixing angle ζ in the manifest left-right symmetric model. The experimental constraints of "Strovink," "Peoples," "MEGA," and "D0" are from Jodidio *et al.* (1986), Derenzo (1969), the MEGA experiment (unpublished), and Abachi *et al.* (1996), respectively. The aimed goal for E614 is also shown (provided by D. R. Gill).

than those previously achieved. Note that only the product $P_\mu \xi$ can be experimentally determined.

Among the many theoretical models that can be studied by precise measurements of standard muon decay, one example is the left-right symmetric model, which invokes a $SU(2)_L \times SU(2)_R \times U(1)$ symmetry (Herczeg, 1986; Langacker and Sankar, 1989). In this class of models there exist heavy right-handed gauge bosons (two charged $W_R^\pm$ and one neutral Z'). In general, they mix with the gauge bosons of the SM and form mass eigenstates $W_{1,2}^\pm$:

$$\begin{pmatrix} W_L^\pm \\ W_R^\pm \end{pmatrix} = \begin{pmatrix} \cos \zeta & -\sin \zeta \\ e^{i\omega} \sin \zeta & e^{i\omega} \cos \zeta \end{pmatrix} \begin{pmatrix} W_1^\pm \\ W_2^\pm \end{pmatrix}, \qquad (96)$$

where ζ is a mixing angle, and ω is a CP-violating phase. For example, the expected constraint on the left-right symmetric model from E614 is presented in Fig. 20.

A schematic view of the E614 detector is shown in Fig. 21. The E614 spectrometer consists of a supercon-
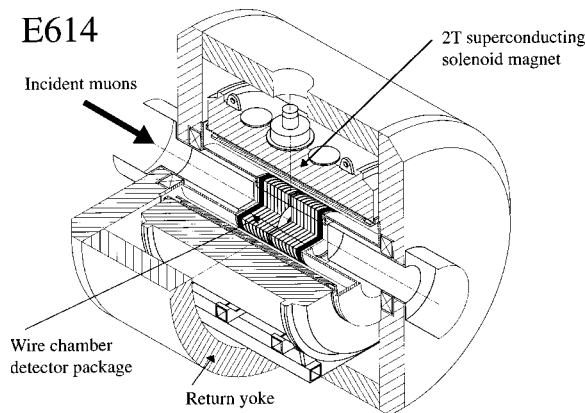

FIG. 21. Schematic view of the E614 detector at TRIUMF (provided by D. R. Gill).

ducting solenoid magnet with tracking chambers. In E614, a surface-muon beam from the M13 beam channel at TRIUMF will be brought into the detector, and stopped in a muon-stopping target made of aluminum located at the center of the apparatus. An array of planar chambers, mounted symmetrically upstream and downstream from the target, will track the trajectories of e^+'s from muon decays under a magnetic field of 2 T with a homogeneity of better than 10^{-4}. The positron spectrum will be measured over a wide range of $0.4 \leq x \leq 1.0$ for the positron energy, and $10 \leq \theta_e \leq 70°$ and $110 \leq \theta_e \leq 170°$ for the angle between the muon spin direction and the positron momentum vector (θ_e), where x is defined in Sec. II.C.1.

Experimentally, it is important to keep the muon polarization fully aligned with the magnetic field direction at the stopping target. Any reduction of P_μ^z, the projection of P_μ on the field direction, must be minimized at a level of 10^{-4}. Possible sources of reduction are a misalignment between the muon-beam axis and the magnetic field at the spectrometer, a fringing field of the spectrometer, a contamination of nonsurface muons (such as cloud muons, which come from pion decays in flight around the target region), multiple scattering of muons in the production target, and possible depolarization of the muon spin in the aluminum muon-stopping target. At the same time, crucial spectrometer requirements are the low-massness of tracking chambers to minimize multiple scattering of positrons and position accuracy of the detector assembly. Detector construction has been started, and physics data collection is expected in 2001.

C. Polarization of e^+ in $\mu^+ \to e^+ \nu_e \bar{\nu}_\mu$ decay

1. Phenomenology

The longitudinal polarization of e^+ (P_L) in $\mu^+ \to e^+ \nu_e \bar{\nu}_\mu$ decay is given in Eq. (38). When the muon is not polarized ($P_\mu = 0$) and the SM values of $\rho = \delta = 3/4$ are taken, P_L leads to

$$P_L(x, \cos \theta_e) = \xi'. \qquad (97)$$

It is independent of the values of x and $\cos \theta_e$. Therefore a measurement of the longitudinal polarization of e^+'s emitted by unpolarized muons would provide a good direct determination of the parameter ξ'.

If the muon is polarized with the SM values of the ρ and δ parameters, P_L is given by

$$P_L(x, \cos \theta_e) = \xi' + \frac{\xi P_\mu \cos \theta_e (2x-1)}{(3-2x) + \xi P_\mu \cos \theta_e (2x-1)} \cdot \frac{(\xi'' - \xi \xi')}{\xi}. \qquad (98)$$

From this, the measurement of P_L as a function of energy (x) and angle (θ_e) would give extra information on the combination of parameters $(\xi'' - \xi \xi')/\xi$. In particular, for $x \approx 1$ and $\cos \theta_e \approx -1$, it leads to

$$P_L(x=1, \cos \theta_e = -1) \approx \xi' + \frac{-\xi P_\mu}{1 - \xi P_\mu} \cdot \frac{(\xi'' - \xi \xi')}{\xi}. \tag{99}$$

The combination $(\xi'' - \xi \xi')/\xi$ is multiplied by an enhancement factor of $\xi P_\mu/(1 - \xi P_\mu)$, which could be large when P_μ is close to unity.

The two transverse polarization components (P_{T1} and P_{T2}) of the e^+ in $\mu^+ \rightarrow e^+ \nu_e \bar{\nu}_\mu$ decay are given in Eqs. (36) and (37). If time-reversal invariance holds, P_{T2}, which is the transverse e^+ polarization normal to the decay plane determined by P_μ and the e^+ momentum direction, should vanish. A nonzero P_{T2} would signal a violation of time-reversal invariance. The electromagnetic final-state interaction, which mimics a T-odd effect, is known to be small. On the other hand, P_{T1}, which is not forbidden by the fundamental symmetries, is sensitive to the Michel parameter, η. The determination of η from P_{T1} is better than that from the isotropic part of the $e^\pm$ energy spectrum, since the latter is more difficult owing to the small x_0 factor ($\sim 10^{-2}$) multiplied by η.

2. Experimental status

The latest measurement of P_L of e^+ in $\mu^+ \rightarrow e^+ \nu_e \bar{\nu}_\mu$ decay was carried out at SIN (Burkard *et al.*, 1985a). A magnetized-iron foil was adopted as a polarimeter for the e^+ polarization, and was tilted by 45° with respect to the e^+ momentum direction. Either Bhabha scattering of e^+ off e^-'s ($e^+ e^- \rightarrow e^+ e^-$) or annihilation in flight ($e^+ e^- \rightarrow \gamma \gamma$) in the magnetized-iron foil was utilized, where the cross sections of those processes have a particular dependence on the relative angle between the $e^\pm$ polarization directions. Since the magnitude and direction of e^- polarization in the magnetized-iron foil is known, the polarization of e^+ from $\mu^+ \rightarrow e^+ \nu_e \bar{\nu}_\mu$ decay can be determined. Both $e^+ e^-$ and $\gamma \gamma$ pairs originating in the foil were detected by four NaI(Tl) crystal detectors located behind the foil. Both unpolarized and polarized muons were studied. From the case of unpolarized muons, $P_L(= \xi') = 0.998 \pm 0.042$ was obtained, whereas the current average value in the Particle Data Group is $P_L = 1.00 \pm 0.04$ (Caso *et al.*, 1998), showing no strong evidence of the right-handed current. For the case of polarized muons, they obtained $(\xi'' - \xi \cdot \xi')/\xi = -0.35 \pm 0.33$, which, however, did not improve the constraints on the coupling constants.

The transverse polarization components, P_{T1} and P_{T2}, of e^+ in $\mu^+ \rightarrow e^+ \nu_e \bar{\nu}_\mu$ decay were measured by the same group (Burkard *et al.*, 1985b). A magnetized-iron foil was used again as a polarimeter, but was placed perpendicular to the e^+ momentum direction. The measurement was based on the fact that two photons from the annihilation of transversely polarized e^+ with e^-'s in a magnetized-iron foil are preferentially emitted in the plane determined by the bisector of the e^+ polarization vector ($\vec{P}_T$) and the e^- polarization vector in a magnetized foil. Their results were $\langle P_{T1} \rangle = 0.016 \pm 0.023$ and

$\langle P_{T2} \rangle = 0.007 \pm 0.023$. From the measured value of P_{T1}, $\eta = -0.007 \pm 0.013$ was obtained.

A new experiment, R-94-10, at PSI (Barnett *et al.*, 1994), is in preparation to measure the transverse polarization, both P_{T_1} and P_{T_2}, of the positrons from polarized $\mu^+ \rightarrow e^+ \nu_e \bar{\nu}_\mu$ decay with a precision of 3×10^{-3}. The experimental principle is the same as the previous one mentioned above. Major improvements are expected to occur from a higher muon-stopping rate due to a higher proton current at the PSI cyclotron, installation of two analyzing foils with an additional wire chamber in between, and replacement of four NaI(Tl) crystals by a 127 hexagonal BGO ($Bi_4 Ge_3 O_{12}$) crystal. An engineering run started in 1999.

Another new experiment, R-97-06 at PSI (van Hove *et al.*, 1997), is under development to measure the longitudinal polarization, P_L, of the positrons emitted antiparallel to the muon spin from polarized $\mu^+ \rightarrow e^+ \nu_e \bar{\nu}_\mu$ decay. As explained in Eq. (99), P_L at $x \approx 1$ and $\cos \theta_e \approx -1$ is sensitive to the combination of $(\xi'' - \xi \xi')/\xi$ with the enhancement factor. R-97-06 aims to measure this observable with an improvement of more than one order of magnitude over the previous experiments at SIN. It will use three solenoidal magnets to track e^+'s from $\mu^+ \rightarrow e^+ \nu_e \bar{\nu}_\mu$ decay with double-sided Si strip detectors. Two magnetized-iron foils with opposite sign of the analyzing power are used as a polarimeter, followed by 127 BGO ($Bi_4 Ge_3 O_{12}$) crystals to detect both $e^\pm$'s and photons. The asymmetry for two different analyzing foils are compared for the two cases of polarized and unpolarized muons, giving a relative measurement to reduce systematic errors. The goal is to measure $(\xi'' - \xi \xi')/\xi$ to about 0.5%. An engineering run with the complete set up took place in late 1999.

V. LEPTON-FLAVOR-VIOLATING MUON DECAYS

The muon system is one of the best places to search for LFV. In Table VIII, the upper limits of various lepton-flavor-violating decays are listed. The sensitivity to LFV is superb in the muon system, mainly due to the fact that a large number of muons (about $10^{14} - 10^{15}$/year) are available at current experiments. The theoretical frameworks for LFV have already been presented in Sec. III. In this section we review phenomenology and experimental results, and mention the prospects for future improvements in each of the forbidden muon LFV processes. These are $\mu^+ \rightarrow e^+ \gamma$ decay, $\mu^+ \rightarrow e^+ e^+ e^-$ decay, $\mu^- - e^-$ conversion in a muonic atom, $\mu^- - e^+$ conversion, and muonium to antimuonium conversion. In the first three processes, lepton flavors change by one unit ($|\Delta L_i| = 1$).

A. $\mu^+ \rightarrow e^+ \gamma$ decay

1. Phenomenology of $\mu^+ \rightarrow e^+ \gamma$ decay

The most popular process of lepton-flavor-violating muon decay is $\mu^+ \rightarrow e^+ \gamma$. From Eq. (54), the Lagrangian for the $\mu^+ \rightarrow e^+ \gamma$ amplitude is given by

TABLE VIII. Experimental limits for the lepton-flavor-violating decays of the muon, tau, pion, kaon, and Z boson.

Reaction	Present limit	Reference
$\mu^+ \to e^+ \gamma$	$<1.2\times10^{-11}$	Brooks $et\ al.$ (1999)
$\mu^+ \to e^+ e^+ e^-$	$<1.0\times10^{-12}$	Bellgardt $et\ al.$ (1988)
$\mu^- \text{Ti} \to e^- \text{Ti}$	$<6.1\times10^{-13}$	Wintz (1998)
$\mu^+ e^- \to \mu^- e^+$	$<8.3\times10^{-11}$	Willmann $et\ al.$ (1999)
$\tau \to e\gamma$	$<2.7\times10^{-6}$	Edwards $et\ al.$ (1997)
$\tau \to \mu\gamma$	$<3.0\times10^{-6}$	Edwards $et\ al.$ (1997)
$\tau \to \mu\mu\mu$	$<1.9\times10^{-6}$	Bliss $et\ al.$ (1998)
$\tau \to eee$	$<2.9\times10^{-6}$	Bliss $et\ al.$ (1998)
$\pi^0 \to \mu e$	$<8.6\times10^{-9}$	Krolak $et\ al.$ (1994)
$K_L^0 \to \mu e$	$<4.7\times10^{-12}$	Ambrose $et\ al.$ (1998)
$K^+ \to \pi^+ \mu^+ e^-$	$<2.1\times10^{-10}$	Lee $et\ al.$ (1990)
$K_L^0 \to \pi^0 \mu^+ e^-$	$<3.1\times10^{-9}$	Arisaka $et\ al.$ (1998)
$Z^0 \to \mu e$	$<1.7\times10^{-6}$	Akers $et\ al.$ (1995)
$Z^0 \to \tau e$	$<9.8\times10^{-6}$	Akers $et\ al.$ (1995)
$Z^0 \to \tau\mu$	$<1.2\times10^{-5}$	Abreu $et\ al.$ (1997)

$$\mathcal{L}_{\mu \to e\gamma} = -\frac{4G_F}{\sqrt{2}} [m_\mu A_R \overline{\mu_R} \sigma^{\mu\nu} e_L F_{\mu\nu}$$

$$+ m_\mu A_L \overline{\mu_L} \sigma^{\mu\nu} e_R F_{\mu\nu} + \text{H.c.}]. \qquad (100)$$

The differential angular distribution of $\mu^+ \to e^+ \gamma$ decay has already been given in Eq. (92) by

$$\frac{dB(\mu^+ \to e^+ \gamma)}{d(\cos\theta_e)} = 192\pi^2 [|A_R|^2(1 - P_\mu \cos\theta_e)$$

$$+ |A_L|^2(1 + P_\mu \cos\theta_e)], \qquad (101)$$

where θ_e is the angle between the muon polarization and the e^+ momentum vectors. Here P_μ is the magnitude of the muon spin polarization. The branching ratio is given by

$$B(\mu^+ \to e^+ \gamma) = \frac{\Gamma(\mu^+ \to e^+ \gamma)}{\Gamma(\mu^+ \to e^+ \nu\bar{\nu})}$$

$$= 384\pi^2(|A_R|^2 + |A_L|^2). \qquad (102)$$

2. Event signature and backgrounds

The event signature of $\mu^+ \to e^+ \gamma$ decay at rest is a e^+ and a photon in coincidence, moving collinearly back-to-back with their energies equal to half that of the muon mass ($m_\mu/2 = 52.8\,\text{MeV}$). The searches in the past were carried out by using positive muon decay at rest to fully utilize its kinematics. A negative muon cannot be used, since it is captured by a nucleus when it is stopped in a material. There are two major backgrounds to the search for $\mu^+ \to e^+ \gamma$. One is a physics (prompt) background from radiative muon decay, $\mu^+ \to e^+ \nu_e \bar{\nu}_\mu \gamma$, when the e^+ and photon are emitted back to back with the two neutrinos carrying off a small amount of energy. The other background is an accidental coincidence of an e^+ in a normal muon decay, $\mu^+ \to e^+ \nu_e \bar{\nu}_\mu$, accompanied by a high-energy photon. Possible sources of the latter would be either $\mu^+ \to e^+ \nu_e \bar{\nu}_\mu \gamma$ decay, annihilation in

flight, or external bremsstrahlung of e^+'s from normal muon decay. These backgrounds are described in more detail in the following sections.

3. Physics background

One of the major physics backgrounds to the search for $\mu^+ \to e^+ \gamma$ decay is radiative muon decay, $\mu^+ \to e^+ \nu_e \bar{\nu}_\mu \gamma$ (branching ratio=1.4% for $E_\gamma > 10\,\text{MeV}$), when the e^+ and photon are emitted back to back with two neutrinos carrying off a small amount of energy. The differential decay width of this radiative muon decay was calculated as a function of the e^+ energy (E_e) and the photon energy (E_γ) normalized to their maximum energies, namely, $x = 2E_e/m_\mu$ and $y = 2E_\gamma/m_\mu$ (Eckstein and Pratt, 1959; Fronsdal and Überall, 1959). The ranges of x and y are shown in Eq. (50). The kinematic case when $x \approx 1$ and $y \approx 1$ is important as a background to $\mu^+ \to e^+ \gamma$. In the approximation $x \approx 1$, $y \approx 1$, and angle between e^+ and photon ($\theta_{e\gamma}$) of almost 180°, the differential decay width of $\mu^+ \to e^+ \nu_e \bar{\nu}_\mu \gamma$ decay is given by (Kuno and Okada, 1996)

$$d\Gamma(\mu^+ \to e^+ \nu\bar{\nu}\gamma) \cong \frac{G_F^2 m_\mu^5 \alpha}{3 \times 2^8 \pi^4} \Bigg[(1-x)^2(1 - P_\mu \cos\theta_e)$$

$$+ \left(4(1-x)(1-y) - \frac{1}{2}z^2 \right)$$

$$\times (1 + P_\mu \cos\theta_e) \Bigg]$$

$$\times dx\,dy\,z\,dz\,d(\cos\theta_e), \qquad (103)$$

where θ_e is the angle between the muon spin and the e^+ momentum direction. The term G_F is the Fermi coupling constant, α is the fine-structure constant, $z = \pi - \theta_{e\gamma}$, and $\cos z$ is expanded as a polynomial of z, since z is small. In Eq. (103), only the terms of up to second order in $(1-x)$, $(1-y)$, and z are kept. At $x \approx 1$ and

$y \approx 1$, the effect of the positron mass is found to be very small, of the order of $(m_e/m_\mu)^2$, and is therefore neglected in Eq. (103). The first term in Eq. (103) represents the e^+ being emitted preferentially opposite to the muon spin direction, whereas in the second term the e^+ is emitted along the muon-spin direction. When $x=1$ and $y=1$ exactly, this differential decay width vanishes. However, in a real experiment, finite detector resolutions introduce background events that would ultimately limit the sensitivity of a search for $\mu^+ \to e^+ \gamma$.

Given the detector resolution, the sensitivity limitation from this physics background can be estimated by integrating the differential decay width over the signal box. It is given by

$$dB(\mu^+ \to e^+ \nu\bar{\nu}\gamma)$$

$$= \frac{1}{\Gamma(\mu^+ \to e^+ \nu\bar{\nu})} \int_{1-\delta x}^{1} dx \int_{1-\delta y}^{1}$$

$$\times dy \int_0^{\min[\delta z, 2\sqrt{(1-x)(1-y)}]} dz \frac{d\Gamma(\mu^+ \to e^+ \nu\bar{\nu}\gamma)}{dx\, dy\, dz},$$

$$= \frac{\alpha}{16\pi}[J_1 \cdot (1 - P_\mu \cos\theta_e)$$

$$+ J_2 \cdot (1 + P_\mu \cos\theta_e)]d(\cos\theta_e), \qquad (104)$$

where δx, δy, and δz are half-widths of the $\mu^+ \to e^+ \gamma$ signal region for x, y, and z, respectively. Here $\Gamma(\mu^+ \to e^+ \nu\bar{\nu})$ is the total muon decay width, and J_1 and J_2 are given as the sixth power of a combination of δx and δy. For the case of $\delta z > 2\sqrt{\delta x\, \delta y}$, they are given by

$$J_1 = (\delta x)^4 (\delta y)^2 \text{ and } J_2 = \frac{8}{3}(\delta x)^3 (\delta y)^3. \qquad (105)$$

When the angular resolution meets $\delta z \leq 2\sqrt{\delta x\, \delta y}$, they are given by

$$J_1 = \frac{8}{3}(\delta x)^3(\delta y)\left(\frac{\delta z}{2}\right)^2 - 2(\delta x)^2\left(\frac{\delta z}{2}\right)^4$$

$$+ \frac{1}{3}\frac{1}{(\delta y)^2}\left(\frac{\delta z}{2}\right)^8, \qquad (106)$$

$$J_2 = 8(\delta x)^2(\delta y)^2\left(\frac{\delta z}{2}\right)^2 - 8(\delta x)(\delta y)\left(\frac{\delta z}{2}\right)^4$$

$$+ \frac{8}{3}\left(\frac{\delta z}{2}\right)^6. \qquad (107)$$

Experimentally, the resolution of the e^+ energy is better than that of the photon energy, i.e., $\delta x < \delta y$. Moreover, the angular resolution δz has been poor in past experiments. Thereby, from Eq. (105), J_2 is much larger than J_1 in most cases.

Figure 22 shows the fraction of the $\mu^+ \to e^+ \nu_e \bar{\nu}_\mu \gamma$ decay for the given δx and δy values with unpolarized muons in the case of $\delta z \geqslant 2\sqrt{\delta x\, \delta y}$. From Fig. 22, it can be seen that both δx and δy of the order of 0.01 are needed to achieve a sensitivity limit at the level of 10^{-15}.
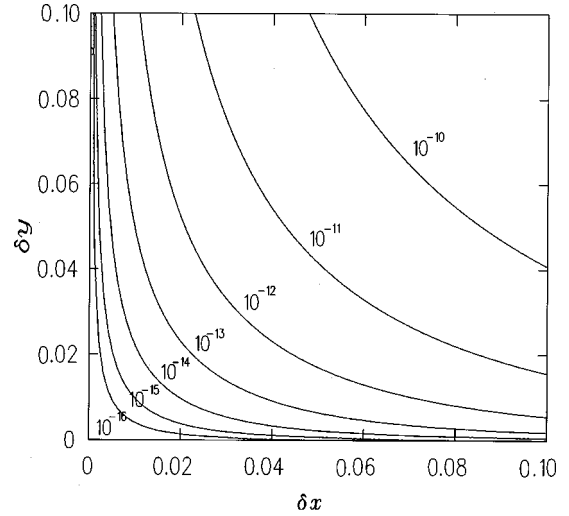
FIG. 22. Effective branching ratio of the physics background from the $\mu^+ \to e^+ \nu_e \bar{\nu}_\mu \gamma$ decay as a function of the e^+ energy resolution δx and photon energy resolution δy. From Kuno and Okada, 1996.

Radiative corrections to radiative muon decay for the case of the physics background to $\mu^+ \to e^+ \gamma$ decay have been calculated to be of the order of several percent, depending on the detector resolution (Arbuzov et al., 1998).

4. Accidental background

With a very high rate of incident muons, the accidental background becomes more important than the physics background. This is usually the case at present experiments and is expected to occur at future experiments as well. The event rate of the accidental background normalized to the total decay rate (B_{acc}) can be estimated by

$$B_{acc} = R_\mu \cdot f_e^0 \cdot f_\gamma^0 \cdot (\Delta t_{e\gamma}) \cdot \left(\frac{\Delta \omega_{e\gamma}}{4\pi}\right), \qquad (108)$$

where R_μ is the instantaneous muon intensity. Here f_e^0 and f_γ^0 are, respectively, the integrated fractions of the spectrum of e^+ and γ in normal muon decay (such as from $\mu^+ \to e^+ \nu_e \bar{\nu}_\mu \gamma$ decay) within the signal region. They include their corresponding branching ratios. The terms $\Delta t_{e\gamma}$ and $\Delta \omega_{e\gamma}$ are, respectively, the full widths of the signal regions for timing coincidence and angular constraint of the back-to-back kinematics.

Given the sizes of the signal region, B_{acc} can be evaluated. Let us take δx, δy, $\delta\theta_{e\gamma}$, and $\delta t_{e\gamma}$ to be, respectively, the half-width of the signal region for e^+, photon energies, angle $\theta_{e\gamma}$, and relative timing between e^+ and photon. Then f_e^0 can be estimated by integrating the Michel spectrum of normal muon decay over $1 - \delta x \leqslant x \leqslant 1$, yielding $f_e^0 \approx 2(\delta x)$. Given the angular resolution, $\delta\theta_{e\gamma}$, the back-to-back resolution ($\Delta\omega_{e\gamma}/4\pi$) is given by $(\Delta\omega_{e\gamma}/4\pi) = (\delta\theta_{e\gamma})^2/4$. As for f_γ^0, if the radiative muon decay $\mu^+ \to e^+ \nu_e \bar{\nu}_\mu \gamma$ is considered as a source of the 52.8-MeV photon, it can be given by integrating Eq. (51)
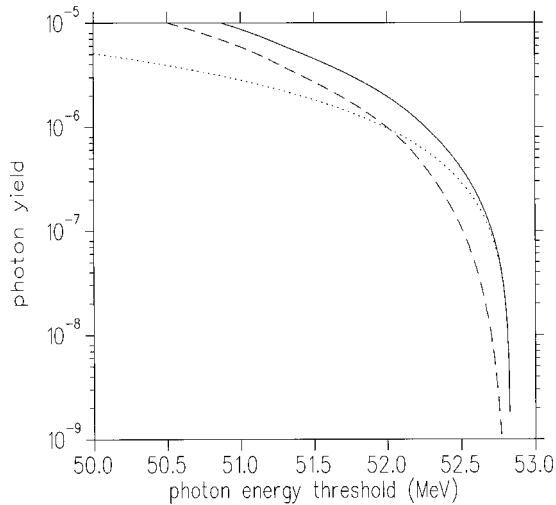
FIG. 23. Integrated rates of backgrounds: dotted line, from annihilation-in-flight; dashed line, from radiative muon decay as a function of the photon energy. The sum of the two is shown by the solid line.
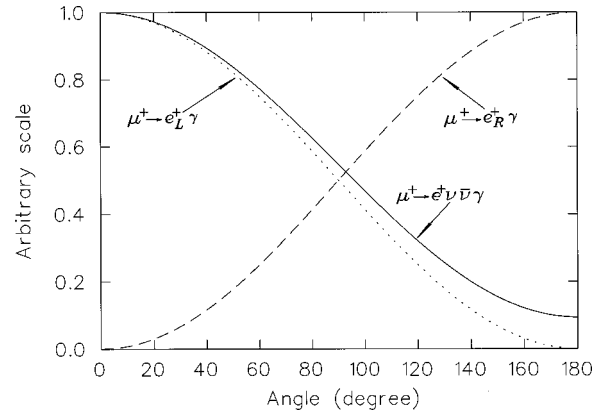

FIG. 24. Angular distribution of e^+ from the physics background of the $\mu^+ \to e^+ \nu_e \bar{\nu}_\mu \gamma$ decay from polarized muons with respect to the muon polarization direction (solid line); dotted line, $\mu^+ \to e_L^+ \gamma$ decay; dashed line, $\mu^+ \to e_R^+ \gamma$ decay. From Kuno and Okada, 1996.

over 2π for θ_γ, and then over the photon energy within the width of the signal region $(1 - \delta y \leqslant y \leqslant 1)$. For unpolarized muons, it is given by

$$f_\gamma^0 = \int_{1-\delta y}^1 dy \int d(\cos\theta_\gamma) \frac{dB(\mu^+ \to e^+ \nu \bar{\nu} \gamma)}{dy\, d(\cos\theta_\gamma)}$$

$$\approx \left(\frac{\alpha}{2\pi}\right)(\delta y)^2[\ln(\delta y) + 7.33]. \tag{109}$$

Equation (109) shows that f_γ^0 for the decay $\mu^+ \to e^+ \nu_e \bar{\nu}_\mu \gamma$ is roughly proportional to $(\delta y)^2$.

The other sources of high-energy photons are annihilation in flight of e^+'s in normal muon decay and external bremsstrahlung. The contribution from annihilation of e^+ in flight depends on the materials along the e^+'s track path. Figure 23 shows, for instance, the contribution of annihilation in flight for the case of e^+'s passing through a muon-stopping target of 50-mg thickness. It indicates that the contribution from the target is smaller than the radiative muon decay, and only becomes important if the photon energy resolution becomes extremely good. However, it is dependent on the total amount of materials in an experimental setup.

From the above, the effective branching ratio of the accidental background is given by

$$B_{acc} = R_\mu \cdot (2\,\delta x) \cdot \left(\frac{\alpha}{2\pi}(\delta y)^2[\ln(\delta y) + 7.33]\right)$$

$$\times \left(\frac{\delta\theta_{e\gamma}^2}{4}\right) \cdot (2\,\delta t_{e\gamma}). \tag{110}$$

For instance, taking some realistic values such as 1% for the e^+ energy resolution [full width at half maximum (FWHM)], a photon energy resolution of 6% (FWHM), $\Delta\omega_{e\gamma} = 3 \times 10^{-4}$ steradian, $\Delta t_{e\gamma} = 1$ ns, and $R_\mu = 3 \times 10^8 \mu^+/s$, B_{acc} is 3×10^{-13}. This shows the accidental background to be severe. Therefore it is critical to make

significant improvements in the detector resolution in order to reduce this background.

5. Muon polarization

The use of polarized muons has been found to be useful in suppressing backgrounds for $\mu^+ \to e^+ \gamma$ searches (Kuno and Okada, 1996; Kuno et al., 1997). For the physical (prompt) background, as already discussed in Sec. V.A.3, the coefficient of J_2 is much larger than J_1, since the resolution of the photon energy is much worse than that of the e^+ energy detection. Therefore the angular distribution of the physics background follows approximately $(1 + P_\mu \cos\theta)$ as long as $\delta y > \delta x$. Figure 24 shows the angular distribution of $\mu^+ \to e^+ \nu_e \bar{\nu}_\mu \gamma$ with, for instance, $\delta y / \delta x = 4$. If we selectively measure the e^+'s in $\mu^+ \to e^+ \gamma$ that move opposite to the muon polarization direction, the background from $\mu^+ \to e^+ \nu_e \bar{\nu}_\mu \gamma$ would be significantly reduced in the search for $\mu^+ \to e_R^+ \gamma$. Furthermore, by varying δx and δy, the angular distribution of the $\mu^+ \to e^+ \nu_e \bar{\nu}_\mu \gamma$ background can change according to Eq. (104), thus providing another means to discriminate the signal from the backgrounds.

Regarding the accidental background, the use of polarized muons has also provided a means for its suppression (Kuno et al., 1997). This is due to the sources of accidental backgrounds having a specific angular distribution when a muon is polarized. For instance, the e^+'s in normal Michel μ^+ decay are emitted preferentially along the muon spin direction, following the $(1 + P_\mu \cos\theta_e)$ distribution described by Eq. (33), whereas the inclusive angular distribution of a high-energy photon (e.g., $\geqslant 50$ MeV) from $\mu^+ \to e^+ \nu_e \bar{\nu}_\mu \gamma$ decay follows the $(1 + P_\mu \cos\theta_\gamma)$ distribution described by Eq. (51), where θ_γ is the angle of the photon direction with respect to the muon spin direction. It should be noted that this inclusive angular distribution was obtained after integrating the energy and direction of the e^+'s, in con-
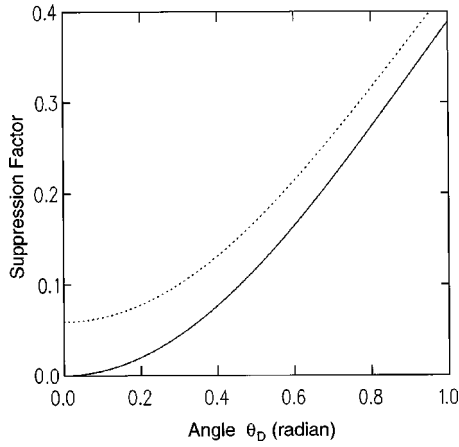
FIG. 25. Suppression factor of the accidental background in a $\mu^+ \to e^+ \gamma$ search as a function of half of the detector opening angle: solid line, 100% muon polarization; dotted line, 97% muon polarization. From Kuno *et al.*, 1997.

trast to the case of the physics background, where only the extreme kinematics of the e^+ and photon being back to back in $\mu^+ \to e^+ \nu_e \bar{\nu}_\mu \gamma$ decay is relevant. In addition, the other sources of high-energy photons, such as external bremsstrahlung and annihilation in flight of e^+'s from the normal muon decay, also follow a $(1 + P_\mu \cos \theta_\gamma)$ distribution.

This inclusive angular distribution of a high-energy photon in $\mu^+ \to e^+ \nu_e \bar{\nu}_\mu \gamma$ implies that the accidental background could be suppressed for $\mu^+ \to e_L^+ \gamma$, where high-energy photons must be detected at the opposite direction to the muon polarization. A similar suppression mechanism of accidental background can be seen for $\mu^+ \to e_R^+ \gamma$ when high-energy positrons are detected in the opposite direction to the muon polarization. As a result, the selective measurements of either e^+'s or photons antiparallel to the muon spin direction would give the same accidental background suppression for $\mu^+ \to e_R^+ \gamma$ and $\mu^+ \to e_L^+ \gamma$ decays, respectively. This favorable situation comes from the fact that the inclusive distributions of both high-energy e^+'s and photons, respectively, in the normal and radiative muon decays follow a $(1 + P_\mu \cos \theta)$ distribution, where θ is either θ_e or θ_γ. The suppression factor η is calculated for polarized muons by

$$\eta \equiv \int_{\cos \theta_D}^1 d(\cos \theta)(1 + P_\mu \cos \theta)$$

$$\times (1 - P_\mu \cos \theta) \bigg/ \int_{\cos \theta_D}^1 d(\cos \theta)$$

$$= (1 - P_\mu^2) + \frac{1}{3} P_\mu^2 (1 - \cos \theta_D)(2 + \cos \theta_D), \quad (111)$$

where θ_D is a half opening angle of detection with respect to the muon polarization direction. The term η is shown in Fig. 25 as a function of θ_D. For instance, for $\theta_D = 300$ mrad, an accidental background can be suppressed to the level of 1/20 (1/10) when P_μ is 100 (97)%.

6. Experimental status of $\mu^+ \to e^+ \gamma$ decay

Experimental searches for $\mu^+ \to e^+ \gamma$ have a long history of more than 50 years. These searches have been actively promoted by intense muon beams available at the meson factories. Experimental efforts have been devoted to improving the detection resolutions of four variables, namely, the positron energy (E_e), the photon energy (E_γ), the timing between the positron and photon ($\Delta t_{e\gamma}$), and the angle between the positron and photon ($\Delta \theta_{e\gamma}$). Various kinds of apparatus have been tried in the past. In Table IX, we list past and present 90%-C.L. upper limits for $\mu^+ \to e^+ \gamma$ decay along with their achieved detection resolutions.

The upper limit quoted by the Particle Data Group (Caso *et al.*, 1998) is $B(\mu^+ \to e^+ \gamma) < 4.9 \times 10^{-11}$, which was obtained by an experiment with the "Crystal Box" detector (Bolton *et al.*, 1988) at Los Alamos National Laboratory (LANL). Its apparatus consisted of 396 NaI(Tl) crystals and cylindrical drift chambers surrounding a muon-stopping target in zero magnetic field.

Since then, a new experimental search for $\mu^+ \to e^+ \gamma$ has been carried out by the MEGA collaboration at LANL. A schematic view of the MEGA spectrometer is shown in Fig. 26. The MEGA detector consists of a magnetic spectrometer for the positron and three concentric pair spectrometers for the photon. They were placed inside a superconducting solenoid magnet of a 1.5-T field. The positron spectrometer comprises eight cylindrical wire chambers and scintillators for timing. The positron energy resolution (FWHM) was from 0.5 MeV (0.95%) to 0.85 MeV (1.6%) for a 52.8-MeV e^+, depending on the number of helical loops of e^+ tracks. For the pair

TABLE IX. Historical progress of search for $\mu^+ \to e^+ \gamma$ since the era of meson factories with 90%-C.L. upper limits. The resolutions quoted are given as a full width at half maximum (FWHM).

Place	Year	ΔE_e	ΔE_γ	$\Delta t_{e\gamma}$	$\Delta \theta_{e\gamma}$	Upper limit	References
TRIUMF	1977	10%	8.7%	6.7 ns		$<3.6 \times 10^{-9}$	Depommier *et al.* (1977)
SIN	1980	8.7%	9.3%	1.4 ns		$<1.0 \times 10^{-9}$	Van der Schaaf *et al.* (1980)
LANL	1982	8.8%	8%	1.9 ns	37mrad	$<1.7 \times 10^{-10}$	Kinnison *et al.* (1982)
LANL	1988	8%	8%	1.8 ns	87mrad	$<4.9 \times 10^{-11}$	Bolton *et al.* (1988)
LANL	1999	1.2%[a]	4.5%[a]	1.6 ns	15mrad	$<1.2 \times 10^{-11}$	Brooks *et al.* (1999)

[a]Shows an average of the numbers given in Brooks *et al.* (1999).
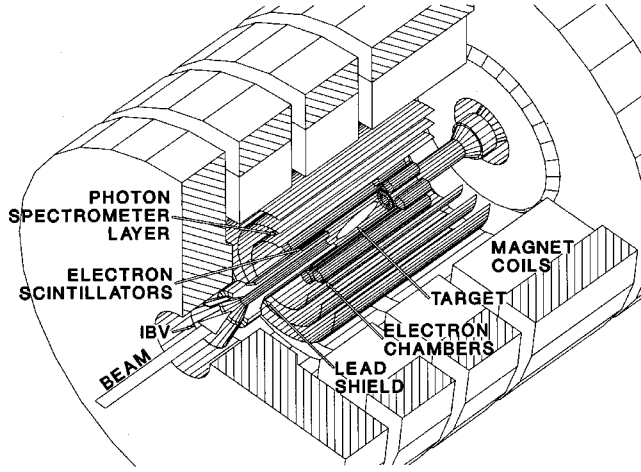
FIG. 26. Schematic layout of the MEGA detector (provided by R. Mischke).

FIG. 27. Kinematics of the $\mu^+ \rightarrow e^+ e^+ e^-$ decay in the muon center-of-mass system, in which $\vec{p}_1$ and $\vec{p}_2$ are the momentum vectors of the two e^+'s and $\vec{p}_3$ is that of the e^-, respectively. Plane I is the decay plane on which $\vec{p}_1$, $\vec{p}_2$, and $\vec{p}_3$ lie. Plane II is the plane in which the muon polarization vectors $\vec{P}$ and $\vec{p}_3$ are located. From Okada, et al., 2000.

spectrometer, each layer had lead converters, multiwire proportional chambers, drift chambers, and scintillators. The photon energy resolutions (FWHM) were 1.7 MeV (3.3%) and 3.0 MeV (5.7%) for the outer and inner Pb conversion layers, respectively. A surface μ^+ beam of 29.8 MeV/c was introduced along the detector axis, and was stopped in the muon-stopping target made of a thin tilted Mylar foil. All of the charged particles from muon decays are confined within the positron spectrometer. The intensity of the muon beam was 2.5×10^8/s with a macroscopic duty factor of 6%. The total number of muons stopped was 1.2×10^{14}. By using the likelihood method, a new limit of 1.2×10^{-11} at 90% C.L. has been reported (Brooks et al., 1999).

Recently, a new experimental proposal, R-99-05, aiming at a sensitivity of 10^{-14} for the $\mu^+ \rightarrow e^+ \gamma$ branching ratio has been approved at PSI (Barkov et al., 1999). This improvement will be obtained by utilizing a continuous muon beam of 100% duty factor at PSI. By keeping the same instantaneous beam intensity as MEGA, the total number of muons available can be increased by a factor of 16. A further improvement is a novel liquid-xenon scintillation detector of the "Mini-Kamiokande" type, which consists of $0.8 \, \text{m}^3$ of liquid xenon viewed by an array of 800 photomultipliers from all sides. The expected resolutions (FWHM) of the photon energy and position are about 1.4% and 4 mm, respectively. As for e^+ detection, a solenoidal magnetic spectrometer with a graded magnetic field is adopted, in which the magnetic field is arranged so that the e^+ from the $\mu^+ \rightarrow e^+ \gamma$ decay follows a trajectory with a constant radius, independent of its emission angle. This allows easier identification of the e^+ in the $\mu^+ \rightarrow e^+ \gamma$ decay. Data collection is expected to start in year 2003.

A search for $\mu^+ \rightarrow e^+ \gamma \gamma$ was also undertaken simultaneously with the $\mu^+ \rightarrow e^+ \gamma$ search, and a 90%-C.L. upper limit of $B(\mu^+ \rightarrow e^+ \gamma \gamma) < 7.2 \times 10^{-11}$ was obtained (Bolton et al., 1988).
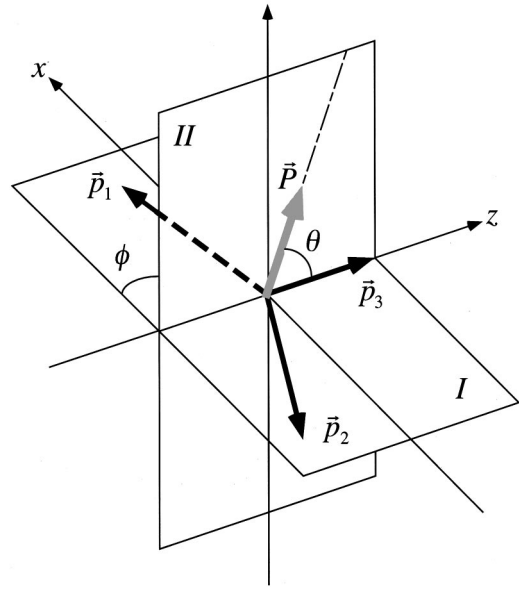
B. $\mu^+ \rightarrow e^+ e^+ e^-$ decay

1. Phenomenology of $\mu^+ \rightarrow e^+ e^+ e^-$ decay

The decay width of $\mu^+ \rightarrow e^+ e^+ e^-$ is determined from the effective Lagrangian (at the scale of m_μ) described by Eqs. (54) and (58) in Sec. III. The relevant interactions are

$$
\begin{aligned}
\mathcal{L}_{\mu \rightarrow eee} = & -\frac{4 G_F}{\sqrt{2}} [m_\mu A_R \overline{\mu_R} \sigma^{\mu\nu} e_L F_{\mu\nu} \\
& + m_\mu A_L \overline{\mu_L} \sigma^{\mu\nu} e_R F_{\mu\nu} + g_1 (\overline{\mu_R} e_L)(\overline{e_R} e_L) \\
& + g_2 (\overline{\mu_L} e_R)(\overline{e_L} e_R) + g_3 (\overline{\mu_R} \gamma^\mu e_R)(\overline{e_R} \gamma_\mu e_R) \\
& + g_4 (\overline{\mu_L} \gamma^\mu e_L)(\overline{e_L} \gamma_\mu e_L) + g_5 (\overline{\mu_R} \gamma^\mu e_R) \\
& \times (\overline{e_L} \gamma_\mu e_L) + g_6 (\overline{\mu_L} \gamma^\mu e_L)(\overline{e_R} \gamma_\mu e_R) \\
& + \text{H.c.}],
\end{aligned} \tag{112}
$$

where the f_{E0} and f_{M0} photonic contributions in Eq. (55) are included in the four-fermion coupling constants.

When muons are polarized, the kinematics of the $\mu^+ \rightarrow e^+ e^+ e^-$ decay is determined by two energy variables and two angle variables of the decay positrons (Okada et al., 1998, 2000). The energy variables are $x_1 = 2E_1/m_\mu$ and $x_2 = 2E_2/m_\mu$, where E_1 (E_2) is the higher (lower) energy of the decay positrons. The allowed regions of x_1 and x_2 are $\frac{1}{2} \leq x_1 \leq 1$ and $1 - x_1 \leq x_2 \leq x_1$, if m_e is neglected compared to m_μ. Let us take the coordinate system shown in Fig. 27, where the z

axis is in the direction of the decay electron momentum ($\vec{p_3}$), and the $z-x$ plane is the decay plane. The positive direction of the x axis is chosen to be in the hemisphere of the higher-energy positron. The two angles (θ, φ) determine the direction of the muon polarization ($\vec{P}_\mu$) with respect to the decay plane.

In this coordinate system, the differential branching ratio of the decay $\mu^+ \rightarrow e^+ e^+ e^-$ is given by

$$
\begin{aligned}
\frac{dB(\mu^+ \rightarrow e^+ e^+ e^-)}{dx_1\, dx_2\, d(\cos\theta)\, d\varphi} = \frac{3}{2\pi} [\, & C_1 \alpha_1(x_1, x_2)(1 + P_\mu \cos\theta) + C_2 \alpha_1(x_1, x_2)(1 - P_\mu \cos\theta) + C_3\{\alpha_2(x_1, x_2) \\
& + P_\mu \beta_1(x_1, x_2)\cos\theta + P_\mu \gamma_1(x_1, x_2)\sin\theta\cos\varphi\} + C_4\{\alpha_2(x_1, x_2) - P_\mu \beta_1(x_1, x_2)\cos\theta \\
& - P_\mu \gamma_1(x_1, x_2)\sin\theta\cos\varphi\} + C_5\{\alpha_3(x_1, x_2) + P_\mu \beta_2(x_1, x_2)\cos\theta + P_\mu \gamma_2(x_1, x_2)\sin\theta\cos\varphi\} \\
& + C_6\{\alpha_3(x_1, x_2) - P_\mu \beta_2(x_1, x_2)\cos\theta - P_\mu \gamma_2(x_1, x_2)\sin\theta\cos\varphi\} \\
& + C_7\{\alpha_4(x_1, x_2)(1 - P_\mu \cos\theta) + P_\mu \gamma_3(x_1, x_2)\sin\theta\cos\varphi\} + C_8\{\alpha_4(x_1, x_2)(1 + P_\mu \cos\theta) \\
& - P_\mu \gamma_3(x_1, x_2)\sin\theta\cos\varphi\} + C_9\{\alpha_5(x_1, x_2)(1 + P_\mu \cos\theta) - P_\mu \gamma_4(x_1, x_2)\sin\theta\cos\varphi\} \\
& + C_{10}\{\alpha_5(x_1, x_2)(1 - P_\mu \cos\theta) + P_\mu \gamma_4(x_1, x_2)\sin\theta\cos\varphi\} + C_{11}P_\mu \gamma_3(x_1, x_2)\sin\theta\sin\varphi \\
& - C_{12}P_\mu \gamma_4(x_1, x_2)\sin\theta\sin\varphi\,],
\end{aligned}
\tag{113}
$$

where P_μ is the magnitude of the polarization vector. The functions α_i, β_i, and γ_i are presented in Appendix C. The coefficients C_i are expressed by g_i ($i = 1$–6), A_L, and A_R. They are given by

$$C_1 = \frac{|g_1|^2}{16} + |g_3|^2, \quad C_2 = \frac{|g_2|^2}{16} + |g_4|^2,$$

$$C_3 = |g_5|^2, \quad C_4 = |g_6|^2, \quad C_5 = |eA_R|^2, \quad C_6 = |eA_L|^2,$$

$$C_7 = \mathrm{Re}(eA_R g_4^*), \quad C_8 = \mathrm{Re}(eA_L g_3^*),$$

$$C_9 = \mathrm{Re}(eA_R g_6^*), \quad C_{10} = \mathrm{Re}(eA_L g_5^*),$$

$$C_{11} = \mathrm{Im}(eA_R g_4^* + eA_L g_3^*),$$

$$C_{12} = \mathrm{Im}(eA_R g_6^* + eA_L g_5^*). \tag{114}$$

In Eq. (113), there are four types of contribution which each have different angular dependences with respect to the muon polarization. They may be categorized as isotropic angular distributions (with even parity P and time-reversal T), $\cos\theta$ or $\sin\theta\cos\varphi$ distributions (which are P odd and T even), and those proportional to $\sin\theta\sin\varphi$ (which are P even and T odd).

The integrated branching ratio and the T-odd asymmetry for the decay $\mu^+ \rightarrow e^+ e^+ e^-$ are given by (Okada *et al.*, 2000)

$$
\begin{aligned}
B(\mu^+ \rightarrow e^+ e^+ e^-) = & \int_{\frac{1}{2}}^{1} dx_1 \int_{1-x_1}^{x_1} dx_2 \int_{-1}^{1} d(\cos\theta) \\
& \times \int_0^\pi d\phi \frac{dB(\mu^+ \rightarrow e^+ e^+ e^-)}{dx_1\, dx_2\, d(\cos\theta)\, d\phi}, \\
= & 2(C_1 + C_2) + (C_3 + C_4)
\end{aligned}
$$

$$+ 32 \left[\ln\left(\frac{m_\mu^2}{m_e^2}\right) - \frac{11}{4} \right](C_5 + C_6)$$

$$+ 16(C_7 + C_8) + 8(C_9 + C_{10}), \tag{115}$$

$$
\begin{aligned}
A_T(\mu^+ \rightarrow e^+ e^+ e^-) = & \frac{1}{P_\mu B(\mu^+ \rightarrow e^+ e^+ e^-)} \\
& \times \Bigg[\int_{\frac{1}{2}}^{1} dx_1 \int_{1-x_1}^{x_1} dx_2 \int_{-1}^{1} d(\cos\theta) \\
& \times \int_0^\pi d\phi \frac{dB(\mu^+ \rightarrow e^+ e^+ e^-)}{dx_1\, dx_2\, d(\cos\theta)\, d\phi} \\
& - \int_{\frac{1}{2}}^{1} dx_1 \int_{1-x_1}^{x_1} dx_2 \int_{-1}^{1} d\cos\theta \\
& \times \int_\pi^{2\pi} d\phi \frac{dB(\mu^+ \rightarrow e^+ e^+ e^-)}{dx_1\, dx_2\, d(\cos\theta)\, d\phi} \Bigg] \\
= & \frac{64}{35} \frac{1}{B(\mu^+ \rightarrow e^+ e^+ e^-)} (3C_{11} - 2C_{12}).
\end{aligned}
\tag{116}
$$

The T-odd asymmetry turns out to be proportional to $(3C_{11} - 2C_{12})$. It arises from interference between the on-shell photon-penguin terms and the four-fermion terms.

If only photon-penguin diagrams contribute to $\mu^+ \rightarrow e^+ e^+ e^-$ decay (namely, the case of $C_5 \neq 0$, $C_6 \neq 0$, with the remainder zero), a model-independent relation between the two branching ratios can be derived, as follows:

TABLE X. Historical progress and summary of searches for $\mu^+ \rightarrow e^+ e^+ e^-$ decay.

Place	Year	90%-C.L. upper limit	Reference
JINR	1976	$< 1.9 \times 10^{-9}$	Korenchenko et al. (1976)
LANL	1984	$< 1.3 \times 10^{-10}$	Bolton et al. (1984)
SIN	1984	$< 1.6 \times 10^{-10}$	Bertl et al. (1984)
SIN	1985	$< 2.4 \times 10^{-12}$	Bertl et al. (1985)
LANL	1988	$< 3.5 \times 10^{-11}$	Bolton et al. (1988)
SIN	1988	$< 1.0 \times 10^{-12}$	Bellgardt et al. (1988)
JINR	1991	$< 3.6 \times 10^{-11}$	Baranov et al. (1991)

$$\frac{B(\mu^+ \rightarrow e^+ e^+ e^-)}{B(\mu^+ \rightarrow e^+ \gamma)} \simeq \frac{\alpha}{3\pi} \left[\ln\left(\frac{m_\mu^2}{m_e^2}\right) - \frac{11}{4} \right] = 0.006. \tag{117}$$

2. Event signature and backgrounds

The event signature of the decay $\mu^+ \rightarrow e^+ e^+ e^-$ is kinematically well constrained, since all particles in the final state are detectable. Muon decay at rest has been used in all past experiments. In this case, the conservation of momentum ($|\Sigma_i \vec{p}_i| = 0$) and energy ($\Sigma_i E_i = m_\mu$) could be effectively used together with the timing coincidence between two e^+'s and one e^-, where $\vec{p}_i$ and E_i ($i = 1-3$) are, respectively, the momentum and energy of each of the e's.

One of the physics background processes is the allowed muon decay $\mu^+ \rightarrow e^+ e^+ e^- \nu_e \bar{\nu}_\mu$, which becomes a serious background when ν_e and $\bar{\nu}_\mu$ have very small energies. Its branching ratio is $(3.4 \pm 0.4) \times 10^{-5}$. The other background is an accidental coincidence of an e^+ from normal muon decay with an uncorrelated $e^+ e^-$ pair, where an $e^+ e^-$ pair could be produced either from Bhabha scattering of e^+, or from the external conversion of the photon in $\mu^+ \rightarrow e^+ \nu_e \bar{\nu}_\mu \gamma$ decay. Since the $e^+ e^-$ pair from photon conversion has a small invariant mass, it could be removed by eliminating events with a small opening angle between e^+ and e^-. This, however, causes a loss in signal sensitivity, in particular for theoretical models in which $\mu^+ \rightarrow e^+ e^+ e^-$ decay occurs mostly through photonic diagrams.

The other background, which comes mainly at the trigger level, comprises fake events with an e^+ curling back to the target, which mimics an $e^+ e^-$ pair. For this background, an $e^+ e^-$ pair forms a relative angle of $180°$, and can therefore be rejected.

3. Experimental status of $\mu^+ \rightarrow e^+ e^+ e^-$ decay

After the pioneering measurement in 1976 using a cylindrical spectrometer, which gave an upper limit of $B(\mu^+ \rightarrow e^+ e^+ e^-) < 1.9 \times 10^{-9}$ (Korenchenko et al., 1976) various experiments to search for $\mu^+ \rightarrow e^+ e^+ e^-$ decay have been carried out, as shown in Table X. In particular, a series of experimental measurements with the SINDRUM magnetic spectrometer at SIN (Bertl et al., 1984, 1985; Bellgardt et al., 1988) were carried out. A surface μ^+ beam with $5 \times 10^6 \mu^+$/s was used, and the muons were stopped in a hollow double-cone target. The e^+'s

and e^-'s were tracked by the SINDRUM spectrometer, which consisted of five concentric multiwire proportional chambers and a cylindrical array of 64 plastic scintillation counters under a solenoid magnetic field of 0.33 T. The momentum resolution was $\Delta p/p = (12.0 \pm 0.3)\%$ (FWHM) at $p = 50$ MeV/c. This experiment gave a 90%-C.L. upper limit of $B(\mu^+ \rightarrow e^+ e^+ e^-) < 1.0 \times 10^{-12}$, assuming a constant matrix element for the $\mu^+ \rightarrow e^+ e^+ e^-$ decay (Bellgardt et al., 1988). They also observed 9070 ± 10 events of $\mu^+ \rightarrow e^+ e^+ e^- \nu_e \bar{\nu}_\mu$ decay. A detailed analysis of the differential decay rate of $\mu^+ \rightarrow e^+ e^+ e^- \nu_e \bar{\nu}_\mu$ decay was studied, and was found to be consistent with the $V - A$ interaction (Kersch et al., 1988).

Another recent experiment to search for $\mu^+ \rightarrow e^+ e^+ e^-$ was performed at the Joint Institute for Nuclear Research (JINR), Dubna, Russia (Baranov et al., 1991). A magnetic 4π spectrometer with cylindrical proportional chambers was used. They obtained an upper limit of 90% C.L. of $B(\mu^+ \rightarrow e^+ e^+ e^-) < 3.6 \times 10^{-11}$, where the matrix element of $\mu^+ \rightarrow e^+ e^+ e^-$ was assumed to be constant.

C. $\mu^- - e^-$ coherent conversion in a muonic atom

1. Phenomenology of $\mu^- - e^-$ conversion

Another prominent process concerning lepton flavor violation is $\mu^- - e^-$ conversion in a muonic atom. When a negative muon is stopped in some material, it is trapped by an atom and forms a muonic atom. After it cascades down the energy levels in the muonic atom, a muon is bound in its $1s$ ground state. The fate of the muon is then either decay in an orbit ($\mu^- \rightarrow e^- \nu_\mu \bar{\nu}_e$) or capture by a nucleus of mass number A and atomic number Z, namely,

$$\mu^- + (A,Z) \rightarrow \nu_\mu + (A, Z-1). \tag{118}$$

However, in the context of physics beyond the standard model, the exotic process of neutrinoless muon capture, such as

$$\mu^- + (A,Z) \rightarrow e^- + (A,Z), \tag{119}$$

is also expected. This process is called $\mu^- - e^-$ conversion in a muonic atom. It violates the conservation of the lepton flavor numbers, L_e and L_μ, by one unit, but conserves the total lepton number, L.

The branching ratio of $\mu^- - e^-$ conversion can be expressed as

$$B[\mu^- + (A,Z) \to e^- + (A,Z)]$$

$$\equiv \frac{\Gamma[\mu^- + (A,Z) \to e^- + (A,Z)]}{\Gamma[\mu^- + (A,Z) \to \text{capture}]},$$

(120)

where Γ is the corresponding decay width.

The final state of the nucleus (A,Z) could be either the ground state or an excited state. In general, the transition to the ground state is dominant, since it is a coherent process where the initial and final nuclear states are the same. The rate of the coherent conversion process over noncoherent ones is enhanced by a factor approximately equal to the number of nucleons in the nucleus, since all of the nucleons participate in the process.

The possible contributions to $\mu^- - e^-$ conversion in a muonic atom can be grouped into two parts: the photonic contribution and the nonphotonic contribution. Therefore, in principle, this process is theoretically interesting, since it occurs by mechanisms which do not contribute to the $\mu^+ \to e^+ \gamma$ process. The study of the photonic contribution was initiated by Weinberg and Feinberg (1959). The nonphotonic contribution was studied later, for instance, by Marciano and Sanda (1977b).

Let us first discuss the photonic transition whose effective Lagrangian is written as

$$\mathcal{L}_{photo} = -e J^\mu_{photo} A_\mu.$$

(121)

The matrix element of the $\mu^-(p_\mu) \to e^-(p_e) \gamma^*(q)$ transition, where p_μ, p_e, and $q = p_\mu - p_e$ are the muon, electron, and virtual photon four-momenta, respectively, is given by

$$M_{photonic} = -e A^*_\mu(q) \langle e^-(p_e) | J^\mu_{photo}(0) | \mu^-(p_\mu) \rangle$$

$$= -e A^*_\mu(q) \bar{u}_e(p_e) \left[(f_{E0}(q^2) \right.$$

$$+ \gamma_5 f_{M0}(q^2)) \gamma_\nu \left(g^{\mu\nu} - \frac{q^\mu q^\nu}{q^2} \right) + (f_{M1}(q^2)$$

$$\left. + \gamma_5 f_{E1}(q^2)) \frac{i \sigma_{\mu\nu} q^\nu}{m_\mu} \right] u_\mu(p_\mu).$$

(122)

Based on Eq. (122), the branching ratio of the coherent $\mu^- - e^-$ conversion through the photonic contribution is given by (Weinberg and Feinberg, 1959)

$$B(\mu^- N \to e^- N) = (8 \alpha^5 m_\mu Z^4_{eff} Z F^2_p \xi^2) \cdot \frac{1}{\Gamma_{capt}}, \quad (123)$$

where Γ_{capt} is the total muon capture rate. Here ξ^2 is given by

$$\xi^2 = |f_{E0}(-m^2_\mu) + f_{M1}(-m^2_\mu)|^2 + |f_{E1}(-m^2_\mu)$$

$$+ f_{M0}(-m^2_\mu)|^2.$$

(124)

We note that in the photonic diagrams, in contrast to $\mu^+ \to e^+ \gamma$, not only f_{E1} and f_{M1}, but also f_{E0} and f_{M0}

can contribute to the $\mu^- - e^-$ conversion. The term Z_{eff} is an effective atomic charge obtained by averaging the muon wave function over the nuclear density (Chiang et al., 1993). This is defined as

$$\frac{\alpha^3 m^3_\mu}{\pi} \frac{Z^4_{eff}}{Z} = \int d^3 x |\Phi_\mu(\vec{x})|^2 \rho_p(\vec{x}) \equiv \langle \Phi_{1s} \rangle^2, \quad (125)$$

where $\Phi_\mu(\vec{x})$ is the nonrelativistic muon wave function for the $1s$ state of the muonic atom and $\rho_p(\vec{x})$ is the proton density in the nucleus normalized as

$$\int d^3 x \, \rho_p(\vec{x}) = 1.$$

(126)

Moreover, F^2_p is the nuclear matrix element squared, given by

$$F_p = \int d^3 x \, e^{-i\vec{p}_e \cdot \vec{x}} \rho_p(\vec{x}) = 4\pi \int \rho_p(r) \frac{\sin m_\mu r}{m_\mu r} r^2 \, dr, \quad (127)$$

where an isotropic proton density in the nucleus is assumed in the second equation in Eq. (127). In Eq. (123), the $\mu^- - e^-$ conversion process is roughly proportional to $(Z_{eff})^4 Z$, whereas the normal muon capture, Γ_{capt}, is proportional to $(Z_{eff})^4$. The enhancement by a factor of Z in the $\mu^- - e^-$ coherent conversion is evident.

Let us next discuss the nonphotonic contribution. The general four-fermion interaction of $\mu^- - e^-$ conversion at the quark level is given by Eq. (59).

At first, this effective Lagrangian at the quark level is converted into that at the nucleon level by using the nucleon form factors (Vergados, 1986; Bernabeu et al., 1993; Faessler et al., 1999). Since the momentum transfer in the $\mu^- - e^-$ conversion process is smaller than the size of the nucleon structure, the momentum dependence of the nucleon form factors can be neglected. In such a case, the matrix element of the quark currents can be replaced by the corresponding nucleon current by using

$$\langle p | \bar{q} \Gamma_K q | p \rangle = G^{(q,p)}_K \bar{p} \Gamma_K p,$$

$$\langle n | \bar{q} \Gamma_K q | n \rangle = G^{(q,n)}_K \bar{n} \Gamma_K n, \quad (128)$$

with $\Gamma_K = (1, \gamma_5, \gamma_\mu, \gamma_\mu \gamma_5, \sigma_{\mu\nu})$ for $K = (S,P,V,A,T)$. For the vector current, $G^{(u,p)}_V = G^{(d,n)}_V = 2$ and $G^{(d,p)}_V = G^{(u,n)}_V = 1$. In general, the isospin invariance requires the relations $G^{(u,p)}_K = G^{(d,n)}_K$, $G^{(u,p)}_K = G^{(d,n)}_K$, and $G^{(s,p)}_K = G^{(s,n)}_K$. The effective Lagrangian at the nucleon level is given by

$$\mathcal{L}_{non-photo} = -\frac{G_F}{\sqrt{2}}\Bigg[\overline{e_L}\mu_R\overline{\Psi}\{(g_{LS}^{(0)}+g_{LS}^{(1)}\tau_3)+(g_{LP}^{(0)}+g_{LP}^{(1)}\tau_3)\gamma_5\}\Psi+\overline{e_R}\mu_L\overline{\Psi}\{(g_{RS}^{(0)}+g_{RS}^{(1)}\tau_3)+(g_{RP}^{(0)}+g_{RP}^{(1)}\tau_3)\gamma_5\}\Psi$$

$$+\overline{e_L}\gamma^\mu\mu_L\overline{\Psi}\gamma_\mu\{(g_{LV}^{(0)}+g_{LV}^{(1)}\tau_3)+(g_{LA}^{(0)}+g_{LA}^{(1)}\tau_3)\gamma_5\}\Psi+\overline{e_R}\gamma^\mu\mu_R\overline{\Psi}\gamma_\mu\{(g_{RV}^{(0)}+g_{RV}^{(1)}\tau_3)+(g_{RA}^{(0)}$$

$$+g_{RA}^{(1)}\tau_3)\gamma_5\}\Psi+\frac{1}{2}\overline{e_L}\sigma^{\mu\nu}\mu_R\overline{\Psi}\sigma_{\mu\nu}\{(g_{LT}^{(0)}+g_{LT}^{(1)}\tau_3)\}\Psi+\frac{1}{2}\overline{e_R}\sigma^{\mu\nu}\mu_L\overline{\Psi}\sigma_{\mu\nu}\{(g_{RT}^{(0)}+g_{RT}^{(1)}\tau_3)\}\Psi+\text{H.c.}\Bigg],$$

(129)

where $\Psi=(p,n)^T$ and the isoscalar and isovector coupling constants $g_{XK}^{(0)}$ and $g_{XK}^{(1)}$ ($X=L,R$, and $K=S,P,V,A,T$) are, respectively, given by

$$g_{XK}^{(0)}=\frac{1}{2}\sum_{q=u,d,s}(g_{XK(q)}G_K^{(q,p)}+g_{XK(q)}G_K^{(q,n)}),\quad(130)$$

$$g_{XK}^{(1)}=\frac{1}{2}\sum_{q=u,d,s}(g_{XK(q)}G_K^{(q,p)}-g_{XK(q)}G_K^{(q,n)}).\quad(131)$$

For coherent μ^--e^- conversion, only the scalar and vector coupling constants can be kept. By using a non-relativistic approximation for the muon wave function, the transition rate becomes

$$B(\mu^-N\to e^-N)=\frac{p_eE_eG_F^2}{8\pi}[|X_L(p_e)|^2$$

$$+|X_R(p_e)|^2]\frac{1}{\Gamma_{capt}},\quad(132)$$

where

$$X_L(p_e)=(g_{LS}^{(0)}+g_{LS}^{(1)}+g_{LV}^{(0)}+g_{LV}^{(1)})ZM_p(p_e)$$

$$+(g_{LS}^{(0)}-g_{LS}^{(1)}+g_{LV}^{(0)}-g_{LV}^{(1)})NM_n(p_e),\quad(133)$$

$$X_R(p_e)=(g_{RS}^{(0)}+g_{RS}^{(1)}+g_{RV}^{(0)}+g_{RV}^{(1)})ZM_p(p_e)$$

$$+(g_{RS}^{(0)}-g_{RS}^{(1)}+g_{RV}^{(0)}-g_{RV}^{(1)})NM_n(p_e),\quad(134)$$

and $N\equiv A-Z$ is the number of neutrons in the nuclei. Here $M_p(p)$ and $M_n(p)$ are given by

$$M_p(p)=\int d^3x\,e^{-i\vec{p}\cdot\vec{x}}\rho_p(\vec{x})\Phi_\mu(\vec{x}),$$

$$M_n(p)=\int d^3x\,e^{-i\vec{p}\cdot\vec{x}}\rho_n(\vec{x})\Phi_\mu(\vec{x}),\quad(135)$$

with the proton and neutron densities, $\rho_p(\vec{x})$ and $\rho_n(\vec{x})$, normalized to unity. If it is assumed that the proton and neutron densities are equal and that the muon wave function does not change very much in the nucleus, by using Eq. (125), Eq. (132) can be transformed into

$$B(\mu^-N\to e^-N)$$

$$=\frac{p_eE_em_\mu^3G_F^2\alpha^3Z_{eff}^4F_p^2}{8\pi^2Z}\{|(Z+N)(g_{LS}^{(0)}+g_{LV}^{(0)})$$

$$+(Z-N)(g_{LS}^{(1)}+g_{LV}^{(1)})|^2+|(Z+N)(g_{RS}^{(0)}+g_{RV}^{(0)})$$

$$+(Z-N)(g_{RS}^{(1)}+g_{RV}^{(1)})|^2\}\cdot\frac{1}{\Gamma_{capt}}.\quad(136)$$

This equation corresponds to Eq. (123) for the photonic case, which was derived in a similar approximation. In Eq. (136), the coherent process is enhanced by a factor equal to the number of nucleons, as can be seen in Eq. (123).

In general, both photonic and nonphotonic contributions might exist. If the nonrelativistic approximation for the muon wave function is used and the momentum transfer of q^2 is replaced by $-m_\mu^2$, the photonic contribution can be regarded as additional terms in the vector coupling constants. They are given by

$$\Delta g_{LV}^{(0)}=\Delta g_{LV}^{(1)}=\frac{2\sqrt{2}\alpha\pi}{G_Fm_\mu^2}(f_{E0}(-m_\mu^2)+f_{M1}(-m_\mu^2)$$

$$+f_{M0}(-m_\mu^2)+f_{E1}(-m_\mu^2)),\quad(137)$$

$$\Delta g_{RV}^{(0)}=\Delta g_{RV}^{(1)}=\frac{2\sqrt{2}\alpha\pi}{G_Fm_\mu^2}(f_{E0}(-m_\mu^2)+f_{M1}(-m_\mu^2)$$

$$-f_{M0}(-m_\mu^2)-f_{E1}(-m_\mu^2)).\quad(138)$$

These contributions must be added to the corresponding vector coupling constants in Eq. (136). In such a case, the interference terms have been taken into account as well.

So far, the nonrelativistic approximation for the muon wave function and a plane wave for the emitted electron have been used to derive the μ^--e^- conversion rates. Possible corrections for this approximation turn out to be important for heavy nuclei. A relativistic treatment based on the Dirac equation was considered and the corrections to the Weinberg-Feinberg formulas were calculated (Shanker, 1979). Recently, the photonic transitions due to f_{M1} and f_{E1} were further examined by properly treating the electric potential in the muonic atom (Czarnecki *et al.*, 1997).

In the case that the photonic contributions of $f_{E1}(q^2)$ and $f_{M1}(q^2)$ dominate over the other contributions, the rate of μ^--e^- conversion can be parametrized by (Czarnecki *et al.*, 1997)

$$B(\mu^-N\to e^-N)=3\times10^{12}(|f_{E1}|^2+|f_{M1}|^2)B(A,Z),\quad(139)$$

where $B(A,Z)$ represents the rate dependence on the mass number (A) and the atomic number (Z) of the target nucleus. This particular case becomes important, for instance, in $SO(10)$ SUSY GUT models. The values of $B(A,Z)$, based on different approximations, are

TABLE XI. Z dependence of the photonic contribution in the $\mu^- - e^-$ conversion estimated by various theoretical models. After Czarnecki et al. (1997).

Models	Al	Ti	Pb	Reference
$B_{WF}(A,Z)$	1.2	2.0	1.6	Weinberg and Feinberg (1959)
$B_S(A,Z)$	1.3	2.2	2.2	Shanker (1979)
$B_{CMK}(A,Z)$	1.1	1.8	1.25	Czarnecki et al. (1997)

tabulated in Table XI, where $B_{WF}(A,Z)$ is from the Weinberg-Feinberg approximation (Weinberg and Feinberg, 1959), $B_S(A,Z)$ is from Shanker (1979), and $B_{CMK}(A,Z)$ is from Czarnecki et al. (1997). From Eq. (139), the ratio of $B(\mu^+\rightarrow e^+\gamma)/B(\mu^- N\rightarrow e^- N)$ is given by

$$\frac{B(\mu^+\rightarrow e^+\gamma)}{B(\mu^- N\rightarrow e^- N)} = \frac{96\pi^3\alpha}{G_F^2 m_\mu^4}\cdot\frac{1}{3\times 10^{12} B(A,Z)}$$

$$\sim \frac{428}{B(A,Z)}. \tag{140}$$

By using the values in Table XI, the ratio $B(\mu^+\rightarrow e^+\gamma)/B(\mu^- N\rightarrow e^- N)$ for different target nuclei can be calculated. One obtains a value of 389 for ^{27}Al, 238 for ^{48}Ti, and 342 for ^{208}Pb. This result indicates that the rate of $\mu^- - e^-$ conversion has a maximum around the medium nuclei ($A\approx 60$), and flattens out or slightly decreases for heavy nuclei. However, the calculations, which took into account the nuclear effect, show a different Z dependence (Chiang et al., 1993; Kosmas and Vergados, 1996; Kosmas et al., 1998).

The $\mu^- - e^-$ conversion rates to the ground state and all excited states have been calculated by either the shell-model closure approximation (Kosmas et al., 1990) or the quasiparticle random-phase approximation (Kosmas et al., 1994). The fraction of the coherent transition to the ground state is dominant. It was calculated specifically for ^{48}Ti to be (95–99)% in the quasiparticle random-phase approximation, which is even larger than in the shell-model closure approximation. Since the transition to excited states is small, possible background associated with deexcitation from those excited states can be minimized. It was also found that among the transitions to excited states, the dipole 1^- state is large both in the photonic and nonphotonic contributions (Kosmas et al., 1994).

2. Event signature and backgrounds

The event signature of the coherent $\mu^- - e^-$ conversion in a muonic atom is a monoenergetic single electron emitted from the conversion with an energy of

$$E_{\mu e} = m_\mu - B_\mu - E_{rec}^0$$

$$\approx m_\mu - B_\mu, \tag{141}$$

where m_μ is the muon mass, and B_μ and E_{rec}^0 are the binding energy of the $1s$ muonic atom and the nuclear-recoil energy, respectively. The nuclear-recoil energy is approximately $E_{rec}^0\approx (m_\mu - B_\mu)^2/(2M_A)$, where M_A is the mass of the recoiling nucleus, which is small. Since B_μ is different for various nuclei, the peak energy of the $\mu^- - e^-$ conversion signal changes. For instance, it varies from $E_{\mu e}=104.3$ MeV for titanium to $E_{\mu e}=94.9$ MeV for lead.

From an experimental point of view, $\mu^- - e^-$ conversion is very attractive. First, the e^- energy of about 105 MeV is far above the end-point energy of the muon decay spectrum (~ 52.8 MeV). Second, since the event signature is a monoenergetic electron, no coincidence measurement is required. The search for this process has the potential to improve the sensitivity by using a high muon rate without suffering from accidental background, which would be serious background for other processes, such as $\mu^+\rightarrow e^+\gamma$ and $\mu^+\rightarrow e^+ e^+ e^-$ decays.

One of the major backgrounds is muon decay in orbit from a muonic atom (also called a bound-muon decay), in which the e^- end-point energy is the same as the energy of the signal. It is discussed in more detail in Sec. V.C.3. The other background sources are (i) radiative pion capture ($\pi^- + (A,Z)\rightarrow(A,Z-1)+\gamma$) or radiative muon captures ($\mu^- + (A,Z)\rightarrow\nu_\mu + (A,Z-1)+\gamma$) followed by internal and external asymmetric $e^+ e^-$ conversion of the photon ($\gamma\rightarrow e^+ e^-$) with e^+ undetected, (ii) electrons in the beam scattering off the target, (iii) muon decay in flight, and (iv) cosmic rays. To eliminate the backgrounds from pions and electrons, the purity of the beam is crucial. Moreover, a highly efficient veto is needed for the cosmic-ray background.

The kinematical endpoint (E_{rmc}^{kin}) of radiative muon capture is given by

$$E_{rmc}^{kin}\approx m_\mu - B_\mu - \Delta_{Z-1}, \tag{142}$$

where Δ_{Z-1} is the difference in the nuclear binding energy of the initial (A,Z) and final $(A,Z-1)$ nucleus involved in radiative muon capture. Therefore an appropriate target with a large Δ_{Z-1} can be selected so as to keep a wide background-free region for the coherent signal. Practically, the empirical end point of radiative muon capture (E_{rmc}^{emp}), which is evaluated by taking account of the radiative-muon-capture spectrum shape given by Primakoff's formula (Primakoff, 1959), is used. The E_{rmc}^{emp} values for Ti were estimated from the observed radiative muon capture on ^{40}Ca (Armstrong et al., 1992). They are 89.7 and 91.4 MeV for ^{48}Ti and ^{46}Ti, respectively (Kaulard et al., 1998), whereas $E_{\mu e}$ is 104.3 MeV.

When the muon is polarized, the angular distribution of e^- in the coherent $\mu^- - e^-$ conversion process is given by

$$\frac{dB(\mu^- N \to e^- N)}{d(\cos\theta_e)}$$

$$= \frac{p_e E_e G_F^2}{16\pi}[|X_L(p_e)|^2(1-P_\mu \cos\theta_e)$$

$$+ |X_R(p_e)|^2(1+P_\mu \cos\theta_e)] \cdot \frac{1}{\Gamma_{capt}}, \qquad (143)$$

where θ_e is the angle between the e^- direction and the muon spin direction. Since the nucleus does not change for the coherent process, the conversion electron carries the information of the original muon spin. The terms X_L and X_R are given in Eqs. (133) and (134), and correspond to the emission of left-handed electrons (e_L^-) and right-handed electrons (e_R^-), respectively. As in polarized $\mu^+ \to e^+\gamma$ decay, in principle, the angular distribution would be useful to discriminate between theoretical models. However, even if negative muons in the beam are 100% spin polarized, they are depolarized during their atomic cascades down to the $1s$ ground state. For a nucleus with zero nuclear spin, the residual polarization is about 16% (Evseev, 1975). For a nucleus with nonzero nuclear spin, it becomes much smaller. This makes discrimination of theoretical models difficult unless high statistics are accumulated. However, if the μ^- polarization is restored, it might provide useful information. One possible way to repolarize a negative muon in a muonic atom is to use a polarized nuclear target (Nagamine and Yamazaki, 1974; Kuno *et al.*, 1986).

3. Muon decay in orbit

Muon decay in orbit (Porter and Primakoff, 1951) is one of the important background sources in the search for $\mu^- - e^-$ conversion in a muonic atom, since the end point of the electron spectrum comes close to the signal region of $\mu^- - e^-$ conversion. Only the high-energy end of the electron energy spectrum is of interest for $\mu^- - e^-$ conversion experiments. At the high-energy end, the effect of the nuclear-recoil energy plays an important role (on its phase space). There have been several studies on its electron energy spectrum with nuclear-recoil energy taken into account (Hänggi *et al.*, 1974; Herzog *et al.*, 1980; Shanker, 1982). With the approximation of a constant nuclear-recoil energy, the electron spectrum with an expansion in powers of the electron energy (E_e) at the end-point energy is given by (Shanker, 1982)

$$N(E_e)dE_e = \left(\frac{E_e}{m_\mu}\right)^2 \left(\frac{\delta_1}{m_\mu}\right)^5 \left[D + E\cdot\left(\frac{\delta_1}{m_\mu}\right)\right.$$

$$\left. + F\cdot\left(\frac{\delta}{m_\mu}\right)\right]dE_e, \qquad (144)$$

where $\delta = E_{\mu e} - E_e$ and $\delta_1 = (m_\mu - B_\mu) - E_{rec} - E_e$. Here $E_{\mu e}$ is the e^- energy of the $\mu^- - e^-$ conversion signal defined in Eq. (141), and E_{rec} is the nuclear-recoil energy given by $E_{rec} \approx E_e^2/(2M_A)$. It should be stressed that the spectrum falls off sharply as the fifth power of
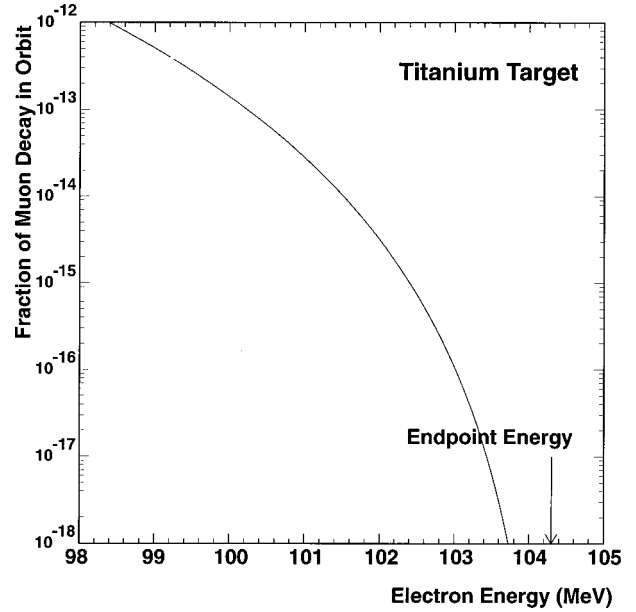

FIG. 28. Energy distribution of electrons from muon decay in orbit normalized to the total nuclear muon-capture rate for a titanium target. This represents an effective branching ratio of muon decay in orbit as a background to the $\mu^- - e^-$ conversion. It was calculated by Shanker's formula in Eq. (144). The energy of the $\mu^- - e^-$ conversion signal in a titanium target is $E_{\mu e} = 104.3$ MeV.

δ_1 towards its end point. The coefficients D, E, and F as well as the end-point energy are tabulated in Shanker (1982). The contributions of the E and F terms to the total rate are about 4% and 8%, respectively, for $Z = 29$ and $E_e = 100$ MeV. Equation (144) agrees with those in Hänggi *et al.* (1974) and Herzog *et al.* (1980). In the evaluation of the leading term D, important are (i) the use of a correct electron wave function incorporating the finite nuclear charge distribution, (ii) the use of the Dirac muon wave function, and (iii) the use of the small component of the muon relativistic wave function. In particular, the effect of (i) is large (Shanker and Roy, 1997).

Experimentally, to avoid any background from muon decay in orbit, the momentum resolution of e^- detection must be improved. Figure 28 shows the effective branching ratio of the muon decay in orbit as a function of E_e for the case of a titanium target, where $E_{\mu e} = 104.3$ MeV. It was calculated using Eq. (144). For a resolution better than 2%, the contribution from muon decay in orbit occurs at a level below 10^{-14}.

What is the asymmetric angular distribution of electrons in muon decay in orbit, if muons are polarized? Numerical calculations can be made by taking into account the angular distribution of electrons from polarized muon decay in orbit (Watanabe *et al.*, 1987). It is given by

$$N(E_e, \theta_e)dE_e\left(\frac{d\Omega_e}{4\pi}\right)$$

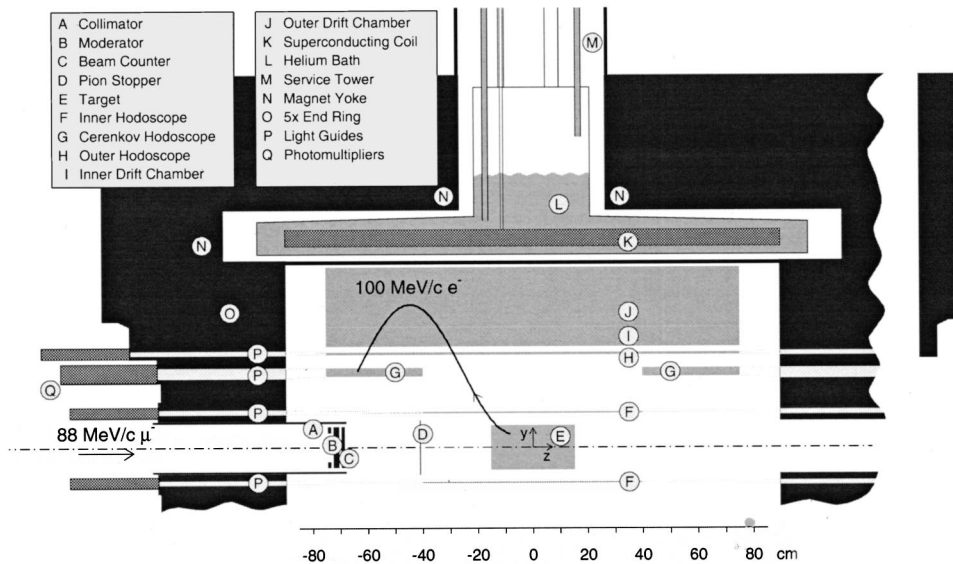$$= N_0(E_e)[1 + \alpha(E_e)P_\mu \cos\theta_e]\left(\frac{d\Omega_e}{4\pi}\right), \qquad (145)$$

FIG. 29. Schematic layout of the SINDRUM II detector (provided by P. Wintz).

where $N_0(E_e)$ is the energy spectrum with zero polarization. Here $\alpha(E_e)$ is the asymmetry parameter, which becomes $\alpha(E_e) = -1$ at the end point, giving a distinct $(1 - P_\mu \cos \theta_e)$ distribution, i.e., electrons are likely to be emitted opposite to the muon polarization direction. At low energy, $\alpha(E_e)$ becomes positive and electrons are emitted along the direction of muon polarization. The Coulomb effect is significant for heavy nuclei, like ^{208}Pb, but very small for light nuclei, like ^{16}O. The calculated results of the decay rate, emitted electron energy spectrum, and asymmetry parameters for muon decay in orbit are tabulated for some nuclei (Watanabe *et al.*, 1993).

4. Experimental status of $\mu^- - e^-$ conversion

The SINDRUM II Collaboration at PSI is carrying out experiments to search for $\mu^- - e^-$ conversion in various nuclei. A schematic view of the SINDRUM II spectrometer is shown in Fig. 29. It consists of a set of concentric cylindrical drift chambers inside a superconducting solenoid magnet of 1.2 T. Negative muons with a momentum of about 90 MeV/c were stopped in a target located at the center of the apparatus, after passing a CH_2 moderator and a beam counter made of plastic scintillators. Charged particles with transverse momentum (with respect to the magnetic field direction) above 80 MeV/c, originating from the target, first hit two layers of plastic scintillation arrays followed by two layers of drift chambers, before eventually hitting plexiglass Cherenkov hodoscopes placed at both ends. Charged particles having transverse momentum below about 80 MeV/c were contained inside, and could not reach the tracking region under a magnetic field of 1.2 T. A momentum resolution of about 2.8% (FWHM) for the energy region of conversion electrons was achieved. For the background rejection, the following are used in an off-line analysis: the e^- energy (E_e), a time delay between the times of charged-particle tracks in the spectrometer and the beam-counter signal (Δt), the position

of the origin of the reconstructed trajectory (Δz), and the polar track angle. Events with small Δt were removed so as to reject prompt backgrounds, such as electron scattering and radiative pion capture.

In a 1993 run with a titanium target, a total of 3 $\times 10^{13}$ stopped μ^-'s were accumulated at a rate of 1.2 $\times 10^7$ μ^-/s from the $\mu E1$ beam line at PSI. The overall efficiency was about 13%. The e^- momentum spectrum for the Ti target in the 1993 data is shown in Fig. 30, where the successive background rejections by prompt veto (i.e. Δt cut) and cosmic-ray suppression are shown. Since no events were found in the signal region, a 90%-C.L. upper limit of 6.1×10^{-13} was obtained (Wintz, 1998). Moreover, for a lead target, it gave $B(\mu^- \text{Pb} \rightarrow e^- \text{Pb}) < 4.6 \times 10^{-11}$ (Honecker *et al.*, 1996); see Table XII.

The next round of the SINDRUM II experiment is under preparation at the $\pi E5$ beam line at PSI. The key element of the next stage is a pion-muon converter to eliminate contamination of pions and electrons in the muon beam. It is needed because a veto of secondary pions and electrons by a beam counter will no longer be
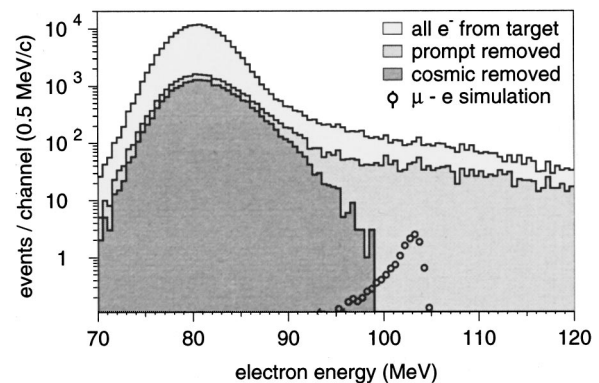

FIG. 30. Electron momentum distributions for the $\mu^- + \text{Ti} \rightarrow e^- + \text{Ti}$ conversion, measured by the SINDRUM II detector, after the consecutive analysis cuts. The expected signal at $B_{\mu e} = 4 \times 10^{-12}$ is shown (provided by P. Wintz).

TABLE XII. History and summary of $\mu^- - e^-$ conversion in various nuclei.

Process	90%-C.L. upper limit	Place	Year	Reference
$\mu^- + Cu \rightarrow e^- + Cu$	$< 1.6 \times 10^{-8}$	SREL	1972	Bryman *et al.* (1972)
$\mu^- + {}^{32}S \rightarrow e^- + {}^{32}S$	$< 7 \times 10^{-11}$	SIN	1982	Badertscher *et al.* (1982)
$\mu^- + Ti \rightarrow e^- + Ti$	$< 1.6 \times 10^{-11}$	TRIUMF	1985	Bryman *et al.* (1985)
$\mu^- + Ti \rightarrow e^- + Ti$	$< 4.6 \times 10^{-12}$	TRIUMF	1988	Ahmad *et al.* (1988)
$\mu^- + Pb \rightarrow e^- + Pb$	$< 4.9 \times 10^{-10}$	TRIUMF	1988	Ahmad *et al.* (1988)
$\mu^- + Ti \rightarrow e^- + Ti$	$< 4.3 \times 10^{-12}$	PSI	1993	Dohmen *et al.* (1993)
$\mu^- + Pb \rightarrow e^- + Pb$	$< 4.6 \times 10^{-11}$	PSI	1996	Honecker *et al.* (1996)
$\mu^- + Ti \rightarrow e^- + Ti$	$< 6.1 \times 10^{-13}$	PSI	1998	Wintz (1998)

working with a high rate (e.g., $10^8 \, \mu^-$/s) at the $\pi E5$ beam line. The pion-muon converter consists of a long straight superconducting solenoid magnet with length of 8.5 m and an inner diameter of 0.4 m. It is located between the pion target and the SINDRUM II spectrometer, and produces the same magnetic field as that of the SINDRUM II spectrometer, 2 T. Low-energy negative muons (called cloud muons) from the production target are injected into the pion-muon-converter. After the 8.5-m flight length, most of the pions in a beam would decay out, resulting in negligible pion contamination. Unfortunately, the original pion-muon-converter magnet did not fulfill the specification at the initial installation stage, and thus caused a severe delay. After its new assembly, the magnet finally achieved its goal. With a lower magnetic field for the pion-muon-converter magnet, data with a gold target were taken in 1997. A new run on gold started in spring 2000.

A new experiment (E940) at the BNL AGS, called the MECO (Muon Electron COnversion) experiment, has been prepared (Bachman *et al.*, 1997). MECO aims to search for $\mu^- + Al \rightarrow e^- + Al$ at a sensitivity below 10^{-16}. It will use a new high-intensity pulsed muon beam, which could yield about $10^{11} \, \mu^-$/s stopped in a target. A schematic layout of the MECO detector is shown in Fig. 31. The MECO apparatus consists of a superconducting solenoid magnet to capture pions from the production target (production solenoid), a curved transport superconducting solenoid magnet system (transport solenoid), and a superconducting solenoid spectrometer, which observes only the 105-MeV signal
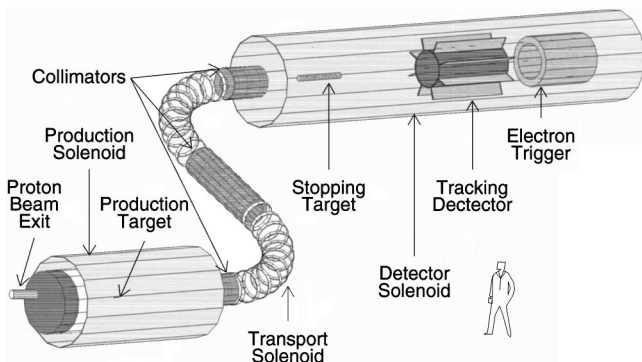

FIG. 31. Schematic layout of the MECO detector (provided by W.R. Molzon).

electrons (detector solenoid). Based on the solenoid-capture scheme originally proposed by MELC (Dzhilkibaev and Lobashev, 1989) it has an axially graded magnetic field (from 3.5 to 2.0 T) to efficiently capture pions from a tungsten target located on the axis of the solenoid magnet. The curved transport solenoid will capture muons from pion decays, and select the momentum and sign of charged particles by using collimators at three positions. Layers of thin aluminum targets where the μ^-'s are stopped are placed in the detector solenoid with an axially graded magnetic field. The conversion electron of 105 MeV is momentum analyzed with a resolution of 300 keV (rms) and an acceptance of 25% in a straw tracking chamber. A pulsed proton beam of about 1-MHz repetition with a pulse length of 30 ns can be extracted at the AGS. A high extinction between the beam pulses (the ratio of the number of protons between pulses to that in the beam pulse) of 10^{-9} is needed to eliminate severe beam backgrounds at a high rate. They expect to observe six signal events for $B(\mu^- Al \rightarrow e^- Al) \approx 10^{-16}$ during a one-year run, with an expected background of 0.4 events.

D. $\mu^- - e^+$ conversion in a muonic atom

1. Phenomenology of $\mu^- - e^+$ conversion

The other neutrinoless muon conversion process is a charge-changing reaction, such as

$$\mu^- + (A,Z) \rightarrow e^+ + (A,Z-2)^*, \qquad (146)$$

which violates the conservation of total lepton number as well as the lepton flavor numbers, L_e and L_μ. This process is closely related to neutrinoless double-β decay ($\beta\beta_{0\nu}$), since both processes require a mechanism involving two nucleons. The final state of the nucleus $(A,Z-2)^*$ could be either the ground state or an excited state. Since the final nucleus is not the same as the initial nucleus, no coherent enhancement is expected, even for the transition to the ground state. The branching ratio of $\mu^- - e^+$ conversion is defined by

$$B[\mu^- + (A,Z) \rightarrow e^+ + (A,Z-2)^*]$$

$$\equiv \frac{\Gamma[\mu^- + (A,Z) \rightarrow e^+ + (A,Z-2)^*]}{\Gamma[\mu^- + (A,Z) \rightarrow \text{capture}]}.$$
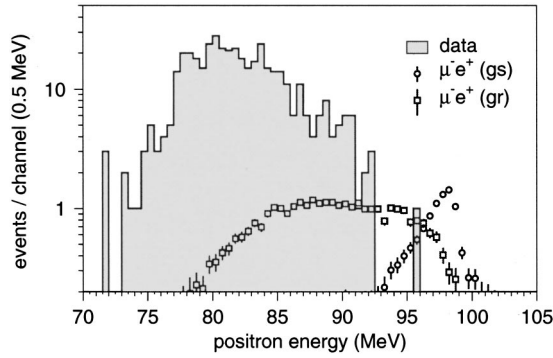
$$(147)$$

FIG. 32. Positron energy spectra of the $\mu^- + \text{Ti} \rightarrow e^+ + \text{Ca}$ reaction; $\mu^- e^+ (\text{gs})$ and $\mu^- e^+ (\text{gr})$ are the expected signals for the transitions to the ground state and to the giant-dipole-resonance states, respectively. The assumed branching ratios for gs and gr are 2.2×10^{-11} and 4.5×10^{-10} (provided by P. Wintz).

Various theoretical models predict experimentally accessible rates. One is the minimum supersymmetric model (MSSM) with R-parity violation, which allows the predicted branching ratio of $\mu^- - e^+$ conversion of the level of 10^{-12}, since the relevant λ and λ' parameters are not constrained (Babu and Mohapatra, 1995). Left-right symmetric models with a low-mass W_R also predict a $\mu^- - e^+$-conversion branching ratio of 10^{-14}, a value estimated by the same authors.

2. Event signature and backgrounds

The energy of the positron from $\mu^- - e^+$ conversion is given by

$$E_{\mu e^+} = m_\mu - B_\mu - E_{rec} - \Delta_{Z-2}$$
$$\approx m_\mu - B_\mu - \Delta_{Z-2}, \tag{148}$$

where Δ_{Z-2} is the difference in the nuclear binding energy between the (A,Z) and $(A,Z-2)$ nuclei, with the excitation energy in the final nucleus taken into account. Usually, it is assumed that a large fraction of the final nucleus could be in the giant-dipole-resonance state, which has a mean energy of 20 MeV and a width of 20 MeV. Therefore the e^+ from $\mu^- - e^+$ conversion would

have a broad momentum distribution corresponding to the width of giant-dipole-resonance excitation.

The principal background is radiative muon capture or radiative pion capture, followed by asymmetric $e^+ e^-$ conversion of the photon. For some nuclei, the end point of the radiative-muon-capture background in Eq. (142) can be selected to be well separated from the signal. The background from radiative pion capture must be reduced by the rejection of pions in the beam.

3. Experimental status of $\mu^- - e^+$ conversion

The SINDRUM II Collaboration at PSI has reported a search for the charge-changing process $\mu^- + \text{Ti} \rightarrow e^+ + \text{Ca}$ in muonic atoms (Kaulard et al. 1998). It was carried out simultaneously with a measurement of $\mu^- + \text{Ti} \rightarrow e^- + \text{Ti}$. The e^+ momentum spectrum is shown in Fig. 32. The results are given separately for the transition to the ground state and that to the giant dipole resonance. They are summarized in Table XIII, together with the previous results.

E. Muonium to antimuonium conversion

A muonium atom is a hydrogenlike bound state of μ^+ and e^-. The spontaneous conversion (or oscillation) of a muonium atom ($\mu^+ e^-$ or Mu) to its antiatom, antimuonium atom ($\mu^- e^+$ or $\overline{\text{Mu}}$,) is another interesting class of muon LFV process. In this $\text{Mu} - \overline{\text{Mu}}$ conversion, the ordinary additive law of conservation of muon and electron numbers is violated by two units ($\Delta L_{e/\mu} = \pm 2$), whereas muon or electron number is conserved multiplicatively (Feinberg and Weinberg, 1961). This possibility was suggested by Pontecorvo in 1957 (Pontecorvo, 1957), even before the muonium atom was observed for the first time at the Nevis cyclotron of Columbia University (Hughes et al., 1960).

1. Phenomenology of $\text{Mu} - \overline{\text{Mu}}$ conversion

Various interactions could induce $|\Delta L_i| = 2$ processes, such as $\text{Mu} - \overline{\text{Mu}}$ conversion, as discussed in Sec. III.E. To discuss the phenomenology of the $\text{Mu} - \overline{\text{Mu}}$ conversion, we take as an example the effective four-fermion

TABLE XIII. Historical progress and summary of $\mu^- - e^+$ conversion in various nuclei; gs and ex, respectively, denote the transitions to the ground state and excited states (mostly giant-dipole-resonance states), respectively.

| Process	90%-C.L. upper limit	Place	Year	Reference
$\mu^- + \text{Cu} \rightarrow e^+ + \text{Co}$	2.6×10^{-8}	SREL	1972	Bryman et al. (1972)
$\mu^- + \text{S} \rightarrow e^+ + \text{Si}$	9×10^{-10}	SIN	1982	Badertsher et al. (1982)
$\mu^- + \text{Ti} \rightarrow e^+ + \text{Ca(gs)}$	9×10^{-12}	TRIUMF	1988	Ahmad et al. (1988)
$\mu^- + \text{Ti} \rightarrow e^+ + \text{Ca(ex)}$	1.7×10^{-10}	TRIUMF	1988	Ahmad et al. (1988)
$\mu^- + \text{Ti} \rightarrow e^+ + \text{Ca(gs)}$	4.3×10^{-12}	PSI	1993	Dohmen et al. (1993)
$\mu^- + \text{Ti} \rightarrow e^+ + \text{Ca(ex)}$	8.9×10^{-11}	PSI	1993	Dohmen et al. (1993)
$\mu^- + \text{Ti} \rightarrow e^+ + \text{Ca(gs)}$	1.7×10^{-12}	PSI	1998	Kaulard et al. (1998)
$\mu^- + \text{Ti} \rightarrow e^+ + \text{Ca(ex)}$	3.6×10^{-11}	PSI	1998	Kaulard et al. (1998)
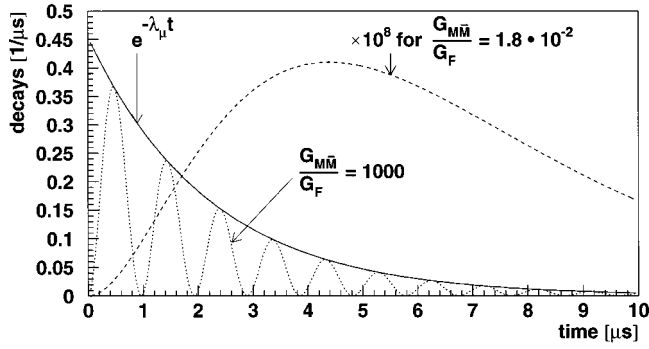
FIG. 33. Time dependence of the probability of antimuonium decay when a pure muonium atom is created initially: solid line, the exponential decay of muonium; dotted line, the decay probability of antimuonium given for $G_{M\bar{M}}/G_F = 1000$; dashed line, for $G_{M\bar{M}}/G_F = 1.8 \times 10^{-2}$. In the latter case, the maximum probability occurs at about twice the muon lifetime. From Willmann and Jungmann, 1997.

interaction of the $(V-A)(V-A)$ type (Feinberg and Weinberg, 1961). It is given by Eq. (93).

In the absence of an external magnetic field, the muonium and the antimuonium atoms have the same ground-state energy levels. The possible new interaction in Eq. (93) would cause a splitting of their energy levels of

$$\delta \equiv 2\langle \bar{M}|H_{\mathrm{Mu\overline{Mu}}}|M\rangle = \frac{8 G_F}{\sqrt{2} n^2 \pi a_0^3}\left(\frac{G_{\mathrm{Mu\overline{Mu}}}}{G_F}\right), \qquad (149)$$

where n is the principal quantum number of the muonium atom, and a_0 is the Bohr radius of the muonium atom. For the ground state of the muonium atom ($n=1$),

$$\delta = 1.5 \times 10^{-12} \cdot \left(\frac{G_{\mathrm{Mu\overline{Mu}}}}{G_F}\right) \quad (\mathrm{eV}). \qquad (150)$$

The $\mathrm{Mu-\overline{Mu}}$ conversion is analogous to $K^0 - \bar{K}^0$ mixing. If a muonium atom is formed at $t=0$ in a vacuum under no external electromagnetic field, it could oscillate into an antimuonium atom with time. For a small δ value, the probability ($p_{\mathrm{Mu\overline{Mu}}}$) is approximately given by (Willmann and Jungmann, 1997)

$$p_{\mathrm{Mu\overline{Mu}}}(t) = \sin^2\left(\frac{\delta t}{2}\right)\cdot\lambda_\mu e^{-\lambda_\mu t} \approx \left(\frac{\delta t}{2}\right)^2 \cdot \lambda_\mu e^{-\lambda_\mu t}, \qquad (151)$$

where $\lambda_\mu = 1/\tau_\mu (= 2.996 \times 10^{-10}\,\mathrm{eV})$ is the muon decay width. The maximum probability of antimuonium decay occurs at $t_{\max} = 2\tau_\mu$. Figure 33 shows the oscillation pattern as a function of time. The total conversion probability after integration over time ($P^0_{\mathrm{Mu\overline{Mu}}}$) in a zero magnetic field is

$$P^0_{\mathrm{Mu\overline{Mu}}} = \int_0^\infty p_{\mathrm{Mu\overline{Mu}}}(t)dt = \frac{|\delta|^2}{2(|\delta|^2 + |\lambda_\mu|^2)}$$

$$= 2.56 \times 10^{-5} \cdot \left(\frac{G_{\mathrm{Mu\overline{Mu}}}}{G_F}\right)^2. \qquad (152)$$
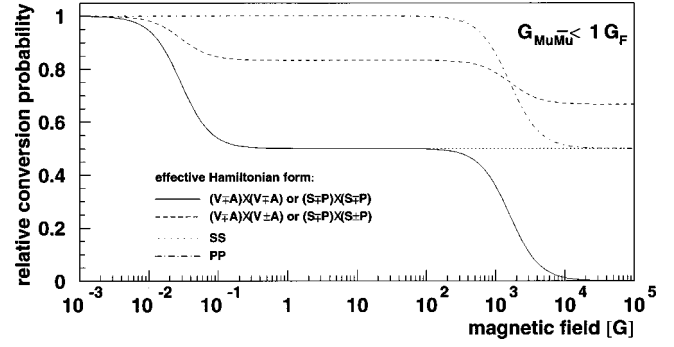

FIG. 34. $\mathrm{Mu-\overline{Mu}}$ conversion rate for different interactions as a function of the external magnetic field. From Willmann and Jungmann, 1997.

The experimental limit constrains the maximum allowed value of $G_{\mathrm{Mu\overline{Mu}}}$. The limit of $G_{\mathrm{Mu\overline{Mu}}}$ is improved by the square root of the conversion probability.

The presence of an external electromagnetic field would remove the degeneracy between the muonium and antimuonium atoms. It would reduce the probability of the muonium-to-antimuonium conversion. The splitting of different muonium energy levels in the presence of a magnetic field is calculated by using the Breit-Rabi formula for the states of their total spin F and its z component, m_F. In a magnetic field, the $(F, m_F) = (1, \pm 1) \to (1, \pm 1)$ transitions become rapidly suppressed, even in a weak field, because of the Zeeman splitting of energy levels. The transitions between different F states are also highly suppressed, even in a zero magnetic field, owing to the muonium $1s$ hyperfine splitting (of 1.846×10^{-5} eV). By taking into account the magnetic field dependences of different energy levels of muonium and antimuonium and their transition rates, Eq. (152) can be modified for unpolarized muons by

$$P_{\mathrm{Mu\overline{Mu}}}(B) = \frac{1}{4}\sum_{F, m_F}\frac{|\delta|^2}{2(|\delta|^2 + |\triangle|^2 + |\lambda_\mu|^2)}$$

$$\equiv P^0_{\mathrm{Mu\overline{Mu}}}\cdot S_B(B), \qquad (153)$$

where $\triangle \equiv E_{Mu}(F, m_F) - E_{\overline{Mu}}(F, m_F)$, and δ and $\triangle$ are functions of the magnitude of the magnetic field (B). The reduction factor $S_B(B)$ has been calculated for possible interactions of different types (Hou and Wong, 1995; Horikawa and Sasaki, 1996). Figure 34 shows the dependence of the $\mathrm{Mu-\overline{Mu}}$ conversion probability on the external magnetic field and different types of coupling. For example, for the traditional $(V-A)(V-A)$ interaction, the conversion rate becomes one-half for a magnetic field of about 100 mG and is further strongly suppressed for a magnetic field greater than 10^3 G.

2. Event signature and backgrounds

In experiments of $\mathrm{Mu-\overline{Mu}}$ conversion, one searches for an antimuonium atom that has been produced from an initial muonium atom. The experimental signature of antimuonium decay is the emission of an energetic e^- from $\mu^- \to e^- \bar{\nu}_\mu \nu_e$ decay with a residual e^+ possessing

TABLE XIV. Historical progress and summary of Mu-$\overline{\text{Mu}}$ conversion.

Place	Year	$G_{\text{Mu}\overline{\text{Mu}}}/G_F$	Reference
TRIUMF	1982	<42	Marshall *et al.* (1982)
TRIUMF	1986	<20	Beer *et al.* (1986)
TRIUMF	1990	<0.29	Huber *et al.* (1990)
LANL	1991	<0.16	Matthias *et al.* (1991)
LANL	1993	<6.9	Ni *et al.* (1993)
PSI	1996	<0.018	Abela *et al.* (1996)
JINR	1997	<0.14	Gordeev *et al.* (1997)
PSI	1999	<0.003	Willmann *et al.* (1999)

an average kinetic energy of 13.5 eV. This corresponds to the binding energy of the $1s$ state of a muonium atom.

The sensitivity to Mu$-\overline{\text{Mu}}$ conversion is known to be suppressed when the muonium atom is in matter. This occurs because a negative muon in antimuonium is easily captured by surrounding atoms. Therefore recent experiments have been performed by using muonium atoms in a vacuum.

There are two major backgrounds. One is the coincidence of a low-energy e^+ and an energetic e^- which are produced by Bhabha scattering of e^+ from μ^+ decay in a muonium atom. The second is the physics (prompt) background from the decay $\mu^+ \to e^+ \nu_e \bar{\nu}_\mu e^+ e^-$ (whose branching ratio is 3.4×10^{-5}), when the e^- becomes energetic and only one of the two e^+'s is detected.

3. Experimental status of Mu$-\overline{\text{Mu}}$ conversion

The historical progress in the searches for Mu$-\overline{\text{Mu}}$ conversion is listed in Table XIV. A recent experiment was carried out at PSI (Willmann *et al.*, 1999). The experiment fully utilized the powerful techniques developed at the previous experiment at LANL (Matthias *et al.*, 1991), which requires the coincidence identification of both particles in the antimuonium decay. Its experimental setup is shown in Fig. 35. Muonium atoms were produced by stopping surface muons in a

SiO_2-powder target, where some fraction diffused out through the target surface with thermal energy in a vacuum. To detect e^- from μ^- decay, a magnetic spectrometer was used. It consisted of five concentric multiwire proportional chambers with 64 segmented hodoscopes at a 0.1-T magnetic field. The e^+ with an average kinetic energy of 13.5 eV was detected by microchannel plate detectors after electrostatic acceleration to 8 keV.
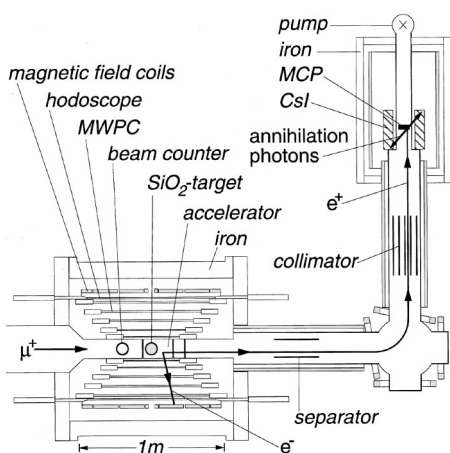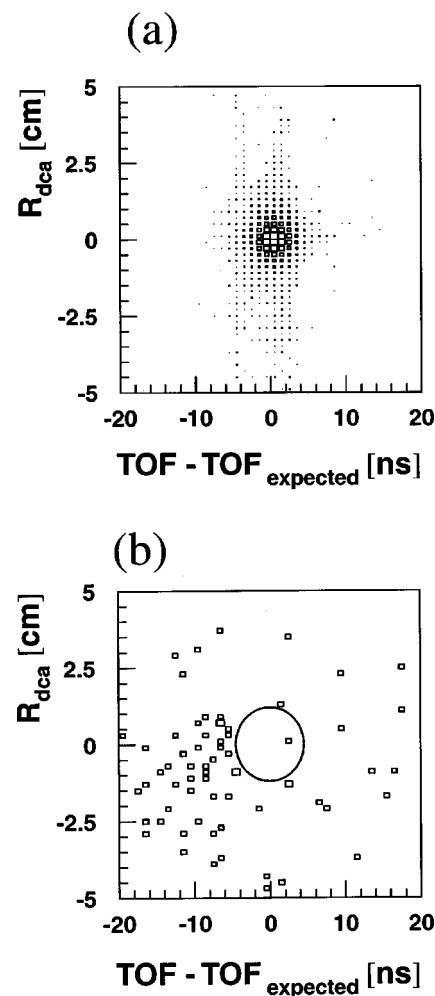
(a)

(b)

FIG. 36. Distribution of the distance of closest approach between the e^+ and e^- trajectories vs their timing difference in the experiment to search for Mu$-\overline{\text{Mu}}$ conversion: (a) Monte Carlo data; (b) experimental data. From Willmann *et al.*, 1999.

FIG. 35. Schematic layout of the detector for muonium-antimuonium conversion at PSI. From Willmann *et al.*, 1999.

TABLE XV. Intensities of existing muon beams.

Facility	Protons	Time structure	Muon intensity	
PSI	1.5 mA	continuous	$3 \times 10^8 \, \mu^+/s$	at 28 MeV/c (surface muons)
	590 MeV	(50 MHz)	$1 \times 10^8 \, \mu^-/s$	at 100 MeV/c
TRIUMF	150 μA	continuous	$2 \times 10^7 \, \mu^+/s$	at 28 MeV/c (surface muons)
	500 MeV	(50 MHz)	$3 \times 10^6 \, \mu^-/s$	at 100 MeV/c
RAL	200 μA	pulsed	$1 \times 10^6 \, \mu^+/s^a$	at 28 MeV/c (surface muons)
	800 MeV	(50 Hz)	$1 \times 10^5 \, \mu^-/s$	at 50 MeV/c
MSL^b	6 μA	pulsed	$1 \times 10^5 \mu^+/s$	at 28 MeV/c (surface muons)
	500 MeV	(20 Hz)	$1 \times 10^4 \, \mu^-/s$	at 55 MeV/c
JINR^c	4 μA	continuous	$3 \times 10^4 \, \mu^+/s$	at 28 MeV/c (surface muons)
	660 MeV		$1 \times 10^3 \, \mu^-/s$	at 100 MeV/c

[a]The highest instantaneous intensity of $2 \times 10^4 \mu^+ s/200$ ns.
[b]Meson Science Laboratory at KEK, using the existing 500-MeV booster ring.
[c]Phasotron, Joint Institute for Nuclear Research, Dubna, Russia.

About 5.7×10^{10} muonium atoms were produced, and their analysis yielded one event satisfying all of the required criteria with the expected background events of 1.7 ± 0.2 due to accidental coincidence. The Monte-Carlo data and experimental data are given in Fig. 36. The 90%-C.L. upper limit on the conversion probability at zero magnetic field is

$$P^0_{\mathrm{Mu\overline{Mu}}} \leq 8.3 \times 10^{-11}/S_B(B), \tag{154}$$

where the factor $S_B(B)$ describes the suppression of $\mathrm{Mu} - \overline{\mathrm{Mu}}$ conversion in an external magnetic field, B. It could be translated into the upper limit on the effective coupling constant, $G_{\mathrm{Mu\overline{Mu}}}$, which is given by

$$G_{\mathrm{Mu\overline{Mu}}} \leq 3.0 \times 10^{-3} G_F \tag{155}$$

at 90%-C.L. upper limit under a 0.1-T magnetic field.

VI. FUTURE PROSPECTS: TOWARDS NEW HIGH-INTENSITY MUON SOURCES

The field of muon-decay physics is presently very productive, even after its long history of over 60 years. Currently, there are several new experiments that are being either prepared or planned. Some of them, which were mentioned in this article, are R77 at RIKEN-RAL and R-99-07 at PSI for the muon lifetime measurement (in Sec. IV.A.2), E614 at TRIUMF to measure the Michel spectrum and its asymmetry (in Sec. IV.B.2), R-94-10 and R-97-07 at PSI to measure the e^+ polarization in polarized $\mu^+ \rightarrow e^+ \nu_e \bar{\nu}_\mu$ decay (in Sec. IV.C.2), R-99-05 at PSI for $\mu^+ \rightarrow e^+ \gamma$ decay (in Sec. V.A.6), the new phase of SINDRUM II at PSI, and E940 (MECO) at BNL for $\mu^- - e^-$ conversion (in Sec. V.C.4). Each of these is aiming at an improvement of about an order of magnitude or more over the previous experiments. The potential progress expected at each of the above experiments is based not only on innovative detection methods, but also on muon beams of high intensity and good quality. In particular, the planned searches for muon LFV processes strongly rely on the beam, such as the pion-muon converter in SINDRUM II and the super-

conducting solenoid capture and transport systems for the MECO experiment. More muon fluxes with less contamination are critical for further improvements.

Currently, two out of the three meson factories are operational. One of the two operational machines, the PSI cyclotron, has increased its proton current, achieving 1.5 mA, the highest proton current in the world. The muon beam intensities for various existing laboratories are listed in Table XV. In addition, the use of higher-energy proton machines, such as the BNL AGS for negative muons, is being considered for the MECO experiment, where a pulsed-beam capability at the AGS and a larger cross section of negative pions at a few tens of GeV of proton energy are to be utilized. In the long-term future, there are several new projects to construct high-intensity proton accelerators: the JAERI/KEK Joint Project (previously JHF) (JAERI/KEK Joint Project, 1999), which consists of a 50-GeV proton synchrotron with a 15-μA beam intensity, and a 3-GeV proton synchrotron with a 330-μA beam intensity; the Spallation Neutron Source at Oak Ridge; and a possible European Spallation Neutron Source. A proton driver for a $\mu^+ \mu^-$ collider (Muon Collider Collaboration, 1996; Ankenbrandt *et al.*, 1999) can probably be included in the long-term future. Note that among the above, only the 50-GeV proton synchotron is planned to have a continuous proton beam by slow beam extraction, whereas the others may only have fast beam extraction of a low repetition rate.

Regarding LFV, besides the study of muon decays, a unique possibility of lepton-flavor-changing Rutherford scattering has been discussed (Abraham and Lampe, 1996). This is the conversion of incident electrons into muons of the same energy by scattering in the external electric field of a massive nucleus. However, the expected cross section is too small to compete with rare muon-decay processes, and the technical details have not yet been discussed.

Significant improvements in low-energy muon physics would be expected if a high-intensity muon source with a beam intensity of $10^{12} - 10^{13} \mu^\pm/s$, a narrow energy
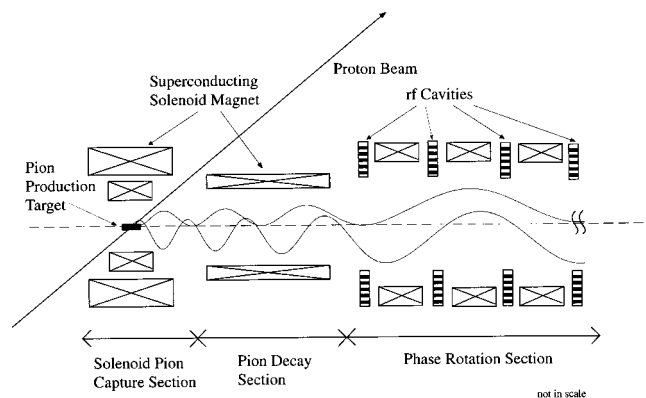
FIG. 37. Schematic layout of a high-intensity muon source.

spread, and less contamination can be realized. The muon beam intensity envisaged would be four or five orders of magnitude higher than that available today. Ideas of such a high-intensity muon source are based on (i) solenoid pion capture, (ii) phase rotation, and (iii) muon cooling. A schematic view of the basic concept is shown in Fig. 37.

In solenoid pion capture, low-energy pions and muons are trapped in a high solenoidal magnetic field (such as 10 T or more). From Monte Carlo simulations with appropriate pion-production cross sections, about 0.3 to 0.1 captured pions (of less than $0.5\,\mathrm{GeV}/c$) per proton are estimated for proton beam energies of 50 GeV to 15 GeV. For a proton intensity of about 10^{13}–10^{14} proton/s (i.e., that at existing and planned proton machines), a large number of captured pions are expected, which is sufficient to attain the aimed intensity of muons.

The phase rotation is to accelerate slow muons and to decelerate fast muons by a strong radio-frequency (rf) electric field, yielding a narrow longitudinal momentum spread. To identify fast and slow muons by their time of flight from the production time, a very narrow pulsed proton beam must be used. An intensity enhancement of a factor of about ten in the longitudinal energy distribution has been estimated from Monte Carlo simulations (Kuno, 1997).

The muon cooling, which is based on ionization cooling (Skrinskii and Parkhomuchum, 1981), is to reduce muon beam emittance. The ionization cooling is based on the repetition of energy loss by ionization and subsequent acceleration to restore the longitudinal momentum. The ionization cooling works only for muons.

These ideas have emerged from studies of a $\mu^+\mu^-$ collider at the high-energy frontier (Muon Collider Collaboration, 1996; Ankenbrandt $et\ al.$, 1999). The physics potential with low-energy muons available from the front end of the $\mu^+\mu^-$ collider complex has been discussed. Although there are many common R&D items between a low-energy muon source and a $\mu^+\mu^-$ collider, there have been discussions on whether the front-end muon collider could be used directly in experiments with muons. The front-end muon collider will run with a pulsed beam of slow repetition (at typically 15 Hz). However, most experiments with muons require a beam with a high duty factor, or a nearly continuous beam,

because of the reduction of the instantaneous rate (Molzon, 1997). The precise requirement of the beam time structure depends on the type of experiments. For instance, searches for $\mu^+\rightarrow e^+\gamma$ and $\mu^+\rightarrow e^+e^+e^-$ must use a continuous beam to reduce the instantaneous rate, whereas searches for μ^--e^- (or μ^--e^+) conversion, Mu$-\overline{\mathrm{Mu}}$ conversion, and a measurement of the muon lifetime need a pulsed beam with a pulse separation in the order of the muon lifetime ($\sim\mu$s). Thus independent R&D items, in particular concerning phase rotation and the muon-cooling system, exist in a low-energy muon source. These technical issues must be pursued separately.

There are several dedicated R&D programs concerning low-energy muon sources with high intensity. One of these is the PRISM project at KEK in Japan (Kuno, 1998). The PRISM project, which is an acronym of Phase-Rotation Intense Secondary Meson beam, would combine solenoid capture, phase rotation, and possibly modest muon cooling to produce a cooled muon beam. The requirement of muon cooling as a secondary beam is not as strict as that at a $\mu^+\mu^-$ collider. Its R&D program starts from a relatively low repetition rate ($\sim$kHz), and aims for higher repetition in the future. Other projects include the MUONS project at TRIUMF (Blackmore $et\ al.$, 1997) and the Super-Super Muon Channel project at the RIKEN-RAL muon facility (Ishida and Nagamine, 1998). In the latter project, a new scheme of the production of cooled μ^+'s by laser ionization of thermal muonium has also been proposed (Nagamine, 1996).

Once a highly intense muon source with a narrow energy spread and less contamination is available, physics programs with stopped muons, in particular, searches for rare muon LFV processes, would be significantly improved. First of all, the potential sensitivity achievable in searches for rare processes is ultimately limited by the number of muons available. Therefore a high-intensity beam is essential. Small beam contamination is necessary to further reduce any background associated with it. A narrow energy spread of the beam will allow a thin muon-stopping target to improve the detection resolution. For instance, if about 10^{19}–10^{20} muons/year are available, a new experiment of μ^--e^- conversion with a sensitivity of 10^{-18} could be possible (Blackmore $et\ al.$, 1997; Kuno, 1999).

The high-intensity muon sources could be used not only for experiments with low-energy muons, but also for experiments with energetic muons if the muons thus produced are injected into additional accelerators for further acceleration. Potential programs might include the measurements of the muon anomalous magnetic moment and the muon electric dipole moment, and also a muon accumulator ring for neutrino sources (Geer, 1998; Autin $et\ al.$, 1999). In addition to particle physics programs, a broad research field from materials science to biology would benefit from new highly intense muon sources, which would definitely open up a new era of muon science.

VII. CONCLUSIONS

We have described the current theoretical and experimental status of the field of muon decay and its potential to search for physics beyond the standard model. Among the many interesting physics topics related to muons, we have discussed precise measurements of normal muon decay and searches for muon LFV processes, in particular stressing the importance of the latter.

The field of LFV in muon decays has received growing attention from both theorists and experimentalists. This surge in interest can be attributed to the fact that many SUSY models predict large branching ratios for such LFV processes, in some cases as large as one or two orders of magnitude below the the present experimental limits. Such enhancements will be accessible and testable at future experiments. Among the SUSY models which predict sizeable LFV effects, one could mention SUSY GUT's, SUSY with right-handed (heavy) Majorana neutrinos, and SUSY with R-parity violation. In particular, LFV in muon decays is sensitive to physics at a very high energy scale, e.g., the GUT scale or the mass scale of a heavy right-handed Majorana neutrino for the see-saw mechanism. Non-SUSY models may also predict large LFV effects, leading one to conclude that the study of LFV in muon decays offers an attractive way of probing new physics phenomena that would be kinematically inaccessible at present and future colliders.

We have described the phenomenology of muon LFV processes of $|\Delta L_i| = 1$ (e.g., $\mu^+ \to e^+ \gamma$ and $\mu^+ \to e^+ e^+ e^-$ decays, and $\mu^- - e^-$ conversion in a muonic atom) and those of $|\Delta L_i| = 2$ (e.g., muonium-to-antimuonium conversion). All of the $|\Delta L_i| = 1$ processes were discussed within the framework of an effective Lagrangian in order to illustrate how the various contributions (such as photonic and nonphotonic) can be separately identified with measurements of the three muon LFV processes. Therefore searches for these three processes are of equal importance. If the muon is polarized, additional information could be obtained by measuring the angular distributions in $\mu^+ \to e^+ \gamma$ decay and $\mu^- - e^-$ conversion, and the T-odd and P-odd correlations in $\mu^+ \to e^+ e^+ e^-$ decay. Furthermore, for $\mu^+ \to e^+ \gamma$ decay, the use of polarized muons would be useful in eliminating background processes in the search. Experimentally, positive muons in a surface muon beam are known to be 100% polarized, and thereby the use of polarized muons will be feasible in the future. We then briefly mentioned the latest experimental results together with future experimental prospects. Recent experiments include MEGA ($\mu^+ \to e^+ \gamma$ decay), SINDRUM II ($\mu^- - e^-$ conversion), and the recent search for Mu$-\overline{\text{Mu}}$ conversion at PSI, whereas future prospects are such as a new phase of SINDRUM II, R-99-05 at PSI ($\mu^+ \to e^+ \gamma$ decay), and E940 (MECO) at BNL ($\mu^- - e^-$ conversion). In addition, precision measurements of normal muon decay, $\mu^+ \to e^+ \nu_e \bar{\nu}_\mu$, have attracted much interest. In the near future, new measurements of the muon lifetime, the Michel spectrum and its asymmetry, and e^+ polarization in polarized $\mu^+ \to e^+ \nu_e \bar{\nu}_\mu$ decay will

be carried out while aiming at an order-of-magnitude improvement. From all of these current and planned experiments, we could expect stronger constraints on parameter spaces of various theoretical models such as SUSY, or if a positive signal is discovered, we would obtain clear evidence of physics beyond the SM.

A new intense muon source with $10^{12} - 10^{13}\,\mu^\pm/s$ would be required to make substantial improvements in low-energy muon physics. The aimed intensity is four or five orders of magnitude higher than that available at present. The ideas for such a muon source are based on (i) solenoid pion capture, (ii) phase rotation, and (iii) muon cooling. These ideas originated from design studies for a $\mu^+ \mu^-$ collider. However, the beam time structure must be of high duty factor for low-energy muon physics, leading to new technical challenges which do not exist for the $\mu^+ \mu^-$ collider R&D studies. To overcome these issues, several R&D programs dedicated to low-energy muons are now being undertaken at KEK, RIKEN, and TRIUMF. With increased muon fluxes, the searches for rare muon LFV processes, as well as precision measurements of muon decay, are expected to be significantly improved.

In summary, muon physics is expected to play a leading role in the search for physics beyond the SM. Experiments with low-energy muons offer extraordinary opportunities for exploring new phenomena which would otherwise be directly inaccessible at future high-energy colliders.

APPENDIX A: RADIATIVE MUON DECAY

The differential branching ratio of the radiative muon decay, $\mu^+ \to e^+ \nu_e \bar{\nu}_\mu \gamma$, is given in Eq. (49). The functions

TABLE XVI. Chiral multiplets in MSSM.

	$Q_i(\tilde{q}_{iL}, q_{iL})$	$U_i^c(\tilde{u}_{iL}^c, u_{iL}^c)$	$D_i^c(\tilde{d}_{iL}^c, d_{iL}^c)$	$L_i(\tilde{l}_{iL}, l_{iL})$	$E_i^c(\tilde{e}_{iL}^c, e_{iL}^c)$	$H_1(H_1, \tilde{H}_1)$	$H_2(H_2, \tilde{H}_2)$
$SU(3)_C$	3	$\bar{3}$	$\bar{3}$	1	1	1	1
$SU(2)_L$	2	1	1	2	1	2	2
$U(1)_Y$	$\frac{1}{6}$	$-\frac{2}{3}$	$\frac{1}{3}$	$-\frac{1}{2}$	1	$-\frac{1}{2}$	$\frac{1}{2}$

appearing in Eq. (49), $F(x,y,d)$, $G(x,y,d)$, and $H(x,y,d)$ in the SM, are given as follows:

$$F = F^{(0)} + rF^{(1)} + r^2 F^{(2)},$$

$$G = G^{(0)} + rG^{(1)} + r^2 G^{(2)},$$

$$H = H^{(0)} + rH^{(1)} + r^2 H^{(2)}, \tag{A1}$$

where $r = (m_e/m_\mu)^2$. The terms m_e and m_μ are the masses of an electron and a muon, respectively. Here, x and y are the normalized electron and photon energies, $x = 2E_e/m_\mu$ and $y = 2E_\gamma/m_\mu$; d is given by $d \equiv 1 - \beta \hat{p}_e \cdot \hat{p}_\gamma$; and $\hat{p}_e$ and $\hat{p}_\gamma$ are unit momentum vectors of the electron and the photon, respectively. Moreover, β is defined as $\beta \equiv |\vec{p}_e|/E_e$.

$$F^{(0)}(x,y,d) = \frac{8}{d}\{y^2(3-2y)+6xy(1-y)$$
$$+2x^2(3-4y)-4x^3\}+8\{-xy(3-y$$
$$-y^2)-x^2(3-y-4y^2)+2x^3(1+2y)\}$$
$$+2d\{x^2y(6-5y-2y^2)$$
$$-2x^3y(4+3y)\}+2\,d^2x^3y^2(2+y), \tag{A2}$$

$$F^{(1)}(x,y,d) = \frac{32}{d^2}\left\{-\frac{y(3-2y)}{x}-(3-4y)+2x\right\}$$
$$+\frac{8}{d}\{y(6-5y)-2x(4+y)+6x^2\}$$
$$+8\{x(4-3y+y^2)-3x^2(1+y)\}$$
$$+6\,dx^2y(2+y), \tag{A3}$$

$$F^{(2)}(x,y,d) = \frac{32}{d^2}\left\{\frac{(4-3y)}{x}-3\right\}+\frac{48y}{d}, \tag{A4}$$

$$G^{(0)}(x,y,d) = \frac{8}{d}\{xy(1-2y)+2x^2(1-3y)-4x^3\}$$
$$+4\{-x^2(2-3y-4y^2)+2x^3(2+3y)\}$$
$$-4\,dx^3y(2+y), \tag{A5}$$

$$G^{(1)}(x,y,d) = \frac{32}{d^2}(-1+2y+2x)+\frac{8}{d}(-xy+6x^2)$$
$$-12x^2(2+y), \tag{A6}$$

$$G^{(2)}(x,y,d) = -\frac{96}{d^2}, \tag{A7}$$

$$H^{(0)}(x,y,d) = \frac{8}{d}\{y^2(1-2y)+xy(1-4y)-2x^2y\}$$
$$+4\{2xy^2(1+y)-x^2y(1-4y)+2x^3y\}$$
$$+2d\{x^2y^2(1-2y)-4x^3y^2\}$$
$$+2\,d^2x^3y^3, \tag{A8}$$

$$H^{(1)}(x,y,d) = \frac{32}{d^2}\left\{-\frac{y(1-2y)}{x}+2y\right\}$$
$$+\frac{8}{d}\{y(2-5y)-xy\}$$
$$+4xy(2y-3x)+6\,dx^2y^2, \tag{A9}$$

$$H^{(2)}(x,y,d) = -\frac{96y}{d^2x}+\frac{48y}{d}. \tag{A10}$$

APPENDIX B: MINIMAL SUPERSYMMETRIC STANDARD MODEL LAGRANGIAN

The Lagrangian for the minimal supersymmetric standard model (MSSM) is described. In SUSY theories, elementary fields are introduced as a pair of bosonic and fermionic fields. Such a pair is called a supermultiplet. There are two types of supermultiplets, a gauge multiplet and a chiral multiplet. A gauge multiplet consists of a gauge field (A_μ^a) and its superpartner, a gauge fermion (or gaugino) field (λ^a), which is a Majorana fermion field in the adjoint representation of the gauge group. In the MSSM, we have to introduce gaugino fields for $SU(3)_C$, $SU(2)_L$, and $U(1)_Y$ gauge groups. A chiral multiplet is a set of a complex scalar field (ϕ) and a left-handed Weyl fermion field (ψ_L). Its complex conjugate is called an antichiral multiplet, which consists of ϕ^* and ψ_R. In the MSSM, these chiral multiplets correspond to matter fields, namely, quark, lepton, and Higgs fields, and their superpartners. The fields in the same chiral multiplet have the same quantum numbers for the gauge groups. Chiral multiplets necessary for the MSSM are listed with their quantum numbers in Table XVI. The right-handed squarks and sleptons are defined as follows: $(\tilde{u}_{iL}^c)^* = \tilde{u}_{iR}$, $(\tilde{d}_{iL}^c)^* = \tilde{d}_{iR}$, and $(\tilde{e}_{iL}^c)^* = \tilde{e}_{iR}$. We sometimes use a notation $\tilde{\phi}$ and $\tilde{\psi}_L$ for superpartners of ϕ and ψ_L and Φ for a supermultiplet (ϕ, ψ_L).

In phenomenological applications of SUSY model, the SUSY Lagrangian consists of two parts, namely, the SUSY-invariant Lagrangian ($\mathcal{L}_{SUSY\,inv}$) and the soft SUSY-breaking terms ($\mathcal{L}_{SUSY\,breaking}$),

$$\mathcal{L} = \mathcal{L}_{SUSY\,inv} + \mathcal{L}_{SUSY\,breaking}. \tag{B1}$$

$\mathcal{L}_{SUSY\,inv}$ can be decomposed into two parts:

$$\mathcal{L}_{SUSY\,inv} = \mathcal{L}_{gauge} + \mathcal{L}_{superpotential}. \tag{B2}$$

$\mathcal{L}_{gauge}$ depends on the gauge coupling constants, and is given by

$$\mathcal{L}_{gauge} = \sum_{gauge\,multiplet} F^{(a)}_{\mu\nu} F^{(a)\mu\nu}$$

$$+ \sum_{chiral\,multiplet} (i\overline{\psi}_{iL}\gamma\cdot\mathcal{D}\psi_{iL} + |\mathcal{D}_\mu\phi_i|^2)$$

$$+ \mathcal{L}_{gaugino-matter} + \mathcal{L}_{D\,term}, \tag{B3}$$

where for each gauge group the $\mathcal{L}_{gaugino-matter}$ and $\mathcal{L}_{D\,term}$ terms are given by

$$\mathcal{L}_{gaugino-matter} = -\sum_i \sqrt{2}g\,\phi_i^\dagger \overline{\lambda}^a T^a \psi_{iL} + \text{H.c.}, \tag{B4}$$

$$\mathcal{L}_{D\,term} = -\sum_a \frac{g^2}{2} \sum_i (\phi_i^\dagger T^a \phi_i)^2. \tag{B5}$$

In addition to the normal gauge interactions defined in the covariant derivatives, these two types of interactions specified by the gauge coupling constants in Eqs. (B4) and (B5) are necessary to keep the SUSY invariance of the Lagrangian. Here $\mathcal{L}_{superpotential}$ is determined from the superpotential $W(\phi_i)$, which is a function of scalar fields of the chiral multiplets,

$$\mathcal{L}_{superpotential} = -\sum_i \left|\frac{W(\phi)}{\partial\phi_i}\right|^2$$

$$- \frac{1}{2}\frac{\partial^2 W(\phi)}{\partial\phi_i\partial\phi_j}\overline{(\psi_{iL})^c}\psi_{jL} + \text{H.c.} \tag{B6}$$

The superpotential therefore generates a set of bosonic and fermionic interactions. From the gauge invariance, the superpotential $[W(\phi_i)]$ for the MSSM is given by

$$W_{MSSM} = (y_e)_{ij} H_1 E_i^c L_j + (y_d)_{ij} H_1 D_i^c Q_j$$

$$+ (y_u)_{ij} H_2 U_i^c Q_j - \mu H_1 H_2, \tag{B7}$$

where the contraction of the $SU(2)$ indices is made by using the antisymmetric tensor, $\varepsilon_{\alpha\beta}$. Moreover, R-parity conservation is required (Sec. III.C.3). By substituting these functions in Eq. (B6), this superpotential would induce the ordinary Yukawa couplings and the Higgsino mass terms, as well as the other interactions that are necessary to ensure SUSY invariance.

The soft SUSY-breaking mass terms are defined as terms that do not introduce quadratic divergence, and essentially serve as mass terms for superpartners. A general form of SUSY-breaking terms in the MSSM is given by

$$\mathcal{L}_{SUSY\,breaking} = -(m_e^2)_{ij}\tilde{e}_{iR}^*\tilde{e}_{jR} - (m_l^2)_{ij}\tilde{l}_{iL}^*\tilde{l}_{jL}$$

$$- (m_d^2)_{ij}\tilde{d}_{iR}^*\tilde{d}_{jR} - (m_u^2)_{ij}\tilde{u}_{iR}^*\tilde{u}_{jR}$$

$$- (m_q^2)_{ij}\tilde{q}_{iL}^*\tilde{q}_{jL} - m_{H_1}^2 H_1^* H_1$$

$$- m_{H_2}^2 H_2^* H_2 - \left[m_0(A_e)_{ij} H_1 \tilde{e}_{iR}^* \tilde{e}_{jR} \right.$$

$$+ m_0(A_d)_{ij} H_1 \tilde{d}_{iR}^* \tilde{q}_{jL}$$

$$+ m_0(A_u)_{ij} H_2 \tilde{u}_{iR}^* \tilde{q}_{jL} - \mu B H_1 H_2$$

$$+ \frac{1}{2}M_1 \overline{\tilde{B}_R}\tilde{B}_L + \frac{1}{2}M_2 \overline{\tilde{W}_R}\tilde{W}_L$$

$$\left. + \frac{1}{2}M_3 \overline{\tilde{G}_R}\tilde{G}_L + \text{H.c.} \right]. \tag{B8}$$

These terms are quadratic terms for scalar quarks, leptons, and Higgs fields, scalar trilinear terms (A terms), and gaugino Majorana mass terms. These terms are supposed to be generated from spontaneous symmetry breaking of SUSY, presumably at some high energy scale in some sector outside the MSSM dynamics, such as the supergravity or the dynamical SUSY-breaking sector. For more details, see, for example, Nilles (1984) or Haber and Kane (1985).

APPENDIX C: DIFFERENTIAL BRANCHING RATIO OF THE $\mu^+\to e^+e^+e^-$ DECAY

The differential branching ratio of the $\mu^+\to e^+e^+e^-$ decay is given in Eq. (113). The kinematical functions appearing in Eq. (113), $\alpha_i(x_1,x_2)$, $\beta_i(x_1,x_2)$, and $\gamma_i(x_1,x_2)$, are given as follows [$x_i\equiv 2E_i/m_\mu(i=1,2)$ are the normalized e^+ energies]:

$$\alpha_1(x_1,x_2) = 8(2-x_1-x_2)(x_1+x_2-1),$$

$$\alpha_2(x_1,x_2) = 2\{x_1(1-x_1)+x_2(1-x_2)\},$$

$$\alpha_3(x_1,x_2) = 8\left\{\frac{2x_2^2-2x_2+1}{1-x_1} + \frac{2x_1^2-2x_1+1}{1-x_2}\right\},$$

$$\alpha_4(x_1,x_2) = 32(x_1+x_2-1),$$

$$\alpha_5(x_1,x_2) = 8(2-x_1-x_2),$$

$$\beta_1(x_1,x_2)$$

$$= 2\frac{(x_1+x_2)(x_1^2+x_2^2)-3(x_1+x_2)^2+6(x_1+x_2)-4}{(2-x_1-x_2)},$$

$$\beta_2(x_1,x_2) = \frac{8}{(1-x_1)(1-x_2)(2-x_1-x_2)}$$

$$\times\{2(x_1+x_2)(x_1^3+x_2^3)-4(x_1+x_2)$$

$$\times(2x_1^2+x_1x_2+2x_2^2)$$

$$+(19x_1^2+30x_1x_2+19x_2^2)$$

$$-12(2x_1+2x_2-1)\},$$

$$\gamma_1(x_1,x_2) = 4 \frac{\sqrt{(1-x_1)(1-x_2)(x_1+x_2-1)}(x_1-x_2)}{(2-x_2-x_1)},$$

$$\gamma_2(x_1,x_2) = 32 \sqrt{\frac{(x_1+x_2-1)}{(1-x_1)(1-x_2)}} \frac{(x_1+x_2-1)(x_2-x_1)}{(2-x_1-x_2)},$$

$$\gamma_3(x_1,x_2) = 16 \sqrt{\frac{(x_1+x_2-1)}{(1-x_1)(1-x_2)}}(x_1+x_2-1)(x_2-x_1),$$

$$\gamma_4(x_1,x_2) = 8 \sqrt{\frac{(x_1+x_2-1)}{(1-x_1)(1-x_2)}}(2-x_1-x_2)(x_2-x_1).$$

$$(C1)$$

REFERENCES

Abachi, S., *et al.* (D0 Collaboration), 1996, Phys. Rev. Lett. **76**, 3271.

Abdurashitov, J.N., *et al.* (SAGE Collaboration), 1996, Phys. Rev. Lett. **77**, 4708.

Abegg, R., *et al.* (TRIUMF E614 Collaboration), 1996, "Precision Measurement of the Michel Parameters of μ^+ Decay," experimental proposal to TRIUMF.

Abela, R., *et al.*, 1996, Phys. Rev. Lett. **77**, 1950.

Abraham, K.J., and B. Lampe, 1996, Phys. Lett. B **367**, 299.

Abreu, P., *et al.* (DELPHI Collaboration), 1997, Z. Phys. C **73**, 243.

Ahmad, S., *et al.*, 1988, Phys. Rev. D **38**, 2102.

Akers, R., *et al.* (OPAL Collaboration), 1995, Z. Phys. C **67**, 555.

Altarelli, G., L. Baulieu, N. Cabibbo, L. Maiani, and R. Petronzio, 1977, Nucl. Phys. B **125**, 285.

Amaldi, U., W. de Boer, and H. Furstenau, 1991, Phys. Lett. B **260**, 447.

Ambrose, D., *et al.* (BNL E871 Collaboration), 1998, Phys. Rev. Lett. **81**, 5734.

Ankenbrandt, C.M., *et al.* (Muon Collider Collaboration), 1999, Phys. Rev. ST Accel. Beams **2**, 081001.

Arbuzov, A.B., O. Krehl, E.A. Kuraev, E.N. Magar, and B.G. Shaikhatdenov, 1998, Phys. Lett. B **432**, 421.

Arisaka, K., *et al.*, 1998, Phys. Lett. B **432**, 230.

Arkani-Hamed, N., H.-C. Cheng, and L.J. Hall, 1996, Phys. Rev. D **53**, 413.

Arkani-Hamed, N., H.-C. Cheng, J.L. Feng, and L.J. Hall, 1996, Phys. Rev. Lett. **77**, 1937.

Arkani-Hamed, N., J.L. Feng, L.J. Hall, and H.-C. Cheng, 1997, Nucl. Phys. B **505**, 3.

Armstrong, D.S., *et al.*, 1992, Phys. Rev. C **46**, 1094.

Athanassopoulos, C., *et al.* (LSND Collaboration), 1998, Phys. Rev. Lett. **81**, 1774.

Autin, B., A. Blondel, and J. Ellis, 1999, Eds., "Prospective Study of Muon Storage Rings at CERN," CERN report, CERN 99-02 and ECFA 99-197.

Babu, K.S., and R.N. Mohapatra, 1995, Phys. Rev. Lett. **75**, 2276.

Bachman, M., *et al.* (MECO Collaboration), 1997, "A Search for $\mu^- N \to e^- N$ with Sensitivity below 10^{-16}," experimental proposal E940 to Brookhaven National Laboratory AGS.

Badertscher, A., *et al.*, 1982, Nucl. Phys. A **377**, 406.

Balke, B., *et al.*, 1988, Phys. Rev. D **37**, 587.

Baranov, V.A., *et al.*, 1991, Sov. J. Nucl. Phys. **53**, 802.

Barber, W.C., *et al.*, 1969, Phys. Rev. Lett. **22**, 902.

Barbieri, R., G. Dvali, and L.J. Hall, 1996, Phys. Lett. B **377**, 76.

Barbieri, R., and L.J. Hall, 1994, Phys. Lett. B **338**, 212.

Barbieri, R., L.J. Hall, and A. Strumia, 1995a, Nucl. Phys. B **445**, 219.

Barbieri, R., L.J. Hall, and A. Strumia, 1995b, Nucl. Phys. B **449**, 437.

Bardin, G., *et al.*, 1984, Phys. Lett. B **137**, 135.

Barkov, L.M., *et al.*, 1999, "Search for $\mu^+ \to e^+ \gamma$ down to 10^{-14} branching ratio," research proposal to PSI.

Barnett, I., *et al.*, 1994, "Measurement of the transverse polarization of positrons from the decay of polarized muons," proposal for an experiment at PSI.

Beer, G.A., *et al.*, 1986, Phys. Rev. Lett. **57**, 671.

Behrends, R.E., R.J. Finkelstein, and A. Sirlin, 1956, Phys. Rev. **101**, 866.

Bellgardt, U., *et al.*, 1988, Nucl. Phys. B **229**, 1.

Beltrami, I., *et al.*, 1987, Phys. Lett. B **194**, 326.

Bernabeu, J., E. Nardi, and D. Tommasini, 1993, Nucl. Phys. B **409**, 69.

Bertl, W., *et al.*, 1984, Phys. Lett. B **140**, 299.

Bertl, W., *et al.*, 1985, Nucl. Phys. B **260**, 1.

Bilenky, S.M., and S.T. Petcov, 1987, Rev. Mod. Phys. **59**, 671.

Bilenky, S.M., S.T. Petcov, and B. Pontecorvo, 1977, Phys. Lett. B **67**, 309.

Bjorken, J.D., K. Lane, and S. Weinberg, 1977, Phys. Rev. D **16**, 1474.

Blackmore, E., *et al.*, 1997, "MUONS at TRIUMF," TRIUMF internal report.

Bliss, D.W., *et al.* (CLEO Collaboration), 1998, Phys. Rev. D **57**, 5903.

Bolton, R.D., *et al.*, 1984, Phys. Rev. Lett. **53**, 1415.

Bolton, R.D., *et al.*, 1988, Phys. Rev. D **38**, 2077.

Borzumati, F., and A. Masiero, 1986, Phys. Rev. Lett. **57**, 961.

Bouchiat, C., and L. Michel, 1957, Phys. Rev. **106**, 170.

Bowser-Chao, D., and W.-K. Keung, 1997, Phys. Rev. D **56**, 3924.

Brooks, M.L., *et al.* (MEGA Collaboration), 1999, Phys. Rev. Lett. **83**, 1521.

Bryman, D.A., M. Blecher, K. Gotow, and R.J. Powers, 1972, Phys. Rev. Lett. **28**, 1469.

Bryman, D.A., *et al.*, 1985, Phys. Rev. Lett. **55**, 465.

Burkard, H., *et al.*, 1985a, Phys. Lett. **150B**, 242.

Burkard, H., *et al.*, 1985b, Phys. Lett. **160B**, 343.

Cao, J.-J., T. Han, X. Zhang, and G.-R. Lu, 1999, Phys. Rev. D **59**, 095001.

Carena, M., G.F. Giudice, and C.E.M. Wagner, 1997, Phys. Lett. B **390**, 234.

Carey, R.M., *et al.*, 1999a, Phys. Rev. Lett. **82**, 1632.

Carey, R.M., *et al.*, 1999b, "A Precision Measurement of the Positive Muon Lifetime Using a Pulsed Muon Beam and the μLan Detector," experimental proposal to PSI.

Carlson, E.D., and P.H. Frampton, 1992, Phys. Lett. B **283**, 123.

Caso, C., *et al.* (Particle Data Group), 1998, Eur. Phys. J. C **3**, 1.

Cavallo, F.R., *et al.*, 1999, "A Precision Measurement of the μ^+ Lifetime (G_F) with the FAST detector," experimental proposal to PSI.

Chaichian, M., and K. Huitu, 1996, Phys. Lett. B **384**, 157.

Chang, D., and W.Y. Keung, 1989, Phys. Rev. Lett. **62**, 2583.

Chattopadhyay, U., and P. Nath, 1996, Phys. Rev. D **53**, 1648.

Cheng, T.P., and L.F. Li, 1977a, Phys. Rev. Lett. **38**, 381.

Cheng, T.P., and L.F. Li, 1977b, Phys. Rev. D **16**, 1425.

Cheng, T.P., and L.F. Li, 1980, Phys. Rev. Lett. **45**, 1908.

Chiang, H.C., E. Oset, T.S. Kosmas, A. Faessler, and J.D. Vergados, 1993, Nucl. Phys. A **559**, 526.

Choi, S.Y., C.S. Kim, Y.J. Kwon, and S.-H. Lee, 1998, Phys. Rev. D **57**, 7023.

Ciafaloni, P., A. Romanino, and A. Strumia, 1996, Nucl. Phys. B **458**, 3.

Cleveland, B.T., *et al.*, 1998, Astrophys. J. **496**, 505.

Cohen, A.G., D.B. Kaplan, and A.E. Nelson, 1996, Phys. Lett. B **388**, 588.

Cohen, E.R., and B.N. Taylor, 1987, Rev. Mod. Phys. **59**, 1121.

Coleman, S., and S.L. Glashow, 1999, Phys. Rev. D **59**, 116008.

Conversi, M., E. Pancini, and O. Piccioni, 1947, Phys. Rev. **71**, 209.

Crittenden, R.R., W.D. Walker, and J. Ballam, 1961, Phys. Rev. **121**, 1823.

Czarnecki, A., W.J. Marciano, and K. Melnikov, 1997, in *Proceedings of Workshop on Physics at the First Muon Collider and at the Front End of the Muon Collider*, Fermilab, edited by S.H. Geer and R. Raja, AIP Conf. Proc. No. 435 (AIP, New York), p. 409.

Czarnecki, A., and W.J. Marciano, 1999, Nucl. Phys. B, Proc. Suppl. **76**, 245.

Danby, G., J.M. Gaillard, K. Goulianos, L.M. Lederman, N. Mistry, M. Schwartz, and J. Steinberger, 1962, Phys. Rev. Lett. **9**, 36.

Depommier, P., 1987, in *Neutrinos*, edited by H.V. Klapdor (Springer, Berlin), p. 265.

Depommier, P., *et al.*, 1977, Phys. Rev. Lett. **39**, 1113.

Depommier, P., and C. Leroy, 1995, Rep. Prog. Phys. **58**, 61.

Derenzo, S.E., 1969, Phys. Rev. **181**, 1854.

Deshpande, N.G., B. Dutta, and E. Keith, 1996, Phys. Rev. D **54**, 730.

Dimopoulos, S., and H. Georgi, 1981, Nucl. Phys. B **193**, 150.

Dimopoulos, S., and L. Hall, 1995, Phys. Lett. B **344**, 185.

Dine, M., and A.E. Nelson, 1993, Phys. Rev. D **48**, 1277.

Dine, M., A.E. Nelson, Y. Nir, and Y. Shirman, 1996, Phys. Rev. D **53**, 2658.

Dine, M., A.E. Nelson, and Y. Shirman, 1995, Phys. Rev. D **51**, 1362.

Dine, M., Y. Nir, and Y. Shirman, 1997, Phys. Rev. D **55**, 1501.

Dohmen, C., *et al.* (SINDRUM II Collaboration), 1993, Phys. Lett. B **317,** 631.

Dubovsky, S.L., and D.S. Gorbunov, 1998, Phys. Lett. B **419**, 223.

Duong, T.V., B. Dutta, and E. Keith, 1996, Phys. Lett. B **378**, 128.

Dzhilkibaev, R.M., and V.M. Lobashev, 1989, Sov. J. Nucl. Phys. **49**, 384.

Eckstein, S.G., and R.H. Pratt, 1959, Ann. Phys. (N.Y.) **8**, 297.

Edwards, K.W., *et al.* (CLEO Collaboration), 1997, Phys. Rev. D **55**, 3919.

Eichenberger, W., R. Engfer, and A. van der Schaaf, 1984, Nucl. Phys. A **412**, 523.

Eitel, K., *et al.* (KARMEN Collaboration), 1999, Nucl. Phys. B, Proc. Suppl. **70**, 210.

Ellis, J., S. Kelly, and D. Nanopoulos, 1991, Phys. Lett. B **260**, 131.

Engfer, R., and H.K. Walter, 1986, Annu. Rev. Nucl. Part. Sci. **36**, 327.

Evseev, V.S., 1975, in *Muon Physics, Vol. III: Chemistry and Solids*, edited by V.W. Hughes and C.S. Wu (Academic, New York), p. 236.

Faessler, A., T.S. Kosmas, S. Kovalemko, and J.D. Vergados, 1999, "Constraints on *R*-parity Violating Supersymmetry from $\mu^- - e^-$ Nuclear Conversion," e-print hep-ph/9904335.

Feinberg, G., 1958, Phys. Rev. **116**, 1482.

Feinberg, G., and S. Weinberg, 1961, Phys. Rev. Lett. **123**, 1439.

Fetscher, W., and H.J. Gerber, 1995, in *Precision Tests of the Standard Electroweak Model*, edited by P. Langacker (World Scientific, Singapore), p. 657.

Fetscher, W., and H.J. Gerber, 1998, Eur. Phys. J. C **3**, 282.

Fetscher, W., H.J. Gerber, and K.F. Johnson, 1986, Phys. Lett. B **173**, 102.

Feynman, R.P., and M. Gell-Mann, 1958, Phys. Rev. **109**, 193.

Fisher, P., B. Kayser, and K.S. McFarland, 1999, Annu. Rev. Nucl. Part. Sci. **49**, 481.

Frampton, P.H., 1992a, Phys. Rev. Lett. **69**, 2889.

Frampton, P.H., 1992b, Phys. Rev. D **45**, 4240.

Frampton, P.H., and B.H. Lee, 1990, Phys. Rev. Lett. **64**, 619.

Frankel, S., 1975, in *Muon Physics II: Weak Interaction*, edited by V.W. Hughes and C.S. Wu (Academic, New York), p. 83.

Freedman, S.J., *et al.*, 1993, Phys. Rev. D **47**, 811.

Fronsdal, C., and H. Überall, 1959, Phys. Rev. **118**, 654.

Fujii, H., Y. Mimura, K. Sasaki, and T. Sasaki, 1994, Phys. Rev. D **49**, 559.

Fujii, H., S. Nakamura, and K. Sasaki, 1993, Phys. Lett. B **299**, 342.

Fukuda, Y., *et al.* (Kamiokande Collaboration), 1996, Phys. Rev. Lett. **77**, 1683.

Fukuda, Y., *et al.* (Super-Kamiokande Collaboration), 1998a, Phys. Rev. Lett. **81**, 1158; **81**, 4279(E).

Fukuda, Y., *et al.* (Super-Kamiokande Collaboration), 1998b, Phys. Rev. Lett. **81**, 1562.

Fukugita, M., and T. Yanagida, 1994, in *Physics and Astrophysics of Neutrinos*, edited by M. Fukugita and A. Suzuki (Springer, Berlin), p. 1.

Gabrielli, E., and U. Sarid, 1997, Phys. Rev. Lett. **79**, 4752.

Geer, S., 1998, Phys. Rev. D **57**, 6989; **59**, 039903(E).

Gell-Mann, M., P. Ramond, and R. Slansky, 1979, in *Supergravity*, edited by D. Freedman and P. van Nieuwenhuizen (North-Holland, Amsterdam), p. 315.

Giovanetti, K.L., *et al.*, 1984, Phys. Rev. D **29**, 343.

Giudice, G.F., and R. Rattazzi, 1999, Phys. Rep. **322**, 419.

Glashow, S.L., 1961, Phys. Rev. Lett. **6**, 196.

Glashow, S.L., P.J. Kerman, and L.M. Krauss, 1999, Phys. Lett. B **445**, 412.

Glashow, S.L., and L.M. Krauss, 1987, Phys. Lett. B **190**, 199.

Gómez, M.E., and H. Goldberg, 1996, Phys. Rev. D **53**, 5244.

Gordeev, V.A., *et al.*, 1997, Phys. At. Nucl. **60**, 1164.

Haber, H.E., and G.L. Kane, 1985, Phys. Rep. **117**, 75.

Hall, L.J., V.A. Kostelecky, and S. Raby, 1986, Nucl. Phys. B **267**, 415.

Halprin, A., 1982, Phys. Rev. Lett. **48**, 1313.

Halprin, A., and A. Masiero, 1993, Phys. Rev. D **48**, 2987.

Hampel, W., *et al.* (Gallex Collaboration), 1999, Phys. Lett. B **447**, 127.

Hänggi, P., R.D. Viollier, U. Raff, and K. Adler, 1974, Phys. Lett. **51B**, 119.

Herczeg, P., and R.N. Mohapatra, 1992, Phys. Rev. Lett. **69**, 2475.

Herczeg, P., 1986, Phys. Rev. D **34**, 3449.

Herczeg, P., 1995, in *Precision Tests of the Standard Electroweak Model*, edited by P. Langacker (World Scientific, Singapore), p. 786.

Herzog, F., and K. Adler, 1980, Helv. Phys. Acta **53**, 53.

Hincks, E.P., and B. Pontecorvo, 1947, Phys. Rev. Lett. **73**, 246.

Hirouchi, M., and M. Tanaka, 1998, Phys. Rev. D **58**, 032004.

Hisano, J., T. Moroi, K. Tobe, and M. Yamaguchi, 1996, Phys. Rev. D **53**, 2442.

Hisano, J., T. Moroi, K. Tobe, and M. Yamaguchi, 1997, Phys. Lett. B **391**, 341; **397**, 357(E).

Hisano, J., T. Moroi, K. Tobe, M. Yamaguchi, and T. Yanagida, 1995, Phys. Lett. B **357**, 579.

Hisano, J., M.M. Nojiri, Y. Shimizu, and M. Tanaka, 1999, Phys. Rev. D **60**, 055008.

Hisano, J., and D. Nomura, 1999, Phys. Rev. D **59**, 116005.

Hisano, J., D. Nomura, Y. Okada, Y. Shimizu, and M. Tanaka, 1998, Phys. Rev. D **58**, 116010.

Hisano, J., D. Nomura, and T. Yanagida, 1998, Phys. Lett. B **437**, 351.

Honecker, W., *et al.* (SINDRUM II Collaboration), 1996, Phys. Rev. Lett. **76**, 200.

Horikawa, K. and K. Sasaki, 1996, Phys. Rev. D **53**, 560.

Hou, W.S., 1996, Nucl. Phys. B, Proc. Suppl. **51A**, 40.

Hou, W.S., and G.G. Wong, 1995, Phys. Lett. B **357**, 145.

Hou, W.S., and G.G. Wong, 1996, Phys. Rev. D **53**, 1537.

Huber, T.M., *et al.*, 1990, Phys. Rev. D **41**, 2709.

Hughes, V.W., and T. Kinoshita, 1999, Rev. Mod. Phys. **71**, S133.

Hughes, V.W., D.W. McColm, K. Ziock, and R. Prepost, 1960, Phys. Rev. Lett. **5**, 63.

Huitu, K., J. Maalampi, M. Raidal, and A. Santamaria, 1998, Phys. Lett. B **430**, 355.

Ishida, K., and K. Nagamine, 1998, in *Proceedings of International Workshop on JHF Science*, Vol. II, edited by J. Chiba, M. Furusaka, H. Miyatake, and S. Sawada (KEK, Tsukuba), p. 12.

JAERI/KEK Joint Project, 1999, unpublished proposal.

Jodidio, A., *et al.*, 1986, Phys. Rev. D **34**, 1967; **37**, 237(E).

Kaulard, J., *et al.*, 1998, Phys. Lett. B **422**, 334.

Kersch, A., N. Kraus, and R. Engfer, 1988, Nucl. Phys. A **485**, 606.

Kim, J.E., P. Ko, and D.G. Lee, 1997, Phys. Rev. D **56**, 100.

King, S.F., and M. Oliveira, 1999, Phys. Rev. D **60**, 035003.

Kinnison, W.W., *et al.*, 1982, Phys. Rev. D **25**, 2846.

Kinoshita, T., and A. Sirlin, 1957, Phys. Rev. **108**, 844.

Kinoshita, T., and A. Sirlin, 1959a, Phys. Rev. Lett. **2**, 177.

Kinoshita, T., and A. Sirlin, 1959b, Phys. Rev. **113**, 1652.

Kitano, R., and K. Yamamoto, 2000, Phys. Rev. D **62**, 073007.

Kobayashi, M., and T. Maskawa, 1973, Prog. Theor. Phys. **49**, 652.

Korenchenko, S.M., *et al.*, 1976, Sov. Phys. JETP **43**, 1.

Kosmas, T.S., and J.D. Vergados, 1990, Nucl. Phys. A **510**, 641.

Kosmas, T.S., and J.D. Vergados, 1996, Phys. Rep. **264**, 251.

Kosmas, T.S., J.D. Vergados, and A. Faessler, 1998, Yad. Fiz. **61**, 1261 [Phys. At. Nucl. **61**, 1161 (1998)].

Kosmas, T.S., J.D. Vergados, O. Civitarese, and A. Faessler, 1994, Nucl. Phys. A **570**, 637.

Krasnikov, N.V., 1994, Mod. Phys. Lett. A **9**, 791.

Krasnikov, N.V., 1996, Phys. Lett. B **388**, 783.

Krolak, P., *et al.*, 1994, Phys. Lett. B **320**, 407.

Kuno, Y., 1997, in *Proceedings of Workshop on Physics at the First Muon Collider and at the Front End of the Muon Collider*, edited by S.H. Geer and R. Raja, AIP Conf. Proc. No. 435 (AIP, New York), p. 261.

Kuno, Y., *et al.*, 1998, in *Proceedings of Workshop on High Intensity Secondary Beam with Phase Rotation*, edited by Y. Kuno and N. Sasao (KEK, Tsukuba), p. 71.

Kuno, Y., *et al.*, 1999, in *Proceedings of Workshop on High Intensity Muon Sources*, edited by Y. Kuno and T. Yokoi (World Scientific, Singapore).

Kuno, Y., A. Maki, and Y. Okada, 1997, Phys. Rev. D **55**, 2517.

Kuno, Y., K. Nagamine, and T. Yamazaki, 1986, Nucl. Phys. A **475**, 615.

Kuno, Y., and Y. Okada, 1996, Phys. Rev. Lett. **77**, 434.

Lagarrigue, A., and C. Peyrou, 1952, Acad. Sci., Paris, C. R. **234**, 873.

Langacker, P., and M. Luo, 1991, Phys. Rev. D **44**, 817.

Langacker, P., and S.U. Sankar, 1989, Phys. Rev. D **40**, 1569.

Lee, A.M., *et al.*, 1990, Phys. Rev. Lett. **64**, 165.

Lee, B.W., S. Pakvasa, R.E. Shrock, and H. Sugawara, 1977, Phys. Rev. Lett. **38**, 937.

Lee, B.W., and R.E. Shrock, 1977, Phys. Rev. D **16**, 1444.

Lenard, A., 1953, Phys. Rev. **90**, 968.

LEP Electroweak Working Group and SLD Heavy Flavor and Electroweak Groups, 1999, "A Combination of Preliminary Electroweak Measurements and Constraints on the Standard Model," preprint; CERN-EP/99-15.

Lobashev, V.M., 1998, in *Proceedings of 18th Workshop on Physics in Collisions*, edited by S. Bianco, A. Calcaterra, P. de Simone, and F.L. Fabbri, Frascati Physics series No. 11, p. 179.

Lokonathan, S., and J. Steinberger, 1955, Phys. Rev. **98**, 240.

Lopez, J.L., D.V. Nanopoulos, and X. Wang, 1994, Phys. Rev. D **49**, 366.

Maki, Z., M. Nakagawa, and S. Sakata, 1962, Prog. Theor. Phys. **28**, 870.

Marciano, W.J., 1999, Phys. Rev. D **60**, 093006.

Marciano, W.J., and A.I. Sanda, 1977a, Phys. Lett. **67B**, 303.

Marciano, W.J., and A.I. Sanda, 1977b, Phys. Rev. Lett. **38**, 1512.

Marciano, W.J., and A. Sirlin, 1988, Phys. Rev. Lett. **61**, 1815.

Marshall, G.M., *et al.*, 1982, Phys. Rev. D **25**, 1174.

Matthias, B., *et al.*, 1991, Phys. Rev. Lett. **66**, 2716.

Michel, L., 1950, Proc. Phys. Soc., London, Sect. A **63**, 514.

Mikheyev, S.P., and A.Yu. Smirnov, 1985, Yad. Fiz **42**, 1441 [Sov. J. Nucl. Phys. **42**, 913 (1985)].

Mohapatra, R.N., 1992, Z. Phys. C **56**, S117.

Mohapatra, R.N., and P.B. Pal, 1998, *Massive Neutrinos in Physics and Astrophysics*, 2nd ed. (World Scientific, Singapore).

Molzon, W.R., 1997, in *Proceedings of Workshop on Physics at the First Muon Collider and at the Front End of the Muon Collider*, edited by S.H. Geer and R. Raja, AIP Conf. Proc. No. 435 (AIP, New York), p. 152.

Moroi, T., 1996, Phys. Rev. D **53**, 6565; **56**, 4424(E).

Muon Collider Collaboration, 1996, "$\mu^+\mu^-$ Collider—A Feasibility Study," preprint; BNL-52503, fermilab-conf-96/092, LBNL-38946.

Nagamine, K., 1996, Nucl. Phys. B, Proc. Suppl. **51A**, 115.

Nagamine, K., and T. Yamazaki, 1974, Nucl. Phys. A **219**, 104.

Nakamura, S., *et al.*, 1998, "Precise Measurement of the μ^+ Lifetime and Test of the Exponential Law," research proposal to RIKEN-RAL (R77).

Neddermeyer, S.H., and C.D. Anderson, 1937, Phys. Rev. **51**, 884.

Ni, B., *et al.*, 1993, Phys. Rev. D **48**, 1976.

Nilles, H.P., 1984, Phys. Rep. **110**, 1.

Nir, Y., and N. Seiberg, 1993, Phys. Lett. B **309**, 337.

Nishijima, K., 1957, Phys. Rev. **108**, 907.

Okada, Y., K. Okumura, and Y. Shimizu, 1998, Phys. Rev. D **58**, 051901.

Okada, Y., K. Okumura, and Y. Shimizu, 2000, Phys. Rev. D **61**, 094001.

Otten, E.W., and Ch. Weinheimer, 1998, in *Proceedings of the First International Symposium on Lepton and Baryon Number Violation*, edited by H.V. Klapdor-Kleingrothaus and I.V. Krivosheina (Institute of Physics, Bristol/Philadelphia), p. 309.

Petcov, S.T., Yad. Fiz. **25**, 641 [Sov. J. Nucl. Phys. **25**, 340 (1977)].

Pich, A., 1997, in *Proceedings of NATO Advanced Study Institute on Masses of Fundamental Particles*, edited by M. Levy, J. Iliopoulos, R. Gastmans, and J.-M. Gerard, Vol. 363 of *NATO Advanced-Study Institute Series B: Physics* (Plenum, New York), p. 173.

Pich, A., and J.P. Silva, 1995, Phys. Rev. D **52**, 4006.

Pontecorvo, B., 1957, Zh. Éksp. Teor. Fiz. **33**, 549 [Sov. Phys. JETP **6**, 429 (1958)].

Porter, C.E., and H. Primakoff, 1951, Phys. Rev. **83**, 849.

Pratt, R., 1958, Phys. Rev. **111**, 646.

Primakoff, H., 1959, Rev. Mod. Phys. **31**, 802.

Raidal, M., 1998, Phys. Rev. D **57**, 2013.

Raidal, M., and A. Santamaria, 1998, Phys. Lett. B **421**, 250.

Rattazzi, R., and U. Salid, 1996, Nucl. Phys. B **475**, 27.

Sakai, N., 1981, Z. Phys. C **11**, 153.

Scheck, F., 1978, Phys. Rep. **44**, 187.

Schwinger, J., 1957, Ann. Phys. (N.Y.) **2**, 407.

Shanker, O., 1979, Phys. Rev. D **20**, 1608.

Shanker, O., 1982, Phys. Rev. D **25**, 1847.

Shanker, O., and R. Roy, 1997, Phys. Rev. D **55**, 7307.

Skrinskii, A.N., and V.V. Parkhomchuk, 1981, Fiz. Elem. Chastits At. Yadra **12**, 557 [Sov. J. Part. Nucl. **12**, 223 (1981)].

Steinberger, J., 1948, Phys. Rev. **74**, 500.

Steinberger, J., and H.B. Wolfe, 1955, Phys. Rev. **100**, 1490.

Swartz, M.L., 1989, Phys. Rev. D **40**, 1521.

Treiman, S.B., F. Wilczek, and A. Zee, 1977, Phys. Rev. D **16**, 152.

Van der Schaaf, A., *et al.*, 1980, Nucl. Phys. A **340**, 249.

Van der Schaaf, A., 1993, Prog. Part. Nucl. Phys. **31**, 1.

Van Hove, P., *et al.*, 1997, "A Precision Measurement of the Michel Parameter ξ'' in Polarized Muon Decay," experimental proposal R-97-06 to PSI.

van Ritbergen, T., and R.G. Stuart, 1999, Phys. Rev. Lett. **82**, 488.

Vergados, J.D., 1986, Phys. Rep. **133**, 1.

Watanabe, R., M. Fukui, H. Ohtsubo, and M. Morita, 1987, Prog. Theor. Phys. **78**, 114.

Watanabe, R., K. Muto, T. Oda, T. Niwa, H. Ohtsubo, R. Morita, and M. Morita, 1993, At. Data Nucl. Data Tables **54**, 165.

Weinberg, S., and G. Feinberg, 1959, Phys. Rev. Lett. **3**, 111; **3**, 244(E).

Wilczek, F., and A. Zee, 1977, Phys. Rev. Lett. **38**, 531.

Willmann, L., *et al.*, 1999, Phys. Rev. Lett. **82**, 49.

Willmann, L., and K.P. Jungmann, 1997, Physics **499**, 43.

Wintz, P., 1998, in *Proceedings of the First International Symposium on Lepton and Baryon Number Violation*, edited by H.V. Klapdor-Kleingrothaus and I.V. Krivosheina (Institute of Physics, Bristol/Philadelphia), p. 534.

Wolfenstein, L., 1978, Phys. Rev. D **17**, 2369.

Yanagida, T., 1979, in *Proceedings of Workshop on Unified Theory and Baryon Number in the Universe*, edited by O. Sawada and A. Sugamoto, New York, KEK Report No. 79-18 (KEK, Tsukuba), p. 95.

Yukawa, H., 1935, Proc. Phys. Math. Soc. Jpn. **17**, 48.

Zee, A., 1985, Phys. Rev. Lett. **55**, 2382.